GIS BASED GEOTHERMAL POTENTIAL ASSESSMENT FOR WESTERN ANATOLIA

A THESIS SUBMITTED TO
THE GRADUATE SCHOOL OF NATURAL AND APPLIED SCIENCES
OF
MIDDLE EAST TECHNICAL UNIVERSITY

BY

NESRİN TÜFEKÇİ

IN PARTIAL FULFILLMENT OF THE REQUIREMENTS
FOR
THE DEGREE OF MASTER OF SCIENCE
IN
GEOLOGICAL ENGINEERING

SEPTEMBER 2006

Approval of the Graduate School of Natural and Applied Sciences

Prof. Dr. Canan ÖZGEN
Director

I certify that this thesis satisfies all the requirements as a thesis for the degree of Master of Science.

Prof. Dr. Vedat DOYURAN
Head of Department

This is to certify that we have read this thesis and that in our opinion it is fully adequate, in scope and quality, as a thesis and for the degree of Master of Science.

Prof. Dr. Nilgün GÜLEÇ	Assist. Prof. Dr. M. Lütfi SÜZEN
Co-Supervisor	Supervisor

Examining Committee Members

Prof. Dr. Nurkan KARAHANOĞLU	(METU, GEOE)	
Assist. Prof. Dr. M. Lütfi SÜZEN	(METU, GEOE)	
Prof. Dr. Nilgün GÜLEÇ	(METU, GEOE)	
Prof. Dr. Vedat TOPRAK	(METU, GEOE)	
Prof. Dr. Mahmut PARLAKTUNA	(METU, PETE)	

I hereby declare that all information in this document has been obtained and presented in accordance with academic rules and ethical conduct. I also declare that, as required by these rules and conduct, I have fully cited and referenced all material and results that are not original to this work.

Name, Last name : Nesrin TÜFEKÇİ

Signature :

ABSTRACT

GIS BASED GEOTHERMAL POTENTIAL ASSESSMENT
FOR
WESTERN ANATOLIA

TÜFEKÇİ, Nesrin

M.Sc., Department of Geological Engineering

Supervisor: Assist. Prof. Dr. M. Lütfi SÜZEN

Co-Supervisor: Prof. Dr. Nilgün GÜLEÇ

September 2006, 107 pages

This thesis aims to predict the probable undiscovered geothermal systems through investigation of spatial relation between geothermal occurrences and its surrounding geological phenomenon in Western Anatolia. In this context, four different public data, which are epicenter map, lineament map, Bouger gravity anomaly and magnetic anomaly maps, are utilized. In order to extract the necessary information for each map layer the raw public data is converted to a synthetic data which are directly used in the analysis. Synthetic data employed during the investigation process include Gutenberg-Richter *b-value* map, distance to lineaments map and distance to major grabens present in the area. Thus, these three layers including directly used magnetic anomaly maps are combined by means of Boolean logic model and Weights of Evidence method (WofE), which are multicriteria decision methods, in a Geographical Information System (GIS) environment. Boolean logic model is based on the simple logic of Boolean operators, while the WofE model depends on the Bayesian probability. Both of the methods use binary maps for their analysis. Thus, the binary map classification is the key point of the analysis. In this study three different binary map classification techniques are applied and thus three output maps were obtained for each of the method. The all resultant maps are evaluated within and among the methods by

means of success indices. The findings reveal that the WofE method is better predictor than the Boolean logic model and that the third binarization approach, which is named as optimization procedure in this study, is the best estimator of binary classes due to obtained success indices. Finally, three output maps of each method are combined and the favorable areas in terms of geothermal potential are produced. According to the final maps the potential sites appear to be Aydın, Denizli and Manisa, of which first two have been greatly explored and exploited since today and thus not surprisingly found as potential in the output maps, while Manisa when compared to first two is nearly virgin.

Keywords: Western Anatolia, Geothermal potential, GIS, Multicriteria Decision Analysis, Weights of Evidence method, Boolean logic model, Gutenberg-Richter relation, Binary classification

ÖZ

BATI ANADOLU'DAKİ JEOTERMAL POTANSİYELİNİN CBS TABANLI DEĞERLENDİRİLMESİ

TÜFEKÇİ, Nesrin

Yüksek Lisans, Jeoloji Mühendisliği Bölümü

Tez Yöneticisi: Yrd. Doç. Dr. M. Lütfi SÜZEN

Ortak Tez Yöneticisi: Prof. Dr. Nilgün GÜLEÇ

Eylül 2006, 107 sayfa

Bu tez, Batı Anadolu'daki keşfedilmemiş olası jeotermal sistemleri, jeotermal oluşumlar ile bunları çevreleyen jeolojik olguların arasındaki ilişkinin incelenmesi aracılığı ile tahmin etmeyi amaçlamaktadır. Bu kapsamda, depremlerin merkez üssü haritası, çizgisellik haritası, Bouger gravite haritası ve Manyetik şiddet haritası olmak üzere dört kamu verisi kullanılmıştır. Herbir harita katmanındaki gerekli bilgiyi çıkarabilmek için ham kamu verileri doğrudan doğruya analizlerde kullanılmak üzere sentetik verilere dönüştürülmüştür. Araştırma sürecinde kullanılan sentetik veriler Gutenberg-Richter *b-değeri* haritası ile çizgiselliklere ve bölgedeki ana grabenlere olan uzaklık haritalarını içermektedir. Böylelikle bu üç katman ile doğrudan doğruya kullanılan manyetik şiddet haritası, Coğrafi Bilgi Sistemleri (CBS) ortamında çok ölçütlü karar metodları olan Boolean mantık modeli ve Kanıtların Delili metodu aracılığı ile birleştirilmiştir. Boolean mantık modeli Boolean operatörlerinin basit mantığına dayanmaktadır. Kanıtların delili metodu ise Bayesian olasılığına bağlıdır. Her iki metod da analizlerinde ikili sınıflandırılmış harita kullanmaktadır. Bu nedenle, ikili harita sınıflaması analizlerin kilit noktasıdır. Bu çalışmada, üç farklı ikili harita sınıflama tekniği uygulanmış olup, her bir metod için üç farklı sonuç haritası elde edilmiştir. Tüm sonuç haritaları, başarı indeksi kullanılarak metoda bağlı olarak kendi içinde ve metodlar arasında değerlendirilmiştir. Bulgulara göre, daha yüksek başarı indeksleri verdikleri için

Kanıtların Delili Metodu Boolean mantık modeline göre daha iyi tahminlerde bulunmakta, ve bu çalışmada Eniyileme Prosedürü olarak adlandırılan üçüncü ikili sınıflama yaklaşımı da ikili sınıfları en iyi hesaplayan prosedür olarak belirlenmiştir. Son olarak herbir metod için elde edilen üç ayrı sonuç haritası birleştirilmiş ve jeotermal potansiyel haritaları elde edilmiştir. Aydın, Denizli ve Manisa son haritalara göre potansiyel olarak belirlenmiştir. Bunlardan ilk ikisi bugüne kadar büyük ölçüde araştırılmış ve işletilmiş olduğu için potansiyel sonuç haritalarında da uygun alanlar olarak ortaya çıkmaları beklenen bir durumdur, fakat, Manisa bu ikisiyle karşılaştırıldığında henüz bakirdir.

Keywords: Batı Anadolu, Jeotermal potansiyel, GIS, Çok Ölçütlü Karar Analizi, Delillerin Ağırlığı Metodu, Boolean Mantık Modeli, Gutenberg-Richter Bağıntısı, İkili Sınıflama

To My Parents

ACKNOWLEDGEMENTS

It is an honor for me to express my admiration and esteem to my supervisor Assist. Prof. Lütfi Süzen for his understanding, continuous support, unlimited trust, supervision and patience throughout the study. His intervention on crucial points rendered the thesis a worthwhile work.

I would like to express my gratitude to Prof. Dr. Nilgün Güleç for her constant support, guidance, trust and friendly attitude.

I am grateful to Assoc. Dr. Nuretdin Kaymaci, for his help, encouragement and comments which enabled me to visualize the related concepts in different aspects.

I gratefully acknowledge Ulaş Avşar, for his outstanding suggestions, tolerance, and guidance.

I would especially express my thanks to my dear friend Başak Şener, the angel of favour in the RS-GIS lab, for her motivation, encouragement, and contributions for the improvement of the document.

I would also like to thank to my dear friend Pınar Ertepınar Kaymakcı, for her support and any assistance.

I would also like to thank to Öykü and Gülsu for their unlimited help, support and patience.

I would also like to thank to my friends Çağıl Kolat, Deniz Gerçek and Sertaç Akar, for their motivational support and their help during the utilization of TNTmips software.

I would also like to acknowledge my room mates Gülderen, Nuray, Ayşe and Yasemin for their support, motivation and sympathy throughout the hard days.

Finally, I would like to express my special thanks to my family who always support and motivate me and who truly merit the dedication of this thesis.

TABLE OF CONTENTS

LIST OF TABLES

TABLE

LIST OF FIGURES

FIGURE

CHAPTER 1

INTRODUCTION

Geothermal energy is a proven resource for direct heat and power generation. In over 30 countries geothermal resources provide directly used heat capacity of 12,000 MW and electric power generation capacity of over 8,000 MW. It meets a significant portion of the electrical power demand in several developing countries.

Table 1.1 is a summary of the peak flow rates, capacity, annual energy utilization (in TJ/year and GWh/year) and capacity factor, wells drilled, professional person-years and investment by country, The capacity factor is an indication of the amount of use (i.e. a load factor of 1.00 would indicate that the system is used at a maximum the entire year). The countries with the largest utilization are China, Iceland and the United States, with Japan and Turkey moving into the top five, together accounting for over half (63.5%) of the world's geothermal energy utilization (Table 1.2). Austria, Canada, Germany, Sweden, Switzerland, and Turkey have produced the largest increase in the past 5 years by almost doubling their use in both capacity and energy use; the increase in the first five of these countries is due to geothermal heat pump installations, and that of Turkey is due mainly to the numerous new district heating systems brought online. (Lund and Freeston, 2001)

Turkey is an energy importing nation with more than half of energy requirements met by imported fuels. Furthermore, air pollution is becoming a significant environmental concern in the country. In this regard, geothermal energy and other renewable energy sources are becoming attractive solution for clean and sustainable energy future for Turkey. According to the geothermal energy potential, Turkey is placed among the richest countries in the world and holds the first place in Europe, it is also among the first seven countries in the world in the abundance of geothermal resources.

Table1.1: Summary of direct use data from individual countries (blanks indicate no value reported)(Lund and Freeston, 2001).

COUNTRY	FLOW kg/s	MWt	TJ/year	GWh/year	Capacity Factor	Well Drilled	Person-year	Funds 10E6$
Algeria	516	100,0	1586	441	0,50		27	
Argentina	2515	25,7	449	125	0,55	9	202	6
Armenia		1,0	15	4	0,48			
Australia	90	34,4	351	98	0,32	0	60	
Austria	210	255,3	1609	447	0,20	17		
Belgium	58	3,9	107	30	0,87			
Bulgaria	1690	107,2	1637	455	0,48		85	0,13
Canada		377,6	1023	284	0,09			
Caribbean Islands		0,1	1	0	0,62	0	0	0,3
Chile		0,4	7	2	0,55			
China	12677	2282,0	37908	10531	0,53			
Colombia	222	13,3	266	74	0,63		68	6,15
Croatia	927	113,9	555	154	0,15	1	91	1,9
Czech Republic		12,5	128	36	0,33		106	0,3
Denmark	44	7,4	75	21	0,32			
Egypt		1,0	15	4	0,58			
Finland		80,5	484	134	0,19			
France	2793	326,0	4895	1360	0,48	1		
Georgia	894	250,0	6307	1752	0,80			
Germany	371	397,0	1568	436	0,13	16		
Greece	258	57,1	385	107	0,21	75	200	
Guatemala		4,2	117	33	0,88	1	10	
Honduras	12	0,7	17	5	0,76		14	
Hungary	677	472,7	4086	1135	0,27	4	20	0,5
Iceland	7619	1469,0	20170	5603	0,44	241	250	90
India	316	80,0	2517	699	1,00	73	14	
Indonesia		2,3	43	12	0,59			
Israel	1672	63,3	1713	476	0,86			
Italy	1656	325,8	3774	1048	0,37	1	50	10
Japan		1167,0	26933	7482	0,73			
Jordan	574	153,3	1540	428	0,32			
Kenya		1,3	10	3	0,25			
Korea	1054	35,8	753	209	0,67	164	42	276
Lithuania	13	21,0	599	166	0,90	6	102	23,94
Macedonia	761	81,2	510	142	0,20	1	55	15
Mexico	4367	164,2	3919	1089	0,76	0	20	0
Nepal	25	1,1	22	6	0,66		8	0,007
Netherlands		10,8	57	16	0,17			
New Zealand	132	307,9	7081	1967	0,73	1	200	50
Norway		6,0	32	9	0,17			
Peru		2,4	49	14	0,65			
Philippines		1,0	25	7	0,79			
Poland	242	68,5	275	76	0,13		166	12
Portugal	49	5,5	35	10	0,20	7		
Romania	890	152,4	2871	797	0,60	14	181	24
Russia	1466	308,2	6144	1707	0,63	306	1043	
Serbia	827	80,0	2375	660	0,94	5	23	
Slovak Republic	623	132,3	2118	588	0,51	4	95	11,75
Slovenia	656	42,0	705	196	0,53	18	43	16,08
Sweden	455	377,0	4128	1147	0,35			
Switzerland	120	547,3	2386	663	0,14	4	58	230
Thailand		0,7	15	4	0,68			
Tunisia		23,1	201	56	0,28			
Turkey	700	820,0	15756	4377	0,61	15	120	25
United Kingdom	25	2,9	21	6	0,23			
United States	4550	3766,0	20302	5640	0,17	44	10	42
Venezuela		0,7	14	4	0,63			
Yemen		1,0	15	4	0,48			
Total	52746	15145,0	190699	52976	0,40	1028	3363	841

Table 1.2: World's top countries using geothermal in direct uses (Fridleiffson, 2001).

Country	Installed MWt	Production GWh/a
China	2282	10531
Japan	1167	7482
USA	3766	5640
Iceland	1469	5603
Turkey	820	4377
New Zeland	308	1967
Georgia	250	1752
Russia	308	1707
France	326	1360
Sweden	377	1147
Hungary	473	1135
Mexico	164	1089
Italy	326	1048
Romania	152	797
Switzerland	547	663

1.1 Purpose and Scope

Geothermal energy is clean, inexpensive, renewable, and can be utilized in various forms. Turkey is one of the geothermal-potential rich countries in the world. Most of the geothermal resources exist in Western Anatolia. Many high-temperature geothermal resources have been explored and a significant number have been under commercial exploitation. However, Turkey is one of the countries which are rich in its geothermal resources, but very low amount of this energy is being utilized. Nevertheless, active tectonics indicates that Turkey has a promising geothermal energy potential. Thus, in order to find out the undiscovered potential sites, the relation among geothermal system and its surroundings should be investigated well so that geothermal data will be interpreted and its relation to geographical and geological information will be obtained.

The purpose of this thesis is to investigate the relationship between the geothermal occurrences and seismicity, lineaments, gravity and magnetic anomaly by means of Geographical Information System so as to determine the probable undiscovered potential sites. Two different methods are used for this purpose, namely Boolean logic model and Weights of Evidence (WofE) method. The first has rather simple logic and its application areas have really wide range, while the latter is mostly used in mineral exploration purposes. The scope of the study on the other hand involves, the presentation of general information on the neotectonic and geological properties of the study area, the presentation of raw publicly available data and synthetic data, the presentation of two different methods with identical samples, the

determination of output potential maps by means of the methods and sensitivity analyses of the application of the methods, and a discussion about the obtained results.

1.2 Geographical Setting of the Study Area

The study area is located at the Western Turkey between the latitudes of 40° and 37,5° and longitudes of 26° and 30° at the eastern coasts of Aegean Sea. The study area includes 9 cities totally and partially. It includes southern parts of Çanakkale and Bursa as well as Balıkesir at North, Kütahya and Uşak at East, Denizli and Aydın are covered entirely at South, whereas entire İzmir at west and Manisa at the central part is also included. Figure 1.1 illustrates the location of the study area within Turkey and the enclosed cities are presented with the boundaries of the study area in the inset map.

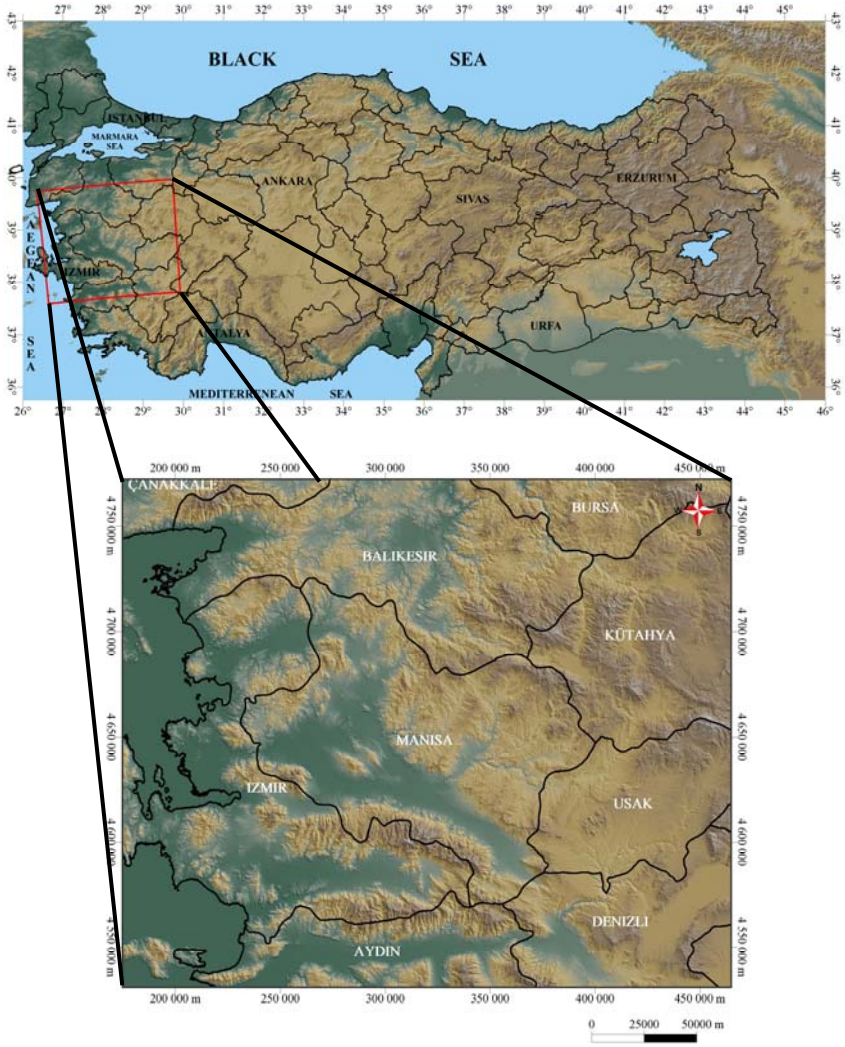

Figure 1.1: Geographical setting of the study area.

1.3 Geothermal Energy in Turkey

Energy demand of Turkey is increasing day by day because of Turkey's rapid development. Although Turkey has various energy resources, the available fossil energy resources do not meet the consumption needs (Akkuş et al, 2005). The reason is that Turkey has no big oil or gas reserves (Demirbaş, 2002), thus more than half of the energy requirement has been supplied by imports (Table 1.3). Oil has the biggest share in total primary energy consumption. The high level of dependence on imported petroleum and natural gas is the dominant factor in Turkey's pattern of energy consumption (Kaygusuz et al, 2004). In 2001, primary energy production and consumption has reached 26 and 74.7 million tons of oil equivalent (Mtoe) respectively. One of the alternative energy resources is the geothermal energy and Turkey, bearing suitable structures for the occurrence, has a significant potential (Table 1.3)(Akkuş et al, 2005).

Thus, Turkey has to evaluate its energy resources in the most economic manner (Akkuş et al, 2005) and has to adopt new long-term energy strategies to reduce the share of fossil fuels in primary energy consumption (Demirbaş, 2002). For this purpose, Turkey should consider the alternative energy resources in addition to fossil types (Akkuş et al, 2005).

Table 1.3: Primary energy production and consumption of Turkey during 1998-2001 (Mtoe) (Ministry of Energy and Natural Resources (MENR), 2002).

	Energy production				**Energy consumption**			
	1998	*1999*	*2000*	*2001*	*1998*	*1999*	*2000*	*2001*
Hard coal	1.678	2.729	1.769	1.255	8.160	11.286	8.149	6.972
Lignite	12.514	12.685	12.830	12.772	12.414	12.984	12.830	13.091
Oil	3.230	3.056	2.925	2.679	32.083	32.916	34.893	30.721
Natural gas	0.684	0.662	0.631	0.284	10.635	12.902	14.071	14.967
Total fossil	18.106	19.132	18.155	16.990	63.292	70.088	69.943	65.751
Hydropower	3.632	2.982	2.656	2.072	3.632	2.982	2.656	2.072
Geothermal	0.256	0.274	0.286	0.310	0.256	0.274	0.286	0.310
Solar	0.098	0.114	0.120	0.130	0.098	0.114	0.120	0.130
Wood	5.512	5.293	5.081	5.060	5.512	5.293	5.081	5.060
Waste&Dung	1.492	1.510	1.376	1.372	1.492	1.510	1.376	1.372
Total renewable	10.878	10.650	9.519	8.945	10.878	10.650	9.519	8.945

The present status and projections of the installed capacity of electricity in Turkey are given in Table 1.4. The table also shows the situation of geothermal power production as compared to the other sources of electricity as of 2000 and projection for 2005. Turkey is poor in fossil fuel reserves as shown in Table 1.4. Excluding lignite, the

coal, oil, and natural gas reserves in the country are quite limited and are far from meeting the domestic demand. On the other hand, Turkey is rich in renewables such as geothermal, solar, wind, biomass and hydropower (Kaygusuz et al, 2004).

Table 1.4: Installed capacity, production capacity and production values in electricity according to fuel types (Kaygusuz et al, 2004).

	2000			2005		
	Installed capacity	**Average production**	**Current production**	**Installed capacity**	**Average production**	**Current production**
	(MW)	(GWh)	(GWh)	(MW)	(GWh)	(GWh)
Hard coal	335	2178	3100	1545	10,678	10,500
Lignite	6669	43,649	36,600	8514	55,629	43,600
Fuel-oil	1287	7575	7260	1287	7575	6000
Diesel and LPG	335	1904	1600	1182	8316	6500
Natural gas	6411	44,155	44,140	13,929	90,938	78,400
Others	14	76	160	54	316	250
Multi fuel[a]	1153	6920	-	800	5200	-
Thermal	16,204	106,456	92,860	27,311	178,652	145,250
Hydraulic	11,115	39,652	31,100	14,780	52,831	46,600
Geothermal	15	90	80	40	277	235
Wind	48	157	145	643	1926	1800
Biogas-waste	10	30	15	10	30	15
Total	27,391	146,385	124,200	42,783	233,716	193,900

Turkey is a country with significant potential in geothermal energy. Geothermal energy in Turkey can be utilized, in selected locations, to cover a share of the electricity demand. Resource assessments have been made many times by the Mineral Research and Exploration Institute of Turkey (Demirbaş, 2002). On the other hand, geothermal electricity is an attractive option because of its relatively low installation and operational costs, and because it is more environmentally friendly than the conventional heat combustion and hydro power plants (Mertoğlu et al, 2003).

Tectonic and volcanic activity zones in Turkey, on which geothermal systems have been developed, are the principal zones for geothermal energy explorations. Young tectonic and volcanic activities occurred in Turkey, have played important role in the formation of geothermal systems (Akkuş et al, 2005).

The potential for geothermal development in Turkey is generally considered large in terms of moderate and low temperature resources (<150 ºC). Therefore, the resources are mostly suitable for direct use applications. (Hepbaşlı and Özgener, 2004).

In Turkey, around 600 geothermal prospects and 170 geothermal fields with a temperature range of 40–242º C have been discovered. The total proven geothermal electricity generation capacity is 200 MWe, while the direct use capacity is 2046 MWt.

This proven potential increases by 5% annually with new exploration and drilling activities. The estimated geothermal power and direct use potential are reported as 4500 MWe and 31,500 MWt, respectively (Hepbaşlı and Özgener, 2004).

Most of the development in Turkey is achieved in geothermal direct-use applications with 65,000 residences equivalence using geothermal heating (750 MWt) including district heating, thermal facilities and 635,000 m^2 geothermal greenhouse heating. Geothermal water is used in nearly 200 spas for balneological purposes (327 MWt). By summing up all these geothermal utilizations, the geothermal direct use installed capacity is 1077 MWt in Turkey in October 2004. The electricity generation has been increased from 90 GWh to 108 GWh in Kizildere geothermal power plant which is the single existing geothermal power plant of Turkey (Mertoğlu,2005).

The Western Anatolian Region, where high temperature geothermal sites have occurred along graben systems, is the most important region for geothermal energy potential (Figure 1.2) (Bozkurt, 2001).

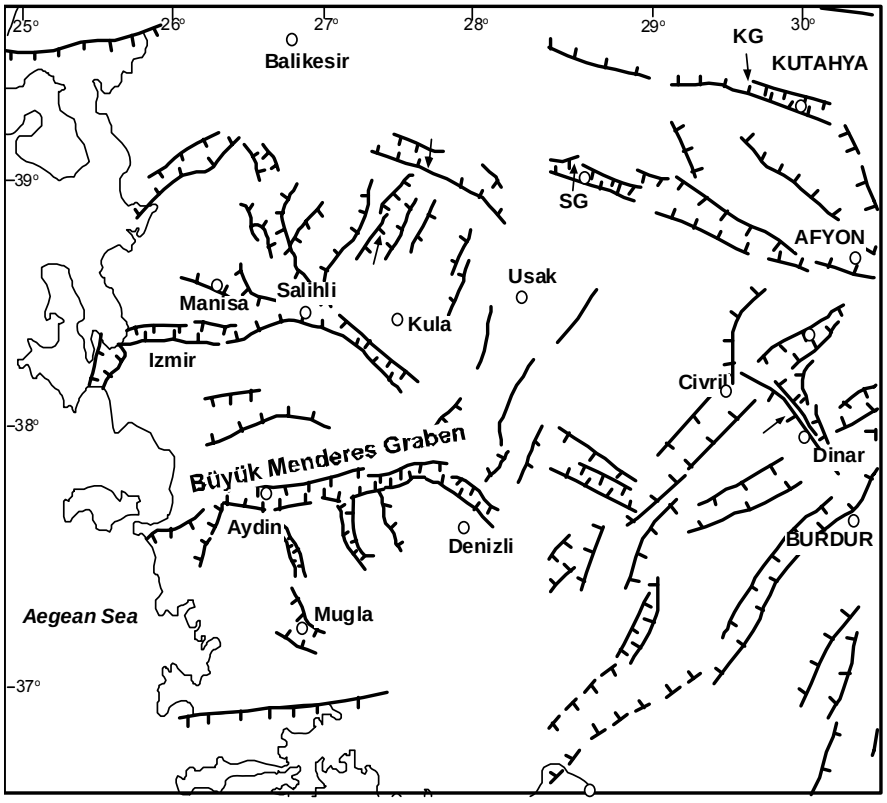

Figure 1.2: Major grabens in Western Anatolia (Modified from Bozkurt, 2001).

The Büyük Menderes fault zone is an important area for this potential (Figure 1.2). After the Denizli-Kızıldere geothermal field in the eastern part of Büyük Menderes graben, the Germencik-Ömerbeyli geothermal field was found in the western part of the same graben in 1982 and is the second highest enthalpy geothermal field in Turkey. According to geological studies, young tectonic activities, regional faults of high slip, young acidic volcanics (dacite-andesite), hydrothermal alterations, fumaroles, and many shallow hot water wells have been determined (Demirbaş, 2002).

According to the parameters affecting the occurrence of geothermal systems, geothermal energy resources are such that they have the opportunity of potential improvements, depending on depth of formation and developing technology (Akkuş et al, 2005).

At present, ten of the geothermal fields of Turkey, most of which are presented in Western Anatolia, are of high enthalpy and are appropriate for the geothermal electric energy generation by binary cycle or by flashing cycle. These fields are: 1) Denizli - Kızıldere Field, 2) Aydın - Germencik - Ömerbeyli Field, 3) Manisa - Salihli - Göbekli Field, 4) Çanakkale - Tuzla Field, 5) Aydın - Salavatlı Field, 6) Kütahya - Simav Field, 7) Manisa - Salihli - Caferbey Field, 8) Izmir - Seferihisar Field, 9) Izmir - Balçova Field, 10) Aydın - Yılmazköy Field (Mertoğlu, 2005).

CHAPTER 2

GEOLOGY

Turkey forms one of the most actively deforming regions in the world and has a long history of disastrous earthquakes. In the formation of the shape of Western Anatolia plate movements played an important role. Thus it is a structurally complex region displaying all the consequences of the effects of extensional, compressional and strike-slip tectonics.

2.1 Brief Information on Tectonic Evolution of Turkey

The continental collision between the African and Eurasian plates resulted in complex deformation of 'Mediterranean Earthquake Belt' within which Turkey is located (Figure 2.1) (Bozkurt, 2001). Both paleotectonic and neotectonic phases are responsible for the tectonic evolution of Turkey. The tectonic event which occurred about the Middle Miocene where African – Arabian and Eurasian plates converged and collided forming The Bitlis – Zagros Suture Zone marks the beginning of the neotectonic period (Mutlu and Güleç, 1998). Actually, the convergence between the African and Eurasian plates began in the Late Cretaceous (Şengör and Yılmaz, 1981; Dewey et al, 1989). On the other hand, the northward subduction of the southern branch of the Neotethys (known as the Bitlis Ocean), continued its evolution through late Middle Miocene (Şengör and Yılmaz, 1981, Dewey et al, 1986; Hempton, 1987; Robertson and Grasso, 1995) and then it was closed during the continent-continent collision across the Arabian Plate in the south and the Eurasian Plate in the north along the Bitlis–Zagros Suture zone (Şengör and Yılmaz, 1981; Dewey et al, 1986). The collision of the Arabian plate with Eurasia, the closure and the suturing of the Neotethyan Bitlis Ocean lasted between late Middle Miocene in the east and Late Pliocene-Quaternary in the west (Şengör and Yılmaz, 1981; Robertson and Grasso, 1995). During the time interval between late Middle Miocene and Early Pliocene, the eastern part of Anatolia has experienced an intracontinental convergence (McKenzie, 1969) which resulted in crustal thickening and uplift of the Anatolian–Iranian plateau (Bozkurt, 2001).

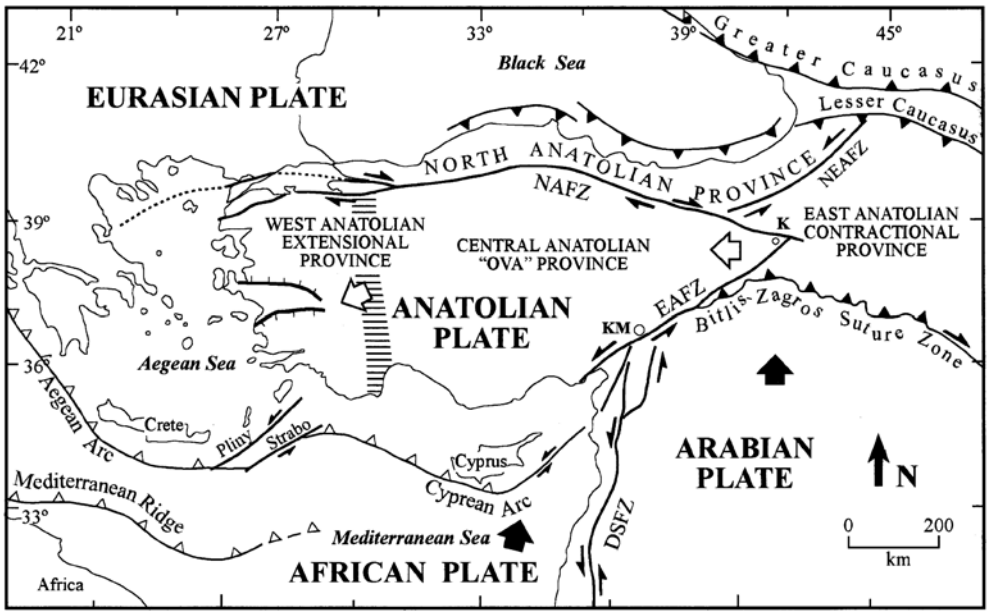

Figure 2.1: Simplified tectonic map of Turkey showing major neotectonic structures and neotectonic provinces (from Şengör et al 1985; Barka 1992). K = Karlıova, KM = Kahramanmaraş, DSFZ = Dead Sea Fault Zone, EAFZ = East Anatolian Fault Zone, NAFZ = North Anatolian Fault Zone, NEAFZ = Northeast Anatolian Fault Zone. Heavy lines with half arrows are strike-slip faults with arrows showing relative movement sense. Heavy lines with filled triangles show major fold and thrust belt: small triangles indicate direction of vergence. Heavy lines with open triangles indicate an active subduction zone, its polarity indicated by the tip of small triangles. The heavy lines with hachures show normal faults: hachures indicate down-thrown side. Bold filled arrows indicate relative movement direction of African and Arabian plates; open arrows, relative motion of Anatolian Plate. The hatched area shows the transition zone between the western Anatolian extensional province and the central Anatolian '*ova*' province from Şengör et al 1985 (The figure and explanations are taken from Bozkurt, 2001).

The neotectonic period, on the other hand, is related to the post-collisional convergence between the respective plates (Şengör et al, 1985) and is governed by three major structures (Figure 2.1) (Bozkurt, 2001):

1. The dextral North Anatolian Fault Zone;
2. The sinistral East Anatolian Fault Zone;
3. The Aegean–Cyprean Arc, a convergent plate boundary where the African Plate to the south is subducting beneath the Anatolian Plate to the north;

The North Anatolian Fault Zone, which is an intracontinental transform fault resulted due to compressional – extensional tectonic regime (tectonic escape/extrusion tectonics) by the Early Pliocene (Bozkurt, 2001).

The NAFZ and EAFZ are narrow zones consisting of small faults. Starting from the Karlıova junction in the east, the EAFZ extends southwestward and connects to the Dead Sea Fault (Figure 2.1) (Arpat and Şaroğlu, 1972, Arpat and Şaroğlu, 1975), whereas the NAFZ extends westwards and, splits into several branches characterized by dominant normal faulting component along with strike–slip component (Canıtez and Üçer, 1967; Mc Kenzie, 1972; Dewey and Şengör, 1979).

The subduction along the Aegean and Cyprean arcs has occurred due to the convergence between the African and Anatolian plates in the Eastern Mediterranean (McKenzie, 1978; Papazachos and Comninakis, 1971; Fytikas et al, 1984; Meulenkamp et al, 1988; Spakman et al, 1988; Mart and Woodside,1994). The African Plate is descending beneath the Anatolian Plate in a N–NE direction. The Aegean arc system plays an important role in the geodynamical evolution of the Aegean region (Bozkurt, 2001). The migration of the trench system to south–southwest resulted in extensional regime in the overriding Aegean plate that subsequently led to the formation of the present-day Aegean Sea (Le Pichon and Angelier, 1981).

Four major neotectonic provinces are recognized in Turkey which are bounded by previously defined three structures, namely NAFZ, EAFZ, and Aegean–Cyprean Arc (Figure 2.1) (Şengör et al., 1985):

1. The East Anatolian contractional province, located east of Karlıova junction where the NAFZ and EAFZ meet, and characterized by N–S shortening due to the still continuing convergence along the BZSZ;
2. The North Turkish province, situated north of the NAF and characterized by limited E–W shortening;
3. The Central Anatolian ‘ova’ province, characterized by NE–SW shortening and NW–SE extension, and by the presence of large, terrestrial sediment filled basins_‘ovas’.
4. The West Anatolian extensional province, characterized by N–S extension resulted from the west southwestward escape of the Anatolian plate along the NAF and EAF;

Here, due to being the study area only the formation of West Anatolian extensional province will be emphasized and its major structural elements will be introduced.

2.2 Western Anatolia Extensional Province and its Structural Elements

Western Anatolia forms one of the most seismically active as well as rapidly extending regions in the world (Eyidoğan and Jackson, 1985; Ambraseys, 1988; Eyidoğan, 1988; Jackson and McKenzie, 1988; Taymaz et al, 1991; Jackson et al, 1992; Taymaz, 1993; Reilinger et al, 1997; Ambraseys and Jackson, 1998; Altunel, 1998, Altunel, 1999 and references therein). The active deformation of western Turkey is governed by interaction of three major plates, namely, Eurasia, Arabia and Africa (Sarı and Şalk, 2005). Most of the deformation in the region have originated from subduction and collision-related processes (Şengör et al., 1985). It is a part of the 'Aegean Extensional Province', which is an extensional region covering parts of Greece, Macedonia, Bulgaria and Albania (Figure 2.1) (Bozkurt, 2001). The cause and origin of crustal extension in the Aegean has been discussed for a long time. Finally four different models explaining the extension of the region have been proposed:

1. *Tectonic escape model:* the westward movement of the Anatolian block along its boundary structures (Dewey and Şengör, 1979; Şengör, 1979, Şengör et al 1985, Şengör, 1987; Görür et al, 1995).
2. *Back-arc spreading model:* back-arc extension caused by the south–southwestward movement of the Aegean Trench system (McKenzie, 1978; Le Pichon and Angelier, 1979; Meulenkamp et al, 1988)
3. *Orogenic collapse model:* the extension is caused by the spreading and thinning of over-thickened crust after the latest Palaeocene collision across Neotethys during the latest Oligocene–Early Miocene (Seyitoğlu and Scott, 1991, Seyitoğlu and Scott, 1992)
4. *Episodic model:* a two-stage graben model that involves westward escape of the Anatolian block following orogenic collapse (Koçyiğit et al, 1999).

Due to the extension of the region Western Anatolia is characterized by east-west trending horsts and deep sediment filled grabens. Approximately E–W trending grabens (e.g. Edremit, Bakırçay, Kütahya, Simav, Gediz, Küçük Menderes, Büyük Menderes, and Gökova grabens) and their basin-bounding active normal faults are the most dominant neotectonic features of Western Turkey (Figure 2.2) (Dumont et al, 1979; Duvarcı, 2001 and references therein). Other, less dominant, structural elements of Western Turkey are the NNE-trending basins and their horsts (e.g. Gördes, Demirci, Selendi, and Uşak-Güre basins; Figure 2.2) (Yılmaz et al., 2000; Şengör, 1987; Nebert, 1960; Bozkuş, 1996 and references therein). The most continuous topographic step structures in western Turkey are oriented approximately E–W and appear to be the

footwalls of major active normal faults. These structures are seen in satellite images, topographic maps and in the field (Yılmaz et al., 2000). Considering the total displacements and extent of strike, the Gediz and Büyük Menderes fault zones are the most important ones (Sarı and Şalk, 2005)

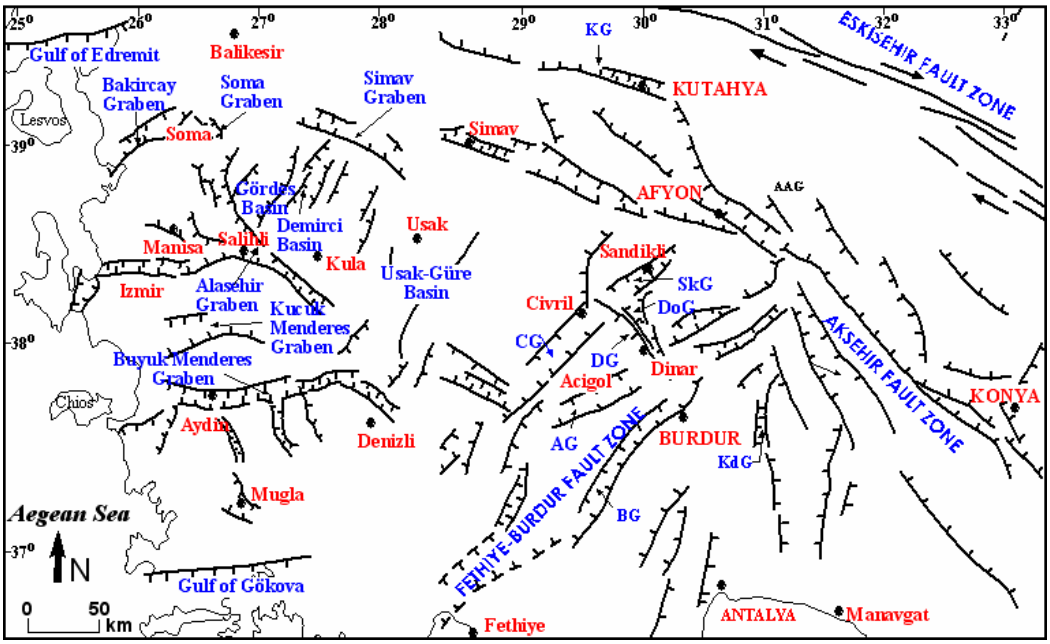

Figure 2.2: Simplifed map showing major structural elements of Western Anatolia. Heavy lines with hachures show normal fault: hachures indicate down-thrown side, other heavy lines show strike-slip faults and the arrows along them show the relative direction of movement (from Bozkurt, 2001).

2.3 Geology of Western Anatolia

The post-orogenic extension is responsible for the geological situation of Western Anatolia, where coexisting lacustrine sediments and coeval volcanic rocks unconformably overly metamorphic rocks, ophiolitic nappes and flysch sediments of the basement. From NW to SE Anatolia, the collisional Izmir– Ankara Zone, the Menderes Massif, and the tectonic units of the western Taurids are observed, which are covered by Cenozoic sedimentary and volcanic rock successions (Möller et al, 2004 and references therein). However, a substantial portion of the study area is composed of Menderes Massif. Thus, in this chapter only the characteristics of Menderes Massif and volcanic rock successions will be introduced.

2.3.1 Menderes Massif

The Menderes Massif is one of the largest metamorphic massifs in Turkey, with a length of about 200 km N–S between the Simav and Gökova grabens, and about 150 km E–W between Denizli and Turgutlu in western Anatolia (Ketin, 1983). It is a structure displaying evidence of Alpine tectonic and magmatic involvement (Blumental, 1951; Başarır, 1970; Izdar, 1971; Dürr et al., 1978; Öztürk and Koçyiğit, 1983).

The Menderes Massif is the oldest rock assemblage of the Anatolian Continent and is composed of high-grade gneisses and schists which are overlain by low-grade schist, marble, phyllite, metaplutonites and metasedimentary rocks associated with recrystallised limestones. Menderes Massif rocks are unconformably overlain by conglomerate, sandstone and limestone intercalations which are known as Mesozoic Kırkbudak formation. These rocks are covered by Cenozoic Toklargözü formation that is composed of coarse clastic rocks and the Eynal formation, which are the uppermost of the Neogene sedimentary rocks in the study area (Gemici and Tarcan, 2002). Neogene terrestrial sediments consist of interbedded conglomerate, sandstone, claystone, siltstone, marl, and limestone and they are observed in the northern and southern parts of the Gediz Graben (Tarcan, 2004). These sediments are mega-sequences of clastic, carbonate- and organic-rich sedimentary rocks deposited as alluvial fans, fluvial carbonate mudflats and ephemeral shallow freshwater carbonate lake deposits (Möller, et al, 2004).

The proposed ages of the Menderes Massif metamorphic rocks and the granodiorite are Precambrian to Paleocene (Dora et al, 1997) and Early Miocene in age (Erdoğan and Güngor, 1992), respectively.

The permeability within the Menderes Massif rocks is highly variable. The carbonates (marbles and dolomitic marbles) of the Menderes Massif rocks are highly fractured and karstified and act as an aquifer for both cold ground waters and thermomineral waters depending on the location. Fractured parts of granodiorite, gneiss and quartz-schist units of the Menderes Massif act as aquifers for low-salinity cold ground waters, hot waters and for thermomineral waters. These rocks form the reservoir for waters to be heated at depth and fractures and faults provide a means for circulation and rise of the heated waters to the surface (Gemici and Tarcan, 2002). Schists and phyllites have relatively low permeability. The Neogene terrestrial sediments, which are made up of alluvial fan deposits including poorly cemented clayey levels, have very low permeability as a whole and may locally act as cap rocks for the geothermal systems. Clayey levels of the Neogene sediments occur as impermeable barrier rocks. Sandy to gravely and limestone levels of this Neogene unit contain minor aquifers (Tarcan et al, 2005).

2.3.2 Volcanic Rock Characteristics

The differential plate motions are responsible for the young, east and west Anatolian volcanic activities (Vengosh, 2002 and references therein). Widespread magmatism developed in the hangingwall plate, along the collisional margin, is characterized by the presence of products of variable petrogenetic affinity (Innocenti et al, 2005). The magmatic activity in the region is characterized by volcanic/plutonic and calc-alkaline/alkaline associations. Compressional phase is represented by calc-alkaline products whereas extensional phase is represented by dominantly alkaline products (Savasçın and Güleç, 1990).

The Aegean–Western Anatolia Volcanic belt extends southward from the Rhodope Massif–Thrace through the Central Aegean Sea and Western Anatolia to the South Aegean Active Volcanic Arc, with an age varying from Upper Eocene to Present (Fytikas et al., 1984). The magmatism develops in three distinct phases of activity.

The oldest phase began in the Late Eocene and ended in the Middle Miocene which is represented by volcanic and plutonic rocks. The magmatic products show an orogenic character with a petrogenetic character ranging from calc-alkaline to dominant high-K calc-alkaline. Andesites and dacites are dominant; however, the basalts and basaltic andesites are scarcely represented (Innocenti et al, 2005).

The second volcanic phase is limited to the Late Miocene–Early Pliocene. It is characterized by the eruption of alkaline rocks with sodic or potassic character. The outcrops of these rocks are observed as patches in Western Anatolia and the Aegean Sea, e.g. Ezine, Urla, Foça, Bodrum, Patmos and Central Aegean Sea. These products generally display a within plate character, although sometimes a slight subduction-related geochemical signature can be noted (Robert et al., 1992; Pe-Piper et al., 1995; Aldanmaz et al., 2000; Yilmaz et al., 2001).

During the third phase, in the Pliocene and Quaternary, two distinct magmatic associations developed. In the Southern Aegean area, an active calc-alkaline volcanic arc (South Aegean Volcanic Arc) evolved as a result of the subduction of the African plate under the Aegean plate whereas in Western Anatolia (Kula region), Na-alkali basalts were erupted (Innocenti et al, 2005).

The volcanic arc and the alkaline basaltic rocks are located south and north of the Actic–Cycladic– Menderes crystalline massif, respectively (Ring et al., 1999). The crystalline massif was the site of an intrusive and effusive acidic magmatic activity of crustal origin during the Middle Miocene–Early Pliocene (Innocenti et al., 1982; Altherr et al., 1982; Delaloye and Bingöl, 2000).

CHAPTER 3

METHODOLOGY

This chapter introduces the methods used in combining maps for geothermal exploration which are integrated with GIS (Figure 3.1). Being the simplest and frequently used application, Boolean logic model is demonstrated first. Next, the Weights of Evidence Method (WofE) which is based on Bayesian probability model is illustrated. In the next chapter the raw public data consisting of geothermal and epicenter databases, lineaments, Bouger gravity and magnetic anomaly maps, is explored to discover the nature of the data and the interrelations among them. In accordance with the findings, the public data is converted to a special form appropriate for utilization of the methods in GIS environment. This form is called synthetic data. Next, in chapter 5 the synthetic data layers are binarized and overlaid by means of two methods presented in this chapter. Then through the accuracy assessment the output maps of both of the methods are compared to find out how they are consistent with each other and how well each method can predict the potential geothermal sites. After, being the most effective factor in the analysis, the precision of the binarization techniques are investigated in sensitivity analysis part. Last, by evaluating the different binary classification techniques and overlay methods the result maps are obtained and discussed in chapter 6.

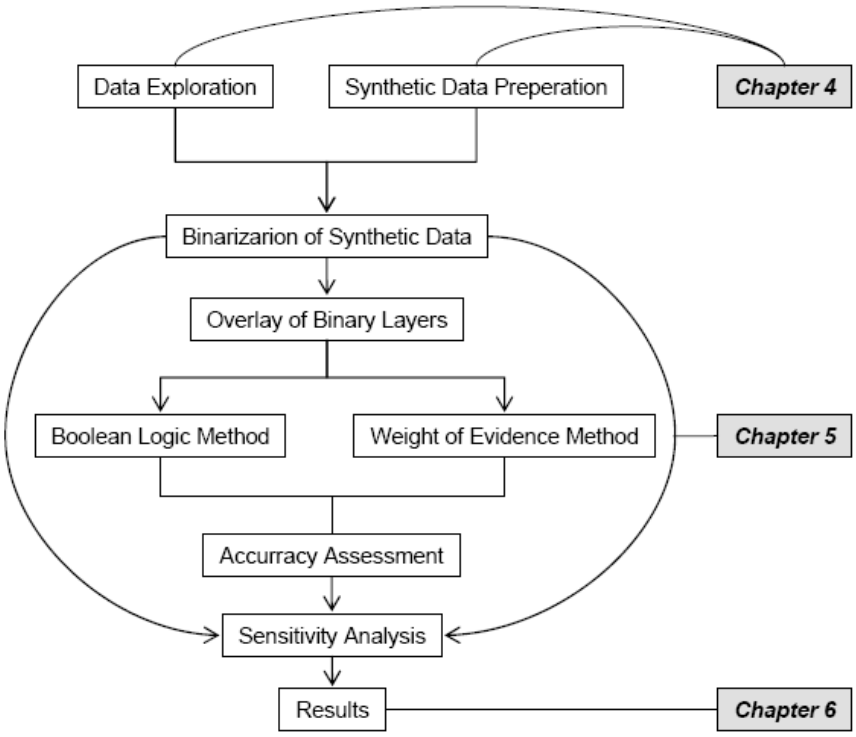

Figure 3.1: The scheme of the followed methodology.

3.1 Boolean Logic Model

In general, logic studies and analyzes the methods of reasoning or argumentation (Whitesitt, 1962). Boolean logic is a kind of algebra, which is a unique, self – contained mathematical system concerned with logical relationships (Adelfio & Nolan, 1964). Similar to mathematical logic it uses logical connectives such as: and, or, not (Lytel, 1963). In this way, Boolean algebra enables one to examine the consequences of several entities by putting them together. However, in Boolean algebra the entities should have some kind of descriptive logical value, like true or false; open, closed; one, zero; etc. This brings out the need of binary variable. In this subchapter, the definition of binary variable and Boolean operators is introduced.

3.1.1 Binary Variable

Boolean algebra is essentially a binary system, because in this algebra something either exists or does not exist. The binary variable assumes two and only two values. It corresponds directly to the “bit” of information theory. The term “bits” means the binary digits and it is a combination of the first two letter of *bi*nary and the last two

terms of digi*ts*. The term “binary”, on the other hand is used to indicate that there are two possible states. The two values of binary variable are commonly represented by as true, false; one, zero; etc (Lytel, 1963; Adelfio & Nolan, 1964).

In GIS applications, binary maps are usually prepared to indicate favorable and unfavorable areas for the particular analysis. The binary maps are generally in raster format, having only two values, 1 and 0. Thus, the pixels having value of “1” are the favorable areas, while the pixels having value of “0” are the unfavorable ones. Suppose for example there is a criterion that the area within 10 km distance of a lineament is accepted as favorable in geothermal occurrence point of view. Then using distance to lineament map, the pixel values equal to or smaller than 10 km will be assigned “1”, while the remaining pixels will have value of “0”. In this way distance to lineament map is recoded so that this binary map shows the favorable areas as “1” and the unfavorable ones as “0”. Figure 3.2a,b shows two imaginary examples of binary maps. Figure 3.2a represents binarized distance to lineament map and Figure 3.2b represents binarized magnetic anomaly map, where negative anomalies are assumed to be favorable.

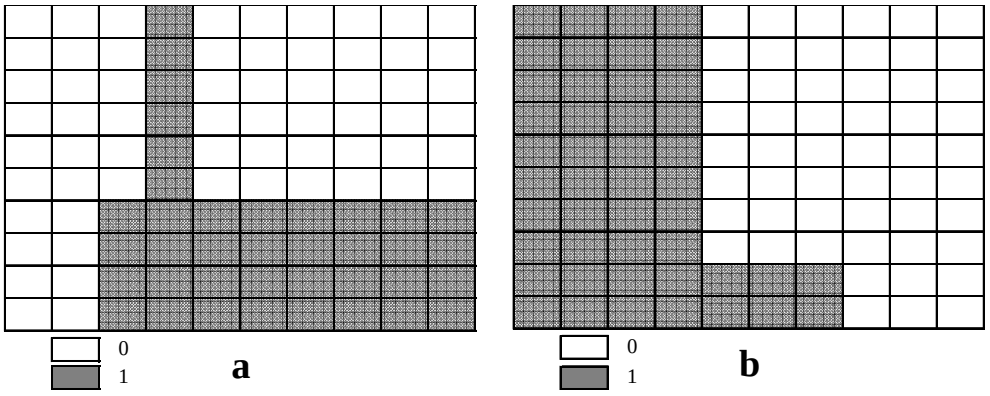

Figure 3.2: a) Binary distance to lineament map; **b)** Binary magnetic anomaly map.

Both maps contain 100 equal sized rectangles, where each rectangle stands for a pixel in the map. The dark pixels have value of 1, favorable areas, while the white ones have value of 0, unfavorable areas.

3.1.2 Boolean Operators

Boolean logic symbolically represents relationships between entities. It lets one to organize concepts together in sets. These sets are controlled by use of 3 primary Boolean logic statements OR, AND, and NOT. Generally, AND narrows the search, OR

broadens the search, and NOT is used to exclude some concepts. The detailed explanations of these statements are as following:

"AND": the AND statement combines variables by logic multiplication. It requires that the all requested concepts are present in the retrieved records. For example, A·B and A·B·C are AND statements. An AND statement such as A·B means both A and B. However, the word both is usually omitted and the statement is simply read A and B. In addition the symbol of multiplication is omitted and the combination is shown as AB, ABC, etc (Adelfio & Nolan, 1964).

"OR": the OR statement is formed by combining variables by logic addition. It requires that any of the requested concepts are present in the retrieved records. For example, A+B and A+B+C are OR statements. A+B is read as either A or B or both. However it is more convenient to read the statement as A or B. There is a special type of OR statement which is known as an exclusive OR statement and is read as A or B but not both. The most common way of indicating XOR statement is a circle around the OR sign as $A \oplus B$ (Adelfio & Nolan, 1964).

"NOT": the NOT statement is exclusion of unwanted variable from the combination of the variables. It is used when a concept is excluded from the search. The NOT operator requires that whatever comes after the NOT operator is not present in the retrieved records. For example, A – B represents the elements within A but not in B. If A and B has some intersecting elements, these elements should be eliminated from elements of A. The NOT operator is also shown as $A\overline{B}$, meaning A but not B.

3.1.3 Operation of Boolean Statements on Binary Variable

The results of Boolean operation to binary variable are shown in Table 3.1. According to the table it can be said that if and only if both of the entities are true then the result of AND operation is true. In OR operation however, if only one of the entities is true then the result is true. The result of NOT operation on the other hand, is true when the entity is false and vice versa.

Table 3.1: Boolean operations on Binary variable (Modified from Lytel, 1963; Hoernes&Heilweil, 1964).

AND		OR		NOT	
0 · 0 = 0	1 · 0 = 0	0 + 0 = 0	1 + 0 = 1	$\bar{1} = 0$	$\bar{0} = 1$
0 · 1 = 0	1 · 1 = 1	0 + 1 = 1	1 + 1 = 1		
The intersection of the terms (multiplication)		Either of the terms or both are present (addition)		The first term but not the second is present (subtraction)	

When these operations are applied to binary maps, the AND operation acts as intersection of favorable areas, OR acts as union of favorable areas, XOR as complementary of intersection of favorable areas. The NOT operation can be used when the favorable area of one of the maps but not the other is necessary to be displayed.

All of the four cases are illustrated using the binary maps in Figure 3.2a and b. The result map of Boolean operation AND retrieves the common part of favorable areas of both maps. Thus, in the result map of AND operation the pixels with value of 1 are those that both distance to lineament and magnetic anomaly maps are favorable, and the remaining pixels with value 0 include unfavorable areas and those that are either favorable in distance to lineament or magnetic anomaly maps but not the both (Figure 3.3c). The result map of Boolean operation OR retrieves the any of favorable areas of both maps. Thus, in the result map of OR operation the pixels with value of 1 are those that either distance to lineament or magnetic anomaly maps or both are favorable, and the remaining pixels with value 0 include unfavorable areas of both maps (Figure 3.3d).

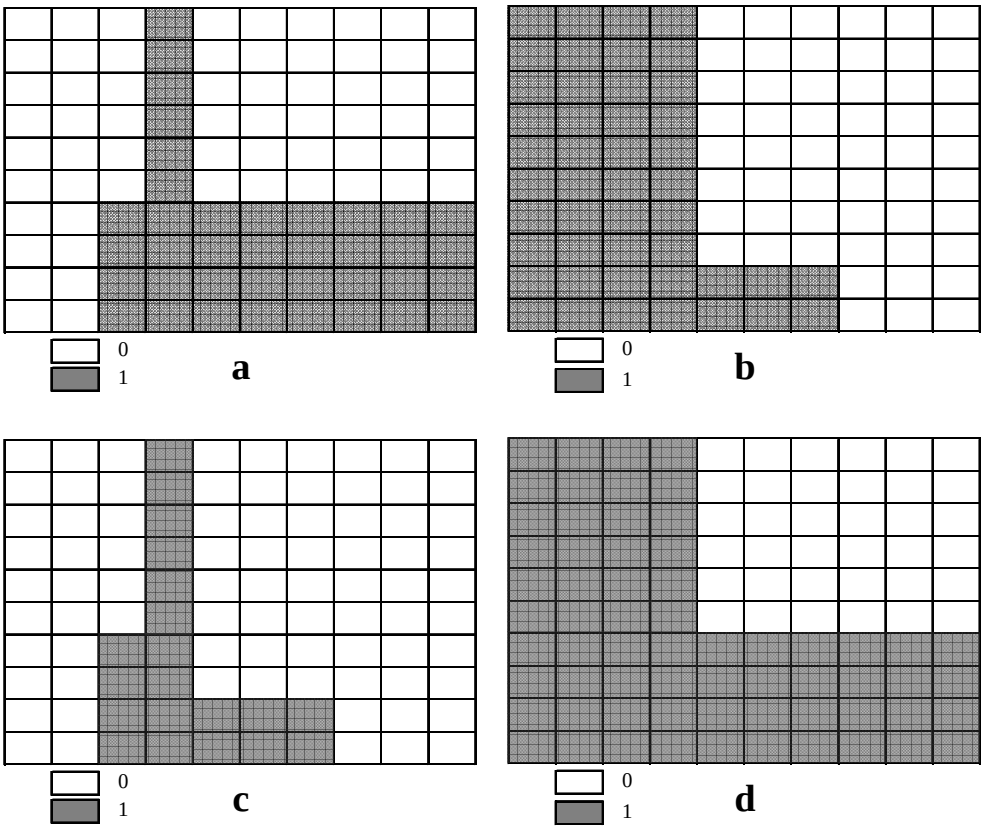

Figure 3.3: a) Binary distance to lineament map; **b)** Binary magnetic anomaly map; **c**) Result of AND operation; **d)** Result of OR operation.

The result map of Boolean operation XOR retrieves the any of favorable areas but not the common part of both maps. Thus, in the result map of XOR operation the pixels with value of 1 are those that either distance to lineament or magnetic anomaly maps but not both are favorable, and the remaining pixels with value 0 include unfavorable and favorable areas of both maps (Figure 3.4c). The result map of Boolean operation NOT is the result of the statement: “Distance to lineament but NOT magnetic anomaly”. It retrieves the favorable areas only in distance to lineament map. The favorable areas of magnetic anomaly and the common favorable areas are excluded. Thus, in the result map of NOT operation the pixels with value of 1 are those that belong only to favorable areas of distance to lineament map, and the remaining pixels with value 0 include unfavorable areas and excluded parts (Figure 3.4d).

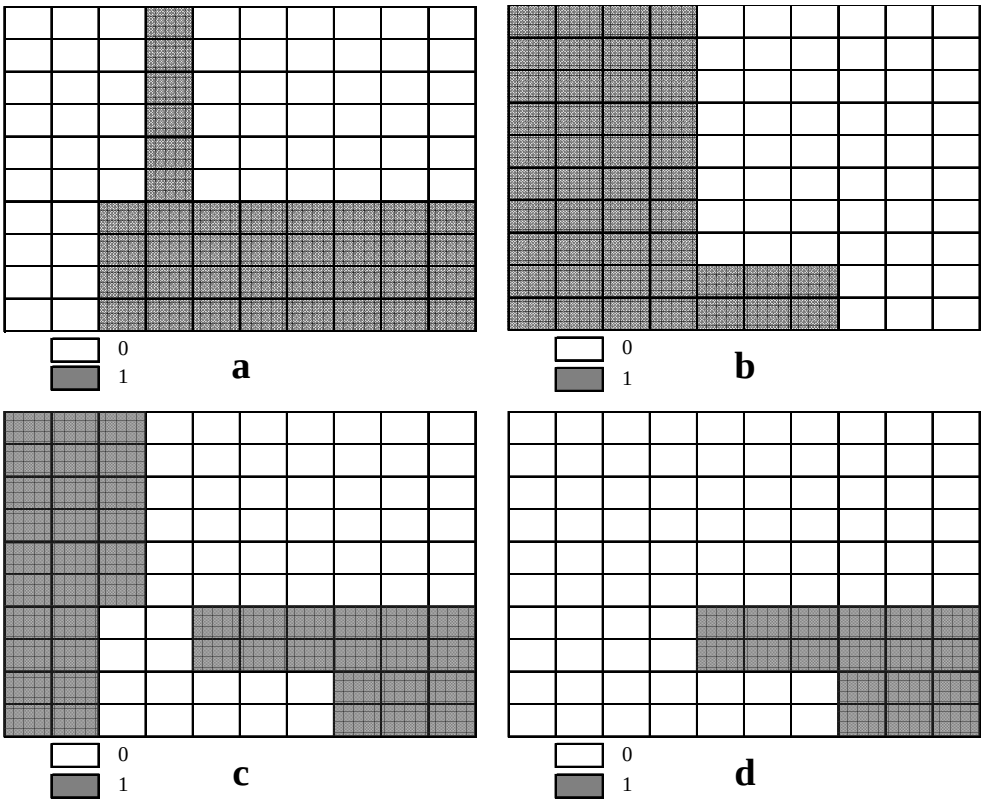

Figure 3.4: a) Binary distance to lineament map; **b)** Binary magnetic anomaly map; **c)** Result of XOR operation; **d)** Result of NOT operation.

3.2 Weights of Evidence Method (WofE)

"Weights of Evidence" is a method depending on Bayesian probability model with assumption of conditional independence. The method is generally used by geologists to investigate probable favorable areas for geologic phenomena (Bonham-Carter 1996). Its application includes combination of spatial data set. Spatial data integration for any geologic occurrence assessment is greatly facilitated using a GIS in association with various softwares. Advanced GIS packages may provide breakthroughs which will bridge the gap between the traditional manual overlay approach and mathematical methods using multivariate statistics and image analysis (Bonham-Carter et.al, 1988).

The WofE method was originally developed for a non-spatial application in medical diagnosis. In this application, the evidence consisted of a set of symptoms, and the hypothesis was "this patient has disease x." For each symptom, a pair of weights was calculated, one for presence of the symptom and one for absence of the symptom. The magnitude of the weights depended on the measured association between the symptom and the occurrence of disease in a large group of patients. The weights could then be used to estimate the probability that a new patient would get the disease, based on the presence or absence of symptoms (Raines et al, 2000).

In geological applications the method uses the statistical association between a training points theme, such as, a theme showing site occurrences and evidential themes, showing map types such as geochemistry, or geophysical measurements to determine the weights. Then using the weights assigned to evidential themes, the response theme which is the final product is obtained (Raines et al, 2000). The final product is a map of posterior probabilities of occurrence of the discrete event within a small unit cell (Agterberg and Cheng, 2002). Namely, response theme is an output map that combines the weights of predictor variables from the evidential themes to express the probability that a unit cell will contain a training point. Evidential themes may have categorical values (e.g., the classes on geology or soil maps) or ordered values (e.g., geochemical concentrations or distance to linear and other spatial objects) (Raines et.al, 2000).

Weight values are quite easy to interpret. A positive weight for a particular evidential-theme value indicates that more training points occur on that theme than would occur due to chance, whereas the converse is true for negative weights. A weight of zero indicates that the training points are spatially uncorrelated to the theme. The range-in-weight values for a particular evidential theme, known as the contrast, gives an overall measure of how important the theme is in the model.

Bonham-Carter (1996) described the way in which the quantitative relationships between the datasets, representing the deposit recognition criteria and known mineral occurrences are analyzed using a statistical method that uses Bayes' Rule.

In this study the basis of WofE method, which are Bayes' Rule of probability, odds formulation and conditional independence will be introduced using the same imaginary examples in subchapter 2.1.

3.2.1 Bayesian Method

Bayes' theorem is a result in probability theory, which relates the conditional and marginal probability distributions of random variables. The probability of an event *A* that is conditional on another event *B* is generally different from the probability of *B* that is conditional on *A*. However, there is a definite relationship between the two, and Bayes' theorem is the statement of that relationship. The Bayesian approach to the problem of combining datasets uses a probability framework. One of the main concepts in the Bayesian approach is the idea of prior and posterior probability (Bonham-Carter, 1996).

A *prior probability* is the probability of one event, regardless of the other event, interpreted as a description of what is known about a variable in the absence of some evidence. The *posterior probability* on the other hand is the conditional probability of the variable taking the evidence into account (Bonham-Carter, 1996).

To clarify the idea the example considers the problem of finding a geothermal occurrence in a region covering 100 km^2 area. Suppose 15 geothermal occurrences are known within the region, and for the purpose of the analysis, each occurrence is assumed to occupy a small unit area or a pixel having 1 km^2 area. According to this assumption the total area occupied is N{T}=100 pixels and geothermal occurrences occupy N{G}=15 pixels (Figure 3.5a). In this case the prior probability of an occurrence will be the proportion of geothermal occurrence pixels to the total number of pixels:

$$P(G) = \frac{N(G_{pix})}{N(Total_{pix})} = \frac{15}{100} = 0.15 \qquad (2.1)$$

This result indicates the probability that any randomly chosen 1 km^2 cell contains a known geothermal occurrence is 0.15. However, suppose that a binary indicator map, such as a magnetic anomaly map, where areas having negative anomalies are represented with black having cell value of 1 and indicating favorable areas for geothermal occurrence covers a part of same area of interest (Figure 3.5b), and that 12 out of 15 occurrence are present where there is negative magnetic anomaly.

Obviously, as negative magnetic anomaly is present the probability of finding a geothermal occurrence is much greater than 0.15; conversely the probability is less than 0.15 if the same anomaly is absent.

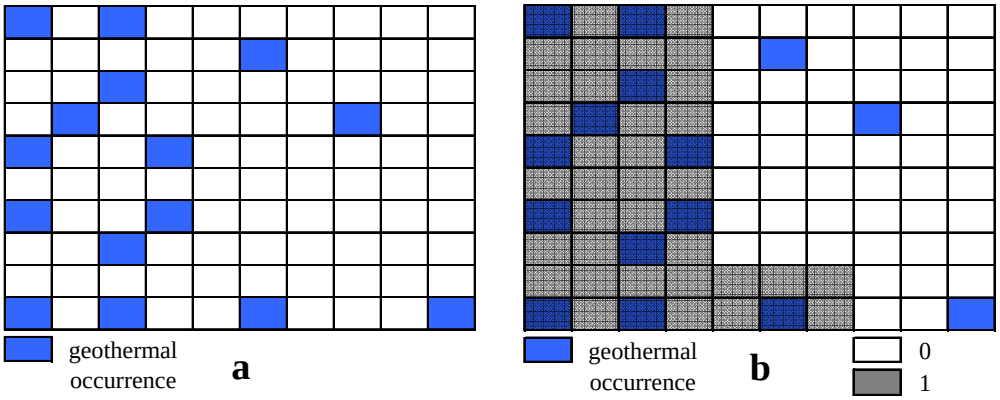

Figure 3.5: **a)** Geothermal occurrence location map; **b)** Binary negative magnetic anomaly and location of the occurrences.

The probability for finding a geothermal occurrence given the presence of the evidence can be expressed by conditional probability:

$$P\{G \mid M\} = \frac{P\{G \cap M\}}{P\{M\}} \tag{2.2}$$

where P{G | M} is the conditional probability of a geothermal occurrence given the presence of a binary pattern of negative magnetic anomaly. According to equation above the probability of existence of a geothermal occurrence given that there is a negative magnetic anomaly is:

$$P\{G \mid M\} = \frac{N\{G \cap M\}}{N\{M\}} = \frac{12}{46} = 0.26$$

where N{G∩M} is the number of pixels where there is both geothermal occurrence and negative magnetic anomaly and similarly N{M} is the total area of pixels occupied by negative magnetic anomaly.

This conditional probability is the posterior probability of geothermal occurrence (0.26), which is about 1.7 times greater than its prior probability (0.15).

In order to obtain an expression relating the posterior probability of geothermal occurrence in terms of the prior probability and the multiplication factor, Bonham-Carter (1996) defines the conditional probability of being on binary map, given the presence of occurrence. According to definition the obtained equation is:

$$P\{M \mid G\} = \frac{P\{M \cap G\}}{P\{G\}} \tag{2.3}$$

which for the present case has the value of 12 / 15 = 0.8. Because P{G∩M} is the same as P{M∩G}, equations (2.2) and (2.3) can be combined to solve P{G | M}, satisfying the relationship:

$$P\{G \mid M\} = P\{G\}\frac{P\{M \mid G\}}{P\{M\}} \tag{2.4}$$

This states that the conditional (posterior) probability of an event, given the presence of a binary pattern equals the prior probability of the event multiplied by the factor P{M | G} / P{M}(Bonham-Carter,1996). According to the example present the numerator of this factor is 0.8 and the denominator is 46 / 100 = 0.46, so the factor is 0.8 / 0.46 = 1.74. Thus, given the presence of negative magnetic anomaly, the posterior probability of a geothermal occurrence is 1.74 times greater than the prior probability.

In the absence of the binary map a similar expression can be derived for the posterior probability of a geothermal occurrence which is:

$$P\left\{G \mid \overline{M}\right\} = P\{G\}\frac{P\left\{\overline{M} \mid G\right\}}{P\left\{\overline{M}\right\}} \tag{2.5}$$

If the corresponding values of the example in Figure 3.5 are substituted into the equation (2.5) the result to be obtained will be:

$$P\left\{G \mid \overline{M}\right\} = P\{G\}\frac{P\left\{\overline{M} \mid G\right\}}{P\left\{\overline{M}\right\}} = 0.15\frac{0.03/0.15}{54/100} = 0.05$$

Thus the probability of finding a geothermal occurrence in the absence of negative magnetic anomaly is rather small than the probability of finding the occurrence in the presence of the same anomaly.

Bayesian method accounts for the basis of odds formulation, which is the primary idea of weights of evidence.

3.2.2 Odds Ratio

Odds are defined as a ratio of the probability that an event will occur to the probability that it will not occur. The WofE method uses the natural logarithm of odds, known as ***logits*** (Bonham-Carter, 1996). It is possible to convert the equation (2.4) to odds by dividing both sides by $P\{\overline{G} \mid M\}$:

$$\frac{P\{G \mid M\}}{P\{\overline{G} \mid M\}} = \frac{P\{G\}P\{R \mid G\}}{P\{\overline{G} \mid M\}P\{M\}} \tag{2.6}$$

According to equation (2.4):

$$P\{\overline{G} \mid M\} = P\{\overline{G}\}\frac{P\{M \mid \overline{G}\}}{P\{M\}} \tag{2.7}$$

When this expression instead of $P\{\overline{G} \mid M\}$ is substituted in equation (2.4):

$$\frac{P\{G \mid M\}}{P\{\overline{G} \mid M\}} = \frac{P\{G\}}{P\{\overline{G}\}} \cdot \frac{P\{M\}}{P\{M\}} \cdot \frac{P\{M \mid G\}}{P\{M \mid \overline{G}\}} \tag{2.8}$$

As previously defined the odd ratio is P{G}/(1-P{G}). Thus equation (2.8) can be expressed in terms of odds such as:

$$O\{G \mid M\} = O\{G\} \cdot \frac{P\{M \mid G\}}{P\{M \mid \overline{G}\}} \tag{2.9}$$

where $O\{G \mid M\}$ is the conditional odds of G given M, $O\{G\}$ is the prior odds of G and the expression $P\{M \mid G\} / P\{M \mid \overline{G}\}$ is known as the **sufficiency ratio LS.** In weights of evidence the natural logarithm of both sides of equation (2.9) are taken and $\log_e$ LS is the positive weight of evidence.

$$\log it\{G \mid M\} = \log it\{G\} + W^{+} \tag{2.10}$$

In the absence of the binary map information the odd equation will be:

$$O\left\{G \mid \overline{M}\right\} = O\{G\} \cdot \frac{P\left\{\overline{M} \mid G\right\}}{P\left\{\overline{M} \mid \overline{G}\right\}} \tag{2.11}$$

the expression $P\left\{\overline{M} \mid G\right\} / P\left\{\overline{M} \mid \overline{G}\right\}$ is called **necessity ratio LN** and the natural logarithm of LN gives the negative weight of evidence.

$$\log it\{G \mid \overline{M}\} = \log it\{G\} + W^{-} \tag{2.12}$$

W^+ is positive, and W^- is negative due to the positive correlation between the points and the binary pattern. Conversely, W^+ would be negative and W^- positive for the case where fewer points occur on pattern than would be expected due to chance. If the occurrences are independent of whether the pattern is present or not, then $W^+ = W^- = 0$, and the posterior equals the prior (Bonham-Carter, 1996).

To clarify the concept let use both maps in Figure 3.2 as evidence maps for geothermal occurrence training points.

Consider there is additional information of distance to lineament map (Figure 3.2a) in addition to previous map shown in Figure 3.5b.

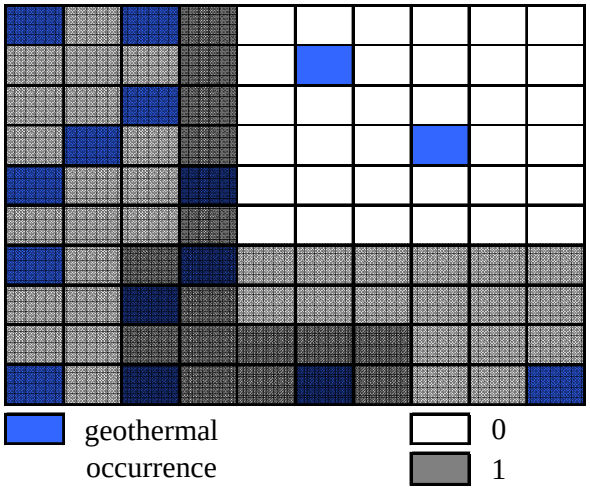

Figure 3.6: Two binary maps of negative magnetic anomaly and 10 km distance to lineament overlaid on geothermal occurrence map. The darkest areas indicate the intersection of two maps.

The following values are present according to Figure 3.6:

N{T}= 100; N{M}= 46; N{L}= 38; N{G}= 15; N{M∩G}= 12; N{L∩G}= 6

From equations (2.10) and (2.12):

$$W_M^+ = In\frac{P\{M \mid G\}}{P\{M \mid \overline{G}\}} = In\frac{0.12/0.15}{0.31/0.85} = In\ 2.1935 = 0.7855$$

$$W_M^- = In\frac{P\{\overline{M} \mid G\}}{P\{\overline{M} \mid \overline{G}\}} = In\frac{0.03/0.15}{0.51/0.85} = In\ 0.3333 = -1.0986$$

$$W_L^+ = In\frac{P\{L \mid G\}}{P\{L \mid \overline{G}\}} = In\frac{0.06/0.15}{0.32/0.85} = In\ 1.0625 = 0.0606$$

$$W_L^- = In\frac{P\{\overline{L} \mid G\}}{P\{\overline{L} \mid \overline{G}\}} = In\frac{0.09/0.15}{0.53/0.85} = In\ 0.9623 = -0.0385$$

The contrast for the negative magnetic anomaly map is 0.7855 – (-1.0986) = 1.8841, and for the distance to lineament map it is 0.0606 – (-0.0385) = 0.0991. This implies that the binary pattern of negative magnetic anomaly is much more associated with the geothermal occurrences than the binary pattern of distance to lineament map.

3.2.3 Combining Datasets

When the evidence from several maps is combined, the weights are calculated from each map independently, and then combined in a single equation. However this requires an assumption of conditional independence of the maps, which is a bivariate assumption.

The conditional probability of a geothermal occurrence, given the presence of two predictive map patterns, say negative magnetic anomaly map M and distance to lineament map L is:

$$P\{G \mid M \cap L\} = \frac{P\{G \cap M \cap L\}}{P\{M \cap L\}} \qquad (2.13)$$

$$P\{G \mid M \cap L\} = \frac{P\{M \cap L \mid G\}\ P\{G\}}{P\{M \cap L\}} = \frac{P\{M \cap L \mid G\}\ P\{G\}}{P\{M \cap L \mid G\}\ P\{G\} + P\{M \cap L \mid \overline{G}\}\ P\{\overline{G}\}} \quad (2.14)$$

Is it is assumed that these two maps are conditionally independent if the following equation is satisfied:

$$P\{M \cap L\} \mid G\} = P\{M \mid G\}\ P\{L \mid G\} \quad (2.15)$$

Substituting this into equation (2.14) leads to the following:

$$P\{G \mid M \cap L\} = P\{G\} \frac{P\{M \mid G\}}{P\{M\}} \frac{P\{L \mid G\}}{P\{L\}} \quad (2.16)$$

Using the odds formulation the posterior odds can be expressed for two map patterns:

$$O\{G \mid M \cap L\} = O\{G\} * LS_M * LS_L \quad (2.17)$$

The log-linear WofE form is:

$$\log it\{G \mid M \cap L\} = \log it\{G\} + W_M^+ + W_L^+ \quad (2.18)$$

There are four different ways of combining two binary map patterns. Equation (2.18) shows the way where both patterns are present. The other three are:

Where M is present and L is absent:

$$\log it\{G \mid M \cap \overline{L}\} = \log it\{G\} + W_M^+ + W_L^- \quad (2.19)$$

Where L is present and M is absent:

$$\log it\{G \mid \overline{M} \cap L\} = \log it\{G\} + W_M^- + W_L^+ \quad (2.20)$$

Where both are absent:

$$\log it\{G \mid \overline{M} \cap \overline{L}\} = \log it\{G\} + W_M^- + W_L^- \quad (2.21)$$

Using 3 binary patterns as evidence, 2^3 or 8 possible combinations and in general with n maps 2^n possible different combinations will be obtained. The general expression for combining i = 1,2…n maps is:

$$\log it\{G \mid B_1 \cap B_2 \cap B_3 \cap .....B_n\} = \log it\{G\} + \sum_{i=1}^{n} W^+ \quad (2.22)$$

If the i-th map pattern is absent instead of present W^+ becomes W^-. If the data is missing for a particular map layer for some locations the weight is set to zero (Bonham – Carter, 1996; Raines et al, 2000).

3.2.4 Conditional Independence

One of the assumptions for the weights of evidence model is conditional independence. Conditional independence can be tested in to ways, which are pairwise test and overall test (Bonham – Carter, 1996).

3.2.4.1 Pairwise Test

This method involves pairwise testing of conditional independence between all possible pairings of the binary maps which are combined. If two maps are said to be statistically independent then the following condition should be satisfied:

$$P\{B_1 \mid B_2\} = P\{B_1\} \qquad and \qquad P\{B_2 \mid B_1\} = P\{B_2\} \quad (2.23)$$

However, if two binary patterns are conditionally independent with respect to a set of occurrences, then the following relationship should be satisfied:

$$P\{B_1 \cap B_2 \mid O\} = P\{B_1 \mid O\}\ P\{B_2 \mid O\} \quad (2.24)$$

When the equation is converted to numbers the following expression is obtained:

$$N\{B_1 \cap B_2 \cap O\} = \frac{N\{B_1 \cap O\}\ N\{B_2 \cap O\}}{N\{O\}} \tag{2.25}$$

The left-hand side of the equation represents the observed number of occurrences, whereas the right hand side represents the expected number of the occurrences in the overlap zone. Thus, conditional independence between two pairs can be tested using X^2 test (Bonham – Carter, 1996).

$$X^2 = \sum_{i=1}^{n} \frac{(Observed_i - Expected_i)^2}{Expected_i} \tag{2.26}$$

The null hypothesis of the X^2 is that the map pairs are conditionally independent. Applying equations (2.25) and (2.26) to the example shown in Figure 3.6 implies:

$$Observed\ Number\ of\ Occurrences = N\{L \cap M \cap G\} = 5$$

$$Expected\ Number\ of\ Occurrences = \frac{N\{L \cap G\}\ N\{M \cap G\}}{N\{G\}} = \frac{6 * 12}{15} = 4.8$$

$$X^2 = \frac{5 - 4.8}{4.8} = \mathbf{0.0417}$$

At a probability level of 95% and one degree of freedom $X^2_{critical}$ = 3.84, which is rather higher than X^2_{test} leading to failure of rejection the null hypothesis of conditional independence.

CHAPTER 4

INPUT DATA AND DATA EXPLORATION

The data used in the analysis are divided mainly in two groups: Raw public data and synthetic data that have been produced from this publicly available data. The raw public data include an inventory about geothermal database, epicenter database, and interpreted lineaments in the area, as well as magnetic anomaly map and Bouger gravity map, which all are supplied by public sources. However, the publicly available data in its current form is not found to be quite suitable to be used as explanatory variables. Hence the synthetic data are processed and transformed version of original raw public data into some meaningful environmental explanatory variables which are then used as inputs of the relevant analysis.

In the raw public data part, the relation between the existing geothermal sites and other public sources are evaluated individually by means of distribution patterns. Depending on the obtained remarks each public layer is transformed to synthetic data layer so as to make the effect of each layer on geothermal occurrences much more evident. Thus, epicenter database is first converted to epicenter density maps and then to Gutenberg-Richter *b* parameter map. Lineaments and attained horst-graben boundaries from the Bouger gravity anomaly map are converted to Distance to lineaments maps. Magnetic anomaly map is decided to be used in its original form due to unclear relationship with the geothermal occurrences (Figure 4.1).

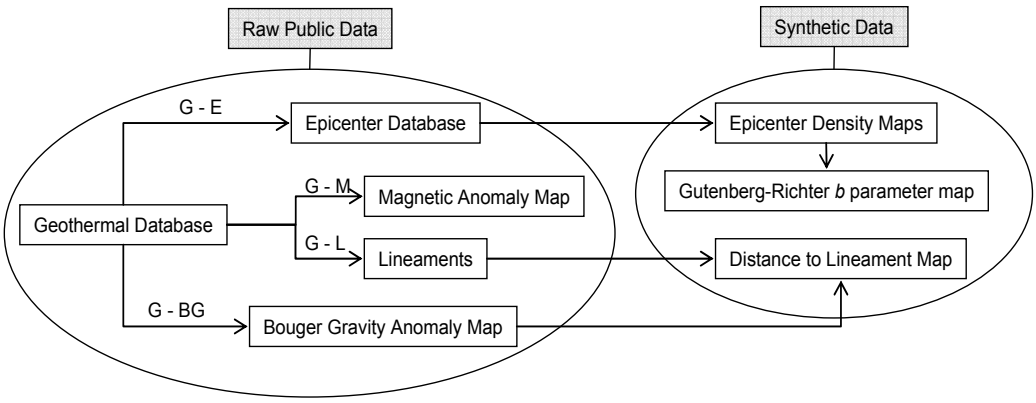

Figure 4.1: The scheme representing the input data and its exploration method.

4.1 Raw Public Data

4.1.1 Geothermal Database

The geothermal database of the Western Anatolia was constructed mainly using the two different versions of Geothermal Inventory of Turkey (1996 and 2005) prepared by General Directorate of Mineral Research and Exploration of Turkey.

The database contains 520 records at total for wells and springs, out of which 342 records fall into the selected study area. The spatial distribution of these wells and springs can be seen in Figure 4.2. The detailed tabulation of the description of the database according to the year of the inventories, spring and well numbers is presented in Table 4.1.

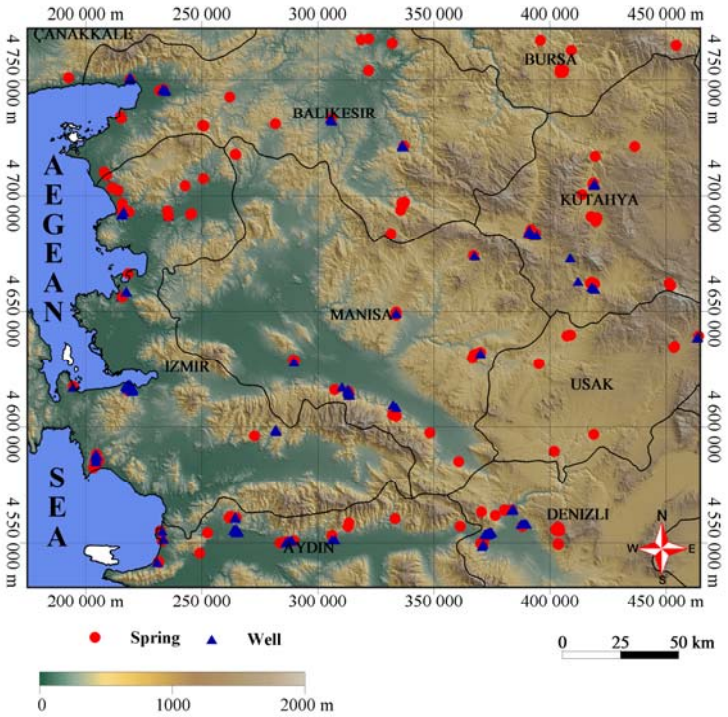

Figure 4.2: Spatial distribution of wells and springs falling within the study area.

It is clear from the Table 4.1 that the geothermal resources in Western Anatolia became important in recent years as the number of explored springs and exploited wells have increased significantly.

Table 4.1: Table containing the numbers of springs and wells for the Western Anatolia and the study area according to 1996 and 2005 Geothermal Inventory of Turkey.

	Western Anatolia		**Study Area**	
	1996	2005	1996	2005
Spring	120	272	73	176
Well	87	248	61	166
Total	**207**	**520**	**134**	**342**

The available public geothermal inventory contain information on type of the geothermal variable (well or spring), well/spring name, district and province of the location, depth and production type for almost all wells, flow rate for wells and for some springs, total flow rate for group of springs, construction years of wells, temperature, pH, conductivity, evaporation remnant and information about the chemistry of the water. All of the occurrences in the inventory have some sketches, but due to the lack of coordinate information, data prepared in MS Excel was imported to MapInfo 7.8 software and by using the nearest village name the occurrences were fixed to their location. Afterwards, the coordinates of the occurrences were extracted and added as new columns to the database, having Latitude-Longitude projection with WGS 84 datum. Then this new database was imported in vector format to TNTmips 6.9 software to become the final geothermal database (Figure 4.3). Using this software the occurrences that fall into the study area were extracted and due to the purpose of the analysis, the projection system was changed into Lambert Conformal Conic projection with European 1950 Mean Datum.

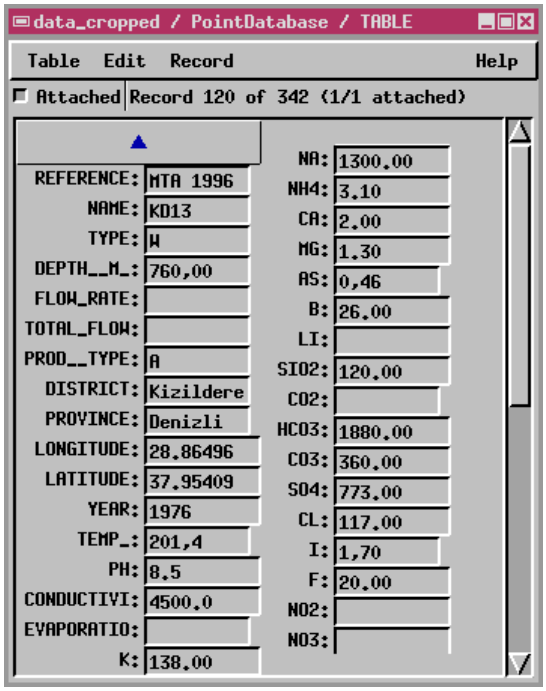

Figure 4.3: Variables within the database.

Following the construction, completion and validation of the database, the data distribution as well as the temperature distribution along the area is investigated.

Average temperature distribution of wells and springs along the study area shows that while the temperature of springs do not vary much, the average temperature of wells have their highest value at the southern part of the area (Figure 4.4). Although it might be considered as a well production issue also it denotes the easiest and hottest location of previous explorations. Furthermore, there exists no significant correlation among the spring temperature and the well temperature, as the spring waters are cooled due to conductive cooling or mixing with cold waters while rising up to the surface.

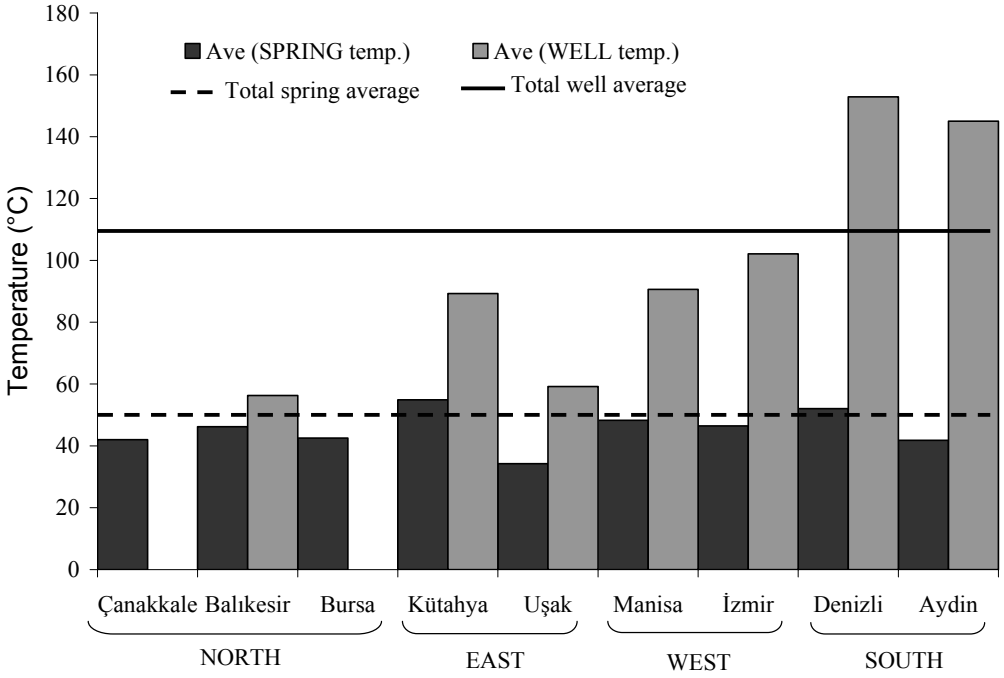

Figure 4.4: Average temperature distribution of wells and springs according to cities and their relevant directions in the study area.

The distribution of wells and springs, namely the occurrences, are not uniform along the study area. According to the histogram in Figure 4.5 it can be concluded that the distribution of the occurrences are accumulated and that these accumulations are along western and southern part (Manisa, İzmir, Denizli, Aydin) of the area as the number of occurrences in these locations have rather high values when compared to northern an eastern parts. Visual inspection does also support this clustering, however, in order to clarify the distribution patterns the distribution of the occurrences should be investigated statistically.

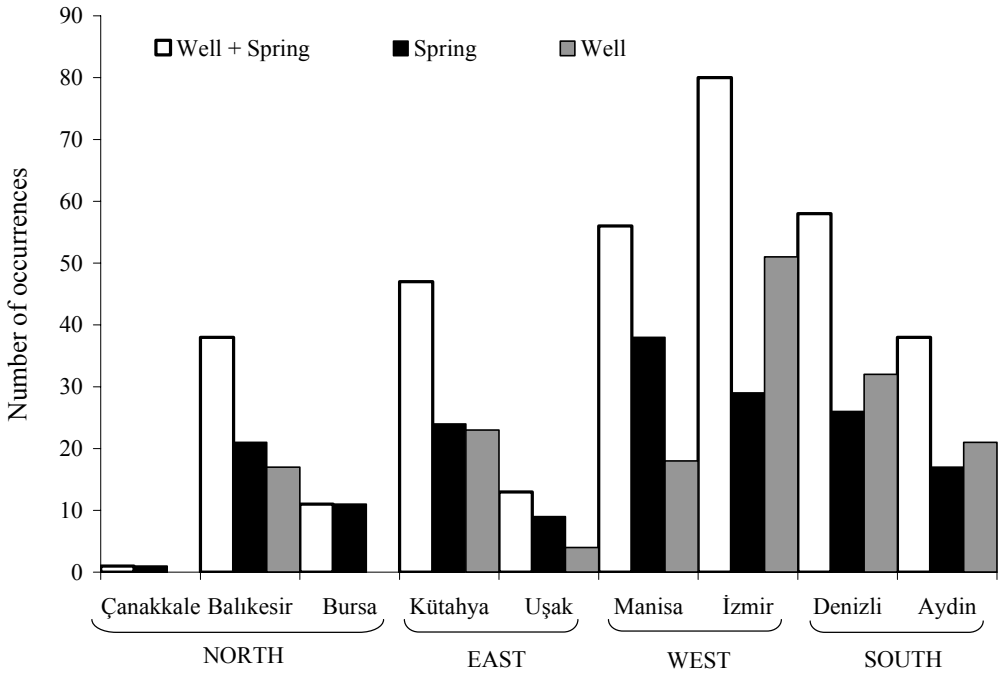

Figure 4.5: Number of geothermal occurrences according to cities and their relevant directions in the study area.

The patterns of points on maps can be classified into three categories: uniform, random and clustered. The ***uniform*** pattern occurs when the density of points in any subarea is equal to the density of points in all other subareas of the same size and shape. A ***random*** pattern can be created if any subarea is likely to contain a point as any other subarea of the same size, regardless of the subareas location, and the placement of a point has no influence on the placement of any other point. In a ***clustered*** pattern, the probability of occurrence of a point varies in some inverse manner with distances to preexisting points (Davis, 2002).

In order to test the distribution of points on a map, first the map area is divided into a number of equal sized subareas. Then the expected number of points in each subarea is found by:

$$E = \frac{N}{k} \tag{4.1}$$

where *N* is the total number of data points and *k* is the number of subareas. Then the variance in number of points per subarea is found using the following equation:

$$s^2 = \frac{\sum_{i=1}^{k}(r_i - N/k)^2}{k-1} \tag{4.2}$$

where r_i is the number of points in the i[th] subarea. After all, the mean (N/k) and the variance (s^2) is compared and the followings are concluded (Davis, 2002):

$N/k > s^2$ Pattern more uniform than random
$N/k = s^2$ Pattern random
$N/k < s^2$ Pattern more clustered than random

In order to investigate point distribution within the study area, wells and springs falling in a 10 km^2 area are assumed to belong to the same geothermal system and a point representing that system is assigned and used rather than using well and spring points separately. In this way, 77 point were assigned and put into analysis. The study area, on the other hand, due to the convenience of the metric system is divided into 100 equal sized subareas having an area of 700 km^2 (Figure 4.6). However, it should be noted that some subareas are occupied by sea which means that one does not expect an occurrence within these subareas (Figure 4.6). Thus, seven subareas falling in Aegean Sea region are excluded from the calculations.

According to this arrangement the expected (mean) number of points and the variance per subarea is found to be as following:

$$E = \frac{N}{k} = \frac{77}{93} = \mathbf{0.83}$$

$$s^2 = \frac{\sum_{i=1}^{k}(r_i - N/k)^2}{k-1} = \frac{(0_i - 0.83)^2 + ... + (4_k - 0.83)^2}{92} = \mathbf{0.84}$$

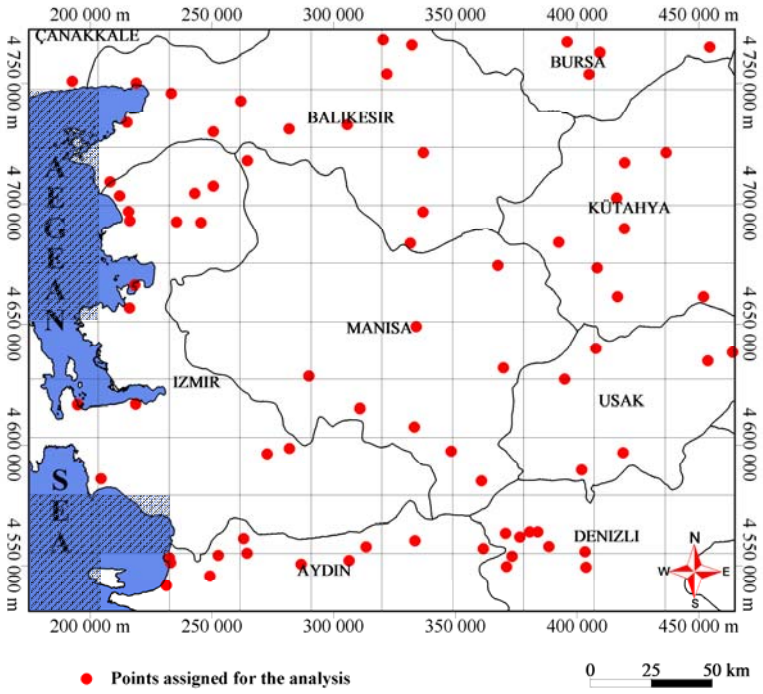

Figure 4.6: Distribution of geothermal systems represented by points within the study area divided into equal sized subareas, the squares with pattern indicate the excluded subareas.

The calculated variance is slightly greater than the mean, but really very close to the mean value. Thus, it is concluded that the point distribution pattern is random to slightly clustered. The clusters can be visualized by rasterizing the polygon vector which has information on its database about the point number in each subarea. The point number attribute for each polygon is presented as cell value in the raster. Additionally, the size of the raster cells is equal to that of the subarea, namely 700 km^2. The cell values range from 1-4, from low clustered to highly clustered distribution (Figure 4.7). Having high clusters in some places while having low clusters in some others, leads to the conclusion that the probability of occurrence of geothermal systems is greater in particular locations. This conclusion arises some questions like: What are the factors affecting this probability? And could they be explained by environmental parameters?

To find an answer to these questions, the possible effects of epicenters, lineaments and in addition to their distribution, the possible effects of magnetic and gravity anomalies on geothermal occurrences will be investigated.

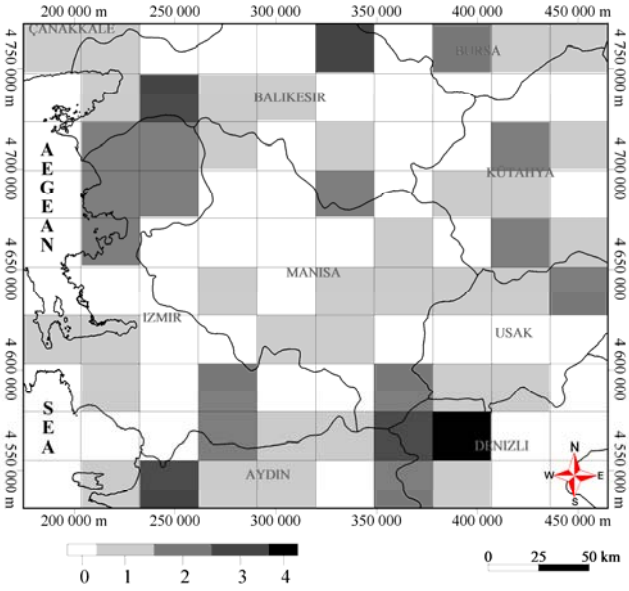

Figure 4.7: Point clusters in raster format.

4.1.2 Epicenter Database

Geothermal systems are common within the seismic zone due to high permeability and convection of hot water in the seismic fractures (Flóvenz et al, 2001). Being the source of fractures, the earthquakes are taken into account as a possible factor affecting the occurrence of a geothermal occurrence. The way in which epicenters affect the point at issue is explored under this subtitle.

The epicenter database was constructed by using the catalogue prepared by Kandilli Observatory which is published in http://www.koeri.boun.edu.tr. This database contains records for 104 years (1900 – 2004) having information on location, magnitude and depth for all epicenter data. However, whole data is not used in the analysis.

In order to avoid bias in detection of earthquakes, and considering that the data collected before 1980 may not reliable due to related instrumental deficiency, the earthquakes occurred between 1980 and 2004 are taken into account. The focal depths and magnitudes of the earthquakes are also restricted. Earthquakes having shallow focal depth (5.0-20.0 km) with magnitude between 3.0 and 7.4 are put into analysis (Oral communication, Kaymakcı, 2006). Shallow focal depths are chosen, because the epicenters near the surface are more likely to affect the surface and create a fracture. The magnitudes lower than 3.0 are eliminated on the other hand, because most of the low magnitudes may belong to aftershocks or classified as background noise but not to the source earthquakes.

After all eliminations are made the epicenters falling into the area of interest are extracted. Table 4.2 tabulates information on number of earthquakes having a particular magnitude and focal depth range, and Figure 4.8 represents the spatial distribution of epicenters.

Table 4.2: Number of earthquakes within classified magnitude and depth ranges with their corresponding cumulative percentages.

		Magnitude range				
		$3 <= M <= 4$	$4 < M <= 5$	$5 < M <= 6$	$M > 6$	***Total***
Depth range	$5 <= D <=10$	15730	1025	48	6	*16809 (78%)*
	$10 < D <= 15$	2917	231	18	0	*3166 (15%)*
	$15 < D <= 20$	1367	177	18	4	*1566 (7%)*
	Total	*20014 (93%)*	*1433 (6.6%)*	*84 (0.39%)*	*10 (0.01%)*	***21541(100%)***

As it is observed the predominant earthquakes within the area are those having shallow depth (5 – 10 km) and low magnitude (3 – 4). However, in order to discover the effect of epicenters on geothermal occurrences, it is vital to find out the distribution of these points along the area and locations where they are clustered.

The distribution manner of epicenters is investigated in same way as it was performed for geothermal occurrences. The same equal sized subareas are used and the point number falling into each subarea is counted and entered to the polygon database of the grid. After the calculation of mean number of points and the variance per subarea, the following is concluded for the distribution of the epicenters:

E = **231.62** < s^2 = **73396.94**…….Clustered distribution

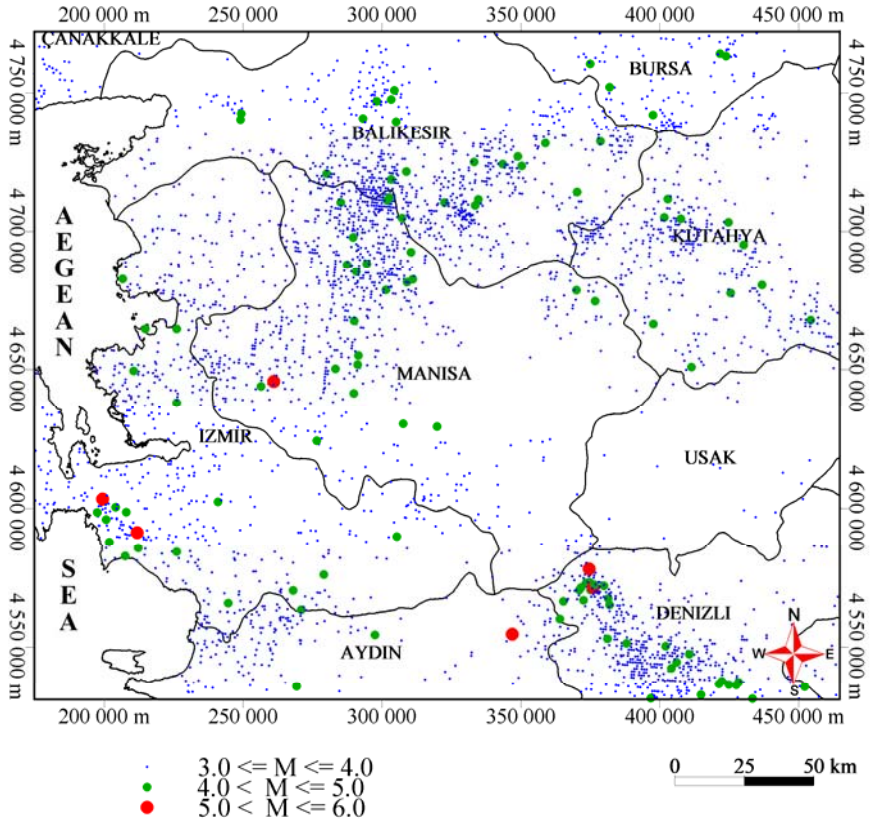

Figure 4.8: Spatial distribution of epicenters within the study area, “M” stands for the magnitude of earthquakes.

Unlike to the geothermal occurrence, the distribution of the epicenters along the region is found out to be highly clustered as the variance is rather greater than the mean. That is to say, the probability of occurrence of epicenters is greater in some locations, and the possible reason is that in these locations the density of faults is greater, namely they are active seismic zones.

Due to the necessity of comparing epicenter and geothermal occurrence clusters, the polygon grid having epicenter number information is rasterized similar to that of geothermal occurrence. The raster cell values range from 0 to 230 as the highest number of epicenter lying within a subarea is 230 (Figure 4.9a). Because the cell values of geothermal occurrence raster map ranges from 0 to 4, the range of the cell values for epicenter density is rearranged by a script so that it has the same range with that of geothermal occurrence density map (Figure 4.9b). In this way, the two maps can be compared easily. However, it should be noted that the comparison will be made for the areas where there is a geothermal cluster; because geothermal clusters having value of “0” may be the non-discovered potential areas. For this reason a mask, having value of “1” for the areas having “geothermal” and value of “0” for the ones with no “geothermal”

is prepared (Figure 4.10). By multiplying the mask with the rearranged epicenter density map, the areas having no “geothermal” will be excluded, while the ones having “geothermal” will still possess the rearranged epicenter density value (Figure 4.11b). The multiplication result and the geothermal occurrence density map is seen side by side in Figure 4.11a,b.

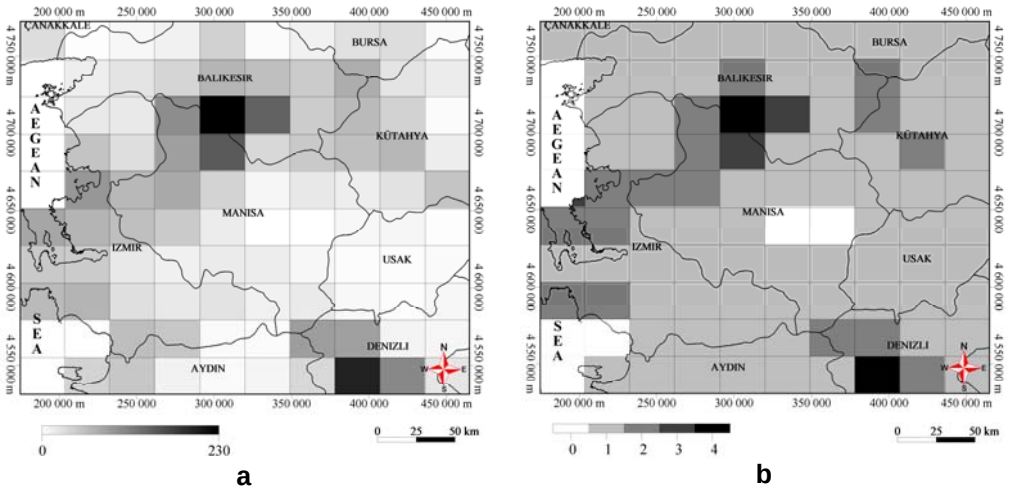

Figure 4.9: a) Raster of epicenter clusters having cell value range: 0-230; **b)** Raster of epicenter clusters having cell value range: 0-4.

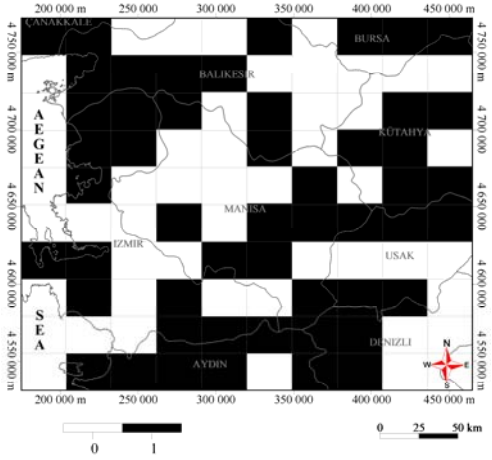

Figure 4.10: Mask multiplied with rearranged epicenter clusters.

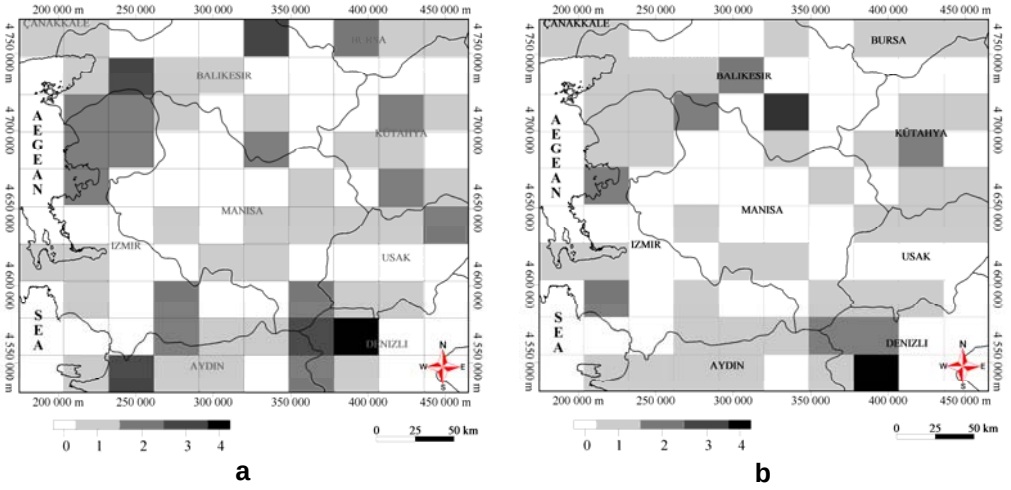

a b

Figure 4.11: a) Geothermal occurrence density map; **b)** Multiplication result of epicenter density map.

If a cell of geothermal density occurrence map is a_{ij}, and a cell of epicenter density map is b_{ij}, for the overlapping pairs of the cells in each map the cell values are compared (a_{11}-b_{11}, a_{12}-b_{12}…….$a_{100\ 100}$-$b_{100\ 100}$) to investigate whether the densities are similar to each other or not. Figure 4.12a summarizes the comparison of to maps and it demonstrates how consistent both of the maps are in terms of density values while Figure 4.12b demonstrates the percentage of success by means of fitting cells.

Epicenter density \ Geothermal density	*0*	*1*	*2*	*3*	*4*
0	0	2	0	0	0
1	0	25	13	3	0
2	0	4	1	1	1
3	0	1	0	0	0
4	0	1	0	0	0

a

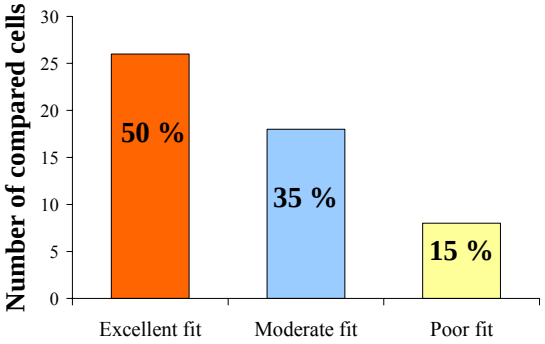

b

Figure 4.12: a) Numeration of compatible and incompatible cells; **b)** Bar diagram of fitted cells.

According to the findings, 50 % of cells fit excellent, while 35 % fit moderately and 15 % have a poor fit (Figure 4.12b). Thus, it can be interpreted that epicenters may have some influence on geothermal occurrences. However, it does not mean that an

area having epicenters should have a geothermal also. Although, this approach can give some idea on how much two different events are related, for prediction of geothermal occurrences, investigating the seismicity and activity characteristics for a location rather than epicenter density alone, may be more realistic.

Hence the activity characteristics map is prepared using the "*b*" parameter in Gutenberg – Richter relation and its importance in geothermal occurrence point of view is introduced in the following chapters.

4.1.3 Lineaments in the Study Area

The lineaments are linear and/or curvilinear features that can be detected on the aerial photographs and satellite images (O'Leary et al, 1976). They are thought to be the surface manifestation of emerged and/or subsurface geological structures.

Faults, being a kind of lineament, allow groundwater to percolate towards the heat source and become heated to high temperatures. Some of this hot geothermal water travels back to the surface through and appear as hot springs. Generally, geothermal systems are associated with areas of active faulting (Bowen, 1989, p. 70), because these active fractures let the meteoric fluids to circulate and penetrate deep to the crust.

The lineament data used in this study is obtained from Dr. Nuretdin Kaymakcı of METU Geological Engineering Department (Ankara, Turkey) and they were interpreted visually using SRTM (http://srtm.usgs.gov/) data (Figure 4.13).

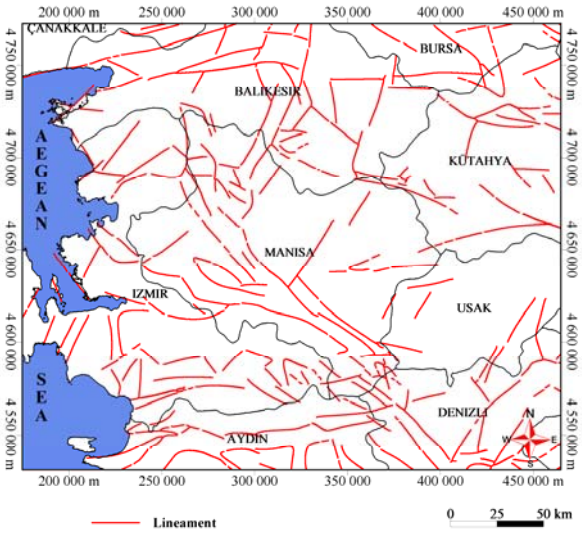

Figure 4.13: Spatial distribution of lineaments in the study area.

In order to find principal statistical trends of the lineaments rose diagram is constructed (Figure 4.14). According to diagram two dominant trends are observed. The one is in NW – SE direction, while the other is in ENE – WSW direction.

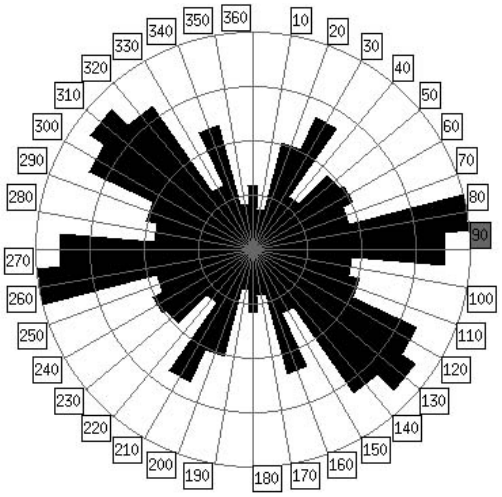

Figure 4.14: Rose diagram representing the trend of lineaments.

It is obvious that the lineaments have some general trend within the area. However, beyond the trends in their distribution, their densities within the study area should be investigated in order to find out their effect on geothermal occurrences.

Just as a set of points can form a pattern that ranges from uniform to clustered, so can set of lines. Of course, lines are more complex than points because they possess length and orientation, as well as location. Their analysis is correspondingly more difficult, and statistical methods suitable for the study of patterns of lines seem less well developed than those applied to patterns of points (Davis, 2002). Suppose, a subarea that contain only two but long lines while another one contain 20 short lines, and some other include 10 lines where 3 of them are long and 7 of them are short. The problem that arises in this case is to decide in which of these three subareas the lineament is more dominant. One should take into account the length of lines as well as their number in each cell to determine the clusters.

In this study, calculation of lineament distribution is performed similar to those of points. However due to the reason that not only the number of lineament in any subarea is important, but also its length, each line is converted to points distance between which is 10m. In this way the importance of line length as well as line number in each subarea is reflected to each polygon grid.

Point number within each subarea is counted and entered to the polygon database of the grid and the calculation of mean number of points and the variance per subarea, leads to the following conclusion:

E = **5080.82** < s^2 = **8737940**…….Clustered distribution

In order to compare lineament and geothermal occurrence clusters, the polygon grid having lineament number information is rasterized similar to that of geothermal occurrence and epicenter. The raster cell values range from 0 to 13638 (Figure 4.15a). Cell value rearrangement is performed using script so that the values range from 0 to 4 (Figure 4.15b). The rearranged map is multiplied by the mask (Figure 4.10) and the product map is compared with geothermal occurrence map (Figures 4.16b and 4.16a respectively).

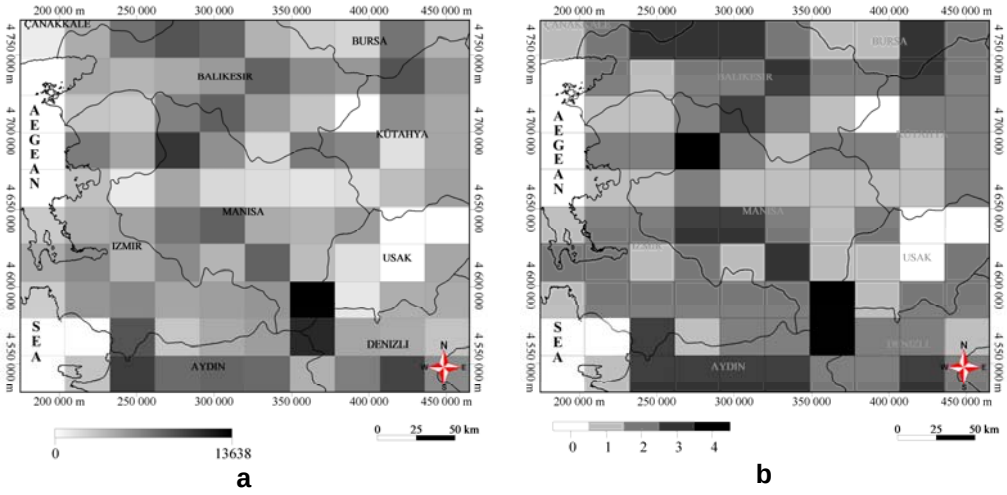

Figure 4.15: a) Raster of lineament clusters having cell value range: 0-13638;
b) Raster of lineament clusters having cell value range: 0-4.

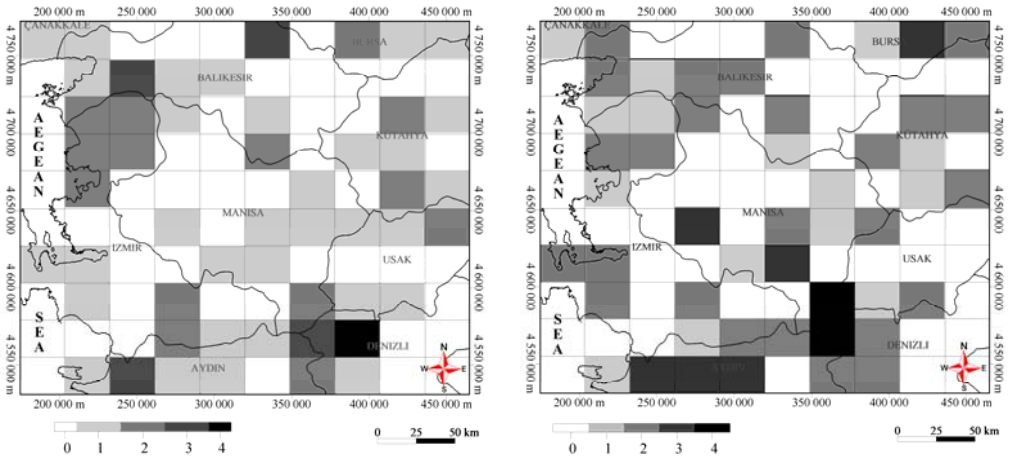

Figure 4.16: a) Geothermal occurrence density map; **b)** Multiplication result of lineament density map.

The same method used for comparing epicenter and geothermal densities is utilized in checking the similarities between lineament density and geothermal occurrence density cells (Figure 4.17a). The empirical evidence has shown that, 27 % of cells fit excellent, while 54 % fit moderately and 19 % have a poor fit (Figure 4.17b). Obviously, lineaments affect geothermal occurrence in some way. However, not only the relation between the distributions but also some other parameters such as distance to lineaments should be investigated in order to introduce how lineaments affect the occurrence of a geothermal.

Lineament density \ Geothermal density	*0*	*1*	*2*	*3*	*4*
0	0	1	1	0	0
1	0	8	7	1	0
2	0	19	5	1	1
3	0	5	0	1	0
4	0	0	1	1	0

a

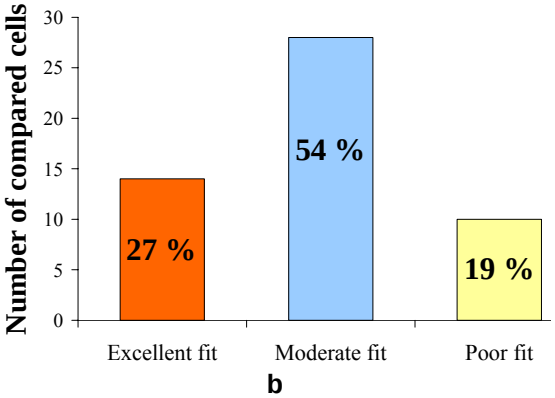

Figure 4.17: a) Numeration of compatible and incompatible cells; **b)** Bar diagram of fitted cells.

4.1.4 Bouger Gravity Anomaly Map

The general aim of gravitational prospecting is to detect underground structures by means of the disturbance they produce at the surface in the earth's gravitational field (Griffiths, 1965).

On the other hand Bouger anomaly is defined as the gravity reduced to a predefined datum level (Parasnis, 1972). It is known as the part of the difference between observed gravity and theoretical gravity at any point on the earth which is due purely to lateral variations of density beneath the surface. Performing latitude, elevation and terrain corrections the Bouger anomalies (BA) can be presented as: (Griffiths, 1965):

$$BA = \textit{Observed gravity} + \textit{Elevation correction} + \textit{Topographic correction} - \textit{Theoretical gravity at the same latitude} \quad (4.3)$$

Gravity anomalies are expressed in milligals. One milligal is one thousand of a gal which is a unit of acceleration named after Galileo. A tenth of a milligal is called gravity unit and is one millionth of the SI unit of acceleration, m/s^2, (Parasnis, 1972).

Isogal maps, namely gravity anomaly maps, look very like topographic contour maps. They show circular, elongated, and irregular areas of high and low gravity. They may also show linear belts of steep gradients (Griffiths, 1965). The anomalies arise from relatively small differences between rock formations and the interpretation is naturally very sensitive to available density values (Parasnis, 1972). Gravity highs, are in many areas associated with anticlines or with horst blocks, both being structures which bring older denser rocks nearer the surface. In other regions gravity highs may be due to the presence of heavy basic intrusions. Conversely sedimentary basins and relatively light acid intrusions usually produce gravity lows. The belts of steep gradients are produced by vertical/sub-vertical contacts between rocks of different density, such as may occur across fault planes (Griffiths, 1965).

The Bouguer gravity map of Turkey is published by the General Directorate of Mining Research and Exploration of Turkey (MTA) on www.mta.gov.tr. The isogal map of the study area was extracted from this 1/2.000.000 scaled map and registered to Lambert Conformal Conic projection system having ED 50 datum. Isogals with 5 mgal interval are digitized and their values are entered to the database of the contour map (Figure 4.18a). Then, continuous surface of Bouger anomaly was interpolated using contour values (Figure 4.18b).

The surface map of Bouger gravity anomaly shows that gravity values increase from E to W towards the Aegean Sea. However, within the majority of the study area

negative gravity anomalies are present. At first sight to the contour map Gediz and Büyük Menderes grabens are observed from the steep gradients of contours, which have generally NW–SE and E–W trends respectively. According to the study performed by Sari and Şalk at 2005, the grabens are thought to be characterized by lower gravity anomaly values due to their thick sedimentary deposits. In other words, negative gravity anomalies are found to be due to the thick Neogene sediments within the Gediz and Büyük Menderes grabens. Higher gravity values on the other hand represent the horsts that consist of high grade metamorphic rocks of the Menderes massif.

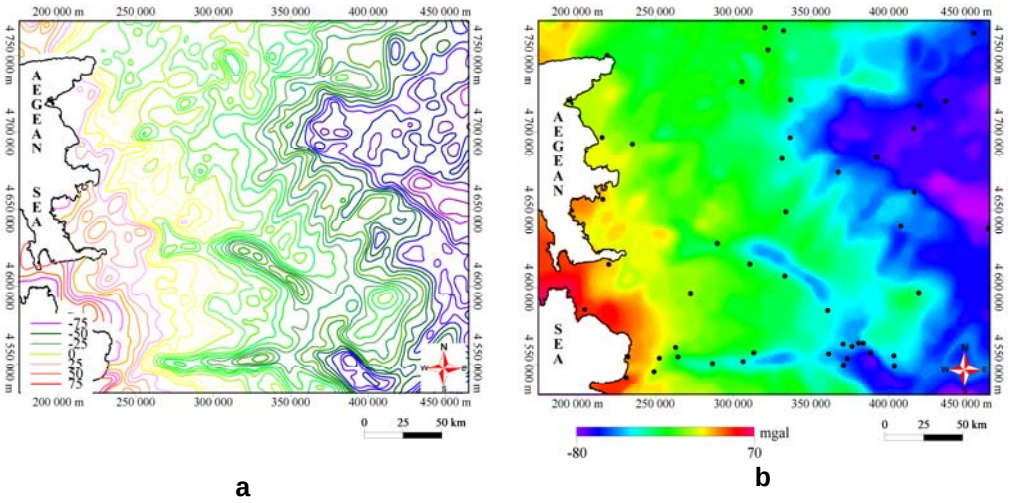

Figure 4.18: a) Bouger gravity anomaly contours; **b)** Continuous surface of Bouger anomaly with overlying occurrences.

Furthermore in literature, regional negative gravity anomalies in the continental stress field are created as a result of the joint effect of a zone of low density and thin oceanic crust (Darracott et al., 1972; Condie, 1976). The positive Bouguer gravity anomaly observed to the west of Menderes-massif is interpreted as a continuation of a positive anomaly belt identified as the concave side of an island arc (Rabinowitz and Ryan, 1970; Özelçi, 1973). Similary, the negative anomaly belt towards central Anatolia from the Denizli area is defined as the continuation of Crete's relatively negative anomaly belt.

Due to the fact that, on both the positive and negative sides of the anomaly map the geothermal occurrences are observed, it is concluded that they have no preference in anomaly value of gravity anomaly point of view. However, when the slope of the gravity map is constructed the hidden relationship between Bouger gravity and

geothermal occurrences come on the scene (Figure 4.19). Steep gradients agree well with the major grabens in the area and so with the occurrences. Thus an assumption like “Geothermal events in major part of Western Anatolia are related to structural features” can be made.

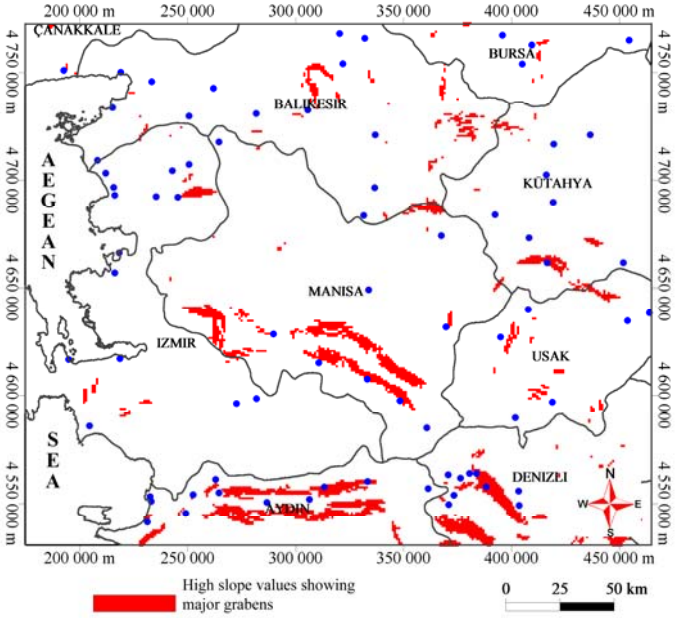

Figure 4.19: Slope map of the gravity anomaly surface.

4.1.5 Magnetic Anomaly Map

The magnetic method of applied geophysics depends upon measuring accurately the anomalies of the local geomagnetic field produced by the variations in the intensity of magnetization in rock formations. The magnetization of rocks is due to partly to induction in the earth’s field and partly to their permanent magnetization. The induced intensity depends primarily upon the magnetic susceptibility and the magnetization field, and the permanent intensity upon the geological history of the rock (Parasnis, 1972).

Most rocks contain small but significant quantities of ferromagnetic materials such as magnetite or hematite. The rocks therefore have a weak magnetization which is likely to be in part induced by the earth’s magnetic field. This magnetization modifies the earth’s field to an extent that can be detected at the surface with sensitive instruments (Griffiths, 1965).

Aeromagnetic surveying is performed using aircraft when a geophysical survey has to be carried out over an extensive area and if access to the area overland is

difficult. Moreover, coverage from the air is usually more complete than from the ground, and there is the very considerable advantage that the geophysical data can be obtained in the form of continuous profiles, rather than as a series of isolated point readings (Griffiths, 1965).

The data of magnetic surveys are presented as contour maps showing lines of equal strength of the anomaly field. On a larger scale, magnetic surveys are used for mapping geological structures. In areas where the sedimentary sequence is very thick it is sometimes possible to delineate the major structural features because the succession includes magnetic horizons. These may be ferruginous sandstones or shale, tuffs, or possibly lava flows. In such circumstances anticlines will produce positive and synclines negative anomalies, faults being indicated by linear belts of somewhat sharp gradient, or by sudden swings in the trend of the contours. In many regions, however, the igneous and metamorphic basement which underlies the sedimentary sequence is the predominant factor controlling the pattern of the anomaly field, for it is usually far more magnetic than the sediments. Where the basement rocks are brought nearer to the surface in structural highs the magnetic anomalies are large and characterized by strong relief. Conversely deep sedimentary basins are likely to show low values of the anomaly and gentle field gradients. The form of the magnetic contours is of course determined to a large extent by the structural trends in the basement itself and in some instances they may be of importance in that they control the later pattern of folding and faulting in the overlying sediments (Parasnis, 1972).

The aeromagnetic anomaly map of Turkey is again published by the General Directorate of Mining Research and Exploration of Turkey (MTA) on www.mta.gov.tr. Its scale is 1/2.000.000 and the contour intervals are 50 gammas. After the extraction of the study area the map is registered to Lambert Conformal Conic projection system having ED 50 datum and the contours are digitized. The contour values are entered to the database of magnetic anomaly contours. After all, for visual purposes the continuous map is prepared (Figure 4.20).

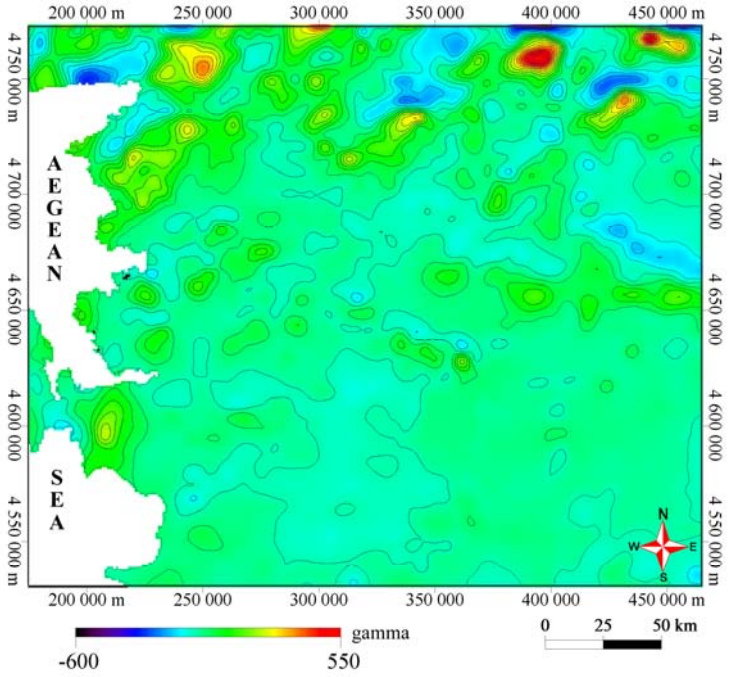

Figure 4.20: Aeromagnetic map of the study area.

It is clear from the magnetic anomaly that the bulk of the area is characterized by low magnetic values. Only some positive patches are observed on the northern part of the area, where scarce geothermal occurrence is encountered (Figure 4.21). Most of the occurrences, on the other hand, are observed where the anomaly shows slight negative variations. This may be due to thickness of sedimentary rocks. As it was defined in geology chapter the dominant rock assemblage in the study area is Menderes Massif which is composed of metamorphic rocks and is overlaid by Neogene sedimentary rocks. In this case one can expect some kind of change in the pattern of the magnetic anomaly as metamorphic rocks are known to be more magnetic than the sediments. However, this kind of change in the pattern is not observed within the area. This can be due very thick cover of the Neogene sedimentary rocks.

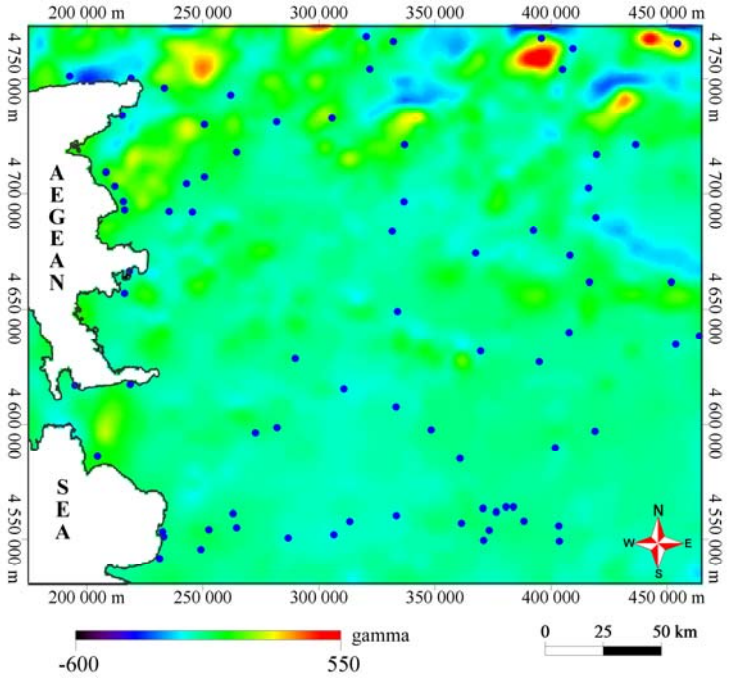

Figure 4.21: Distribution of geothermal occurrences on magnetic anomaly map.

At first sight, one can claim that the occurrences are observed at negative magnetic anomalies. However, a considerable amount of the area has already negative anomalies ranging from 0 to -600 and in this case it is not so easy to comment on magnetic anomaly preference of geothermal waters. The way of evaluation of this data will be introduced and its possible effect on the occurrences will be calculated in the next chapter.

4.2 Synthetic Data

Raw data usually contain some unknown pattern. Thus, it should be processed and converted to a form having somewhat known geometry and location. Thus it will be suitable for statistical and spatial analysis. In the previous subchapters the general relation of geothermal occurrence – epicenter and lineament was stated. However, the reason of this relation is the issue that will make it possible to analyze potential sites. Thus, the epicenter data, being an indicator of near faults and activity of the area, and the faults, possessing pathway characteristics for the heated water, will be further processed in order to obtain synthetic datasets.

4.2.1 Epicenters

Epicenters being vertical projections of the points of earthquakes origin occurred deep within the earth are generally mapped to show the seismicity of a specific area. Seismicity maps on the other hand reflect the activity of the nearby fractures within the area. Simply, it can be said that the more the epicenter, much more is the activity. However, not only the epicenter number, density in other words, is the determining factor in activity, but also their occurrence frequency. Gutenberg and Richter (1944) have found a relationship between the recurrence of earthquakes and their magnitude. The relation and its parameters are actually used as inputs in seismic hazard calculations. However, in this study one of these parameters "*b*" will be used as an indicator of low/high magnitude seismicity.

4.2.1.1 Background Information on Gutenberg-Richter Parameters

The Gutenberg – Richter law was developed from a set of regional data that included many different seismic sources. For specific sites, rather than large regions, the earthquake generating characteristics of individual faults is important (Kramer, 1996). For particular earthquake sources, seismicity recurrence characteristics are calculated. The sources are explicitly defined as being of uniform earthquake potential, that is, the chance of an earthquake of a given size occurring is the same throughout the source. Sources may range from small planar faults to large seismotectonic provinces. Each source is characterized by an earthquake probability distribution or *recurrence relationship*. A recurrence relationship indicates the chance of an earthquake of a given size occurring anywhere inside the source during a specified period of time. A maximum or upper bound earthquake is chosen for each source which represents the maximum event to be considered. This maximum event does not represent the only earthquake to be considered, but rather the upper limit of earthquakes of all sizes that will enter into the analysis for each source. Recurrence relationships for individual sources have classically been represented by straight line plots through data sets (Reiter, 1990).

Gutenberg and Richter (1944) gathered data for southern California earthquakes over a period of many years and organized the data according to the number of earthquakes that exceeded different magnitudes during that time period. They divided the number of exceedences of each magnitude by the length of the time period to define a *mean annual rate of exceedence*, λ_m of an earthquake of magnitude *m*. As would be expected, the mean annual rate of exceedence of small earthquakes is greater than that of large earthquakes. The reciprocal of the annual rate of exceedence for a particular magnitude is commonly referred to as *return period* of earthquakes

exceeding that magnitude. When the logarithm of the annual rate of exceedence of southern California earthquakes was plotted against earthquake magnitude, a linear relationship was observed. The resulting Gutenberg – Richter law for earthquake recurrence was expressed as:

$$\log \lambda_m = a - bm \tag{4.4}$$

where λ_m is the mean annual rate of exceedence of magnitude m, a is the logarithm of the mean yearly number of earthquakes of magnitude greater than or equal to zero, and b (the *b value*) describes the relative likelihood of large and small earthquakes (Kramer, 1996). The "a" value can be thought as an activity rate whose relative size describes the overall rate of earthquake occurrence (Reiter, 1990). The Gutenberg – Richter law is illustrated schematically in Figure 4.22 (Kramer, 1996). The ordinate shows the logarithm of the number of earthquakes of a given size or larger, while the abscissa shows increasing size (Reiter, 1990). As the *b value* increases, the number of larger magnitude earthquakes decreases compared to those of smaller magnitudes (Kramer, 1996). Thus, shallow slope would imply a relatively higher proportion of large earthquakes than steep slope (Reiter, 1990).

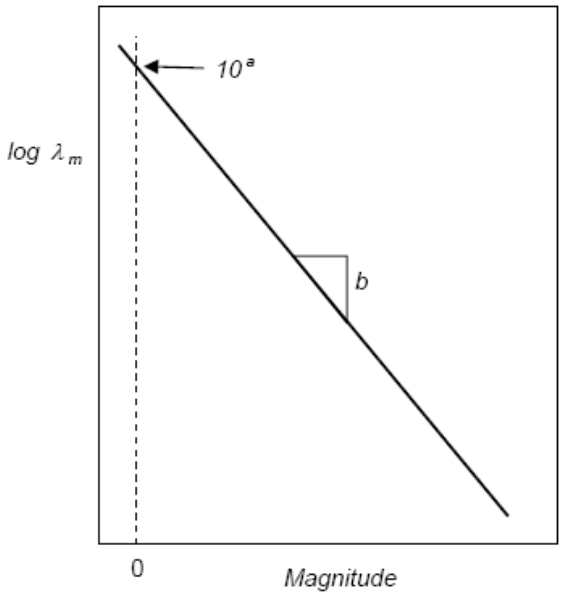

Figure 4.22: Gutenberg – Richter recurrence law, showing meaning of "*a*" and "*b*" parameters (Kramer, 1996).

Recurrence relationships provide the analysts with a tool for incorporating descriptions of the whole earthquake history. These relationships are largely data dependent. The database from which these relationships are derived consists of the historical and instrumental seismic record (Reiter, 1990) and the "*a*" and "*b*" parameters are generally obtained by regression on this database of seismicity from the source zone of interest (Kramer, 1996).

4.2.1.2 Epicenter Density Maps

In order to find the *mean annual rate of exceedence*, λ_m, ordinate of the Gutenberg – Richter relation, the number of earthquakes that exceeded different magnitudes between 1980 and 2004, are expressed by means of density maps which are prepared with "point density" extension of TNTmips 6.9. The epicenter density maps are in raster format having equal sized cells with side size of 1km. Each raster cell contains information on epicenter quantity falling within a circle having 10 km radius around that cell. As mentioned above in Gutenberg – Richter relation, the number of earthquakes occurred around a seismic source are counted first. For determination of the seismic sources, the earthquake generating characteristics of individual faults are important. Here, instead of selecting faults as sources, a continuous map representing epicenter density within a circle having radius of 10 km is prepared. However, the radius size is not an arbitrarily chosen value. It is already mentioned that the maximum depth of epicenter was selected to be 20 km for this study. Assuming that most of the faults in Western Anatolia have normal fault character having 60° dip amount, then the furthest epicenter from a fault will have about 10 km (20 / tan 60 ≈ 10) distant from that fault (Figure 4.23). Thus, considering that each fault is a single source, then the continuous map of 10 km density takes the source and the nearby epicenter number into account.

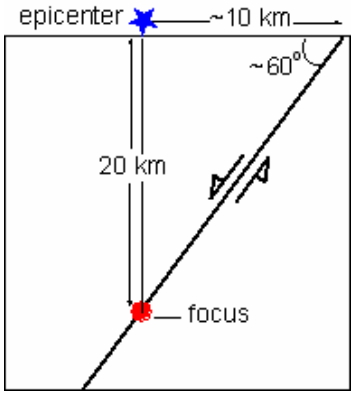

Figure 4.23: Depth – distance to fault relation for an epicenter.

Following the idea above 9 earthquake magnitudes are chosen to be threshold values for density maps. These magnitude values are 3.0, 3.2, 3.5, 3.7, 4.0, 4.2, 4.5, 4.7, 5.0. As it was previously presented the existing minimum earthquake magnitude is 3.0 and the maximum is 7.4 (17 August 1999 Earthquake). However, the earthquake magnitudes greater than 5.0 are scarcely observed (0.4 %) within the area (Table 4.2). Thus, upper and lower values of magnitude thresholds are chosen to be 5.0 and 3.0 respectively. The other 7 intermediate values are nearly equally distributed between the upper and lower thresholds. The optimum number of threshold values is chosen in order to obtain much precise graph and thus *"b"* value.

4.2.1.3 Gutenberg – Richter *b* Parameter Map

Density maps alone, only give the number of earthquakes occurred within an area, however, they do not provide the seismic character of that area. Gutenberg – Richter's *b* parameter, on the other hand, is a kind of indicator of density related to magnitude and time. Thus, using this map it will be investigated whether the geothermal occurrences are related to low magnitude earthquakes or high magnitude earthquakes.

The *b value* in Gutenberg – Richter law is the slope of the linear relationship between the magnitude and recurrence. Because the relationship has decreasing recurrence interval with increasing magnitude, the *b values* will always be negative. Thus, if the absolute value of *b* is large, then it means that low magnitude earthquakes occur much more frequently within their source when compared to high magnitude earthquakes.

In order to obtain the *b value* map the following procedure is applied:

1. First the density maps are obtained for the earthquake magnitudes previously defined (3.0, 3.2, 3.5, 3.7, 4.0, 4.2, 4.5, 4.7, 5.0) separately.

2. As the density maps are in raster format each pixel within the raster contain information on number of earthquakes with a search radius of 10 km. On the other hand, the area of each pixel is 1 km^2 and each pixel in the density maps is divided by recurrence interval which is constant. For this study, as earthquakes occurred between 1980 and 2004 is taken into account, hence the recurrence interval come out to be 25 years. In this way, a raster, in which, each of its pixels contain mean annual occurrence of earthquakes is obtained.

3. The logarithm of each cell is taken excluding those having value of “0” (no eq) to prevent pixels having undefined values. Generally the density maps with higher magnitudes have “0” valued pixels as the number of large earthquakes are relatively rare within the area (Table 2.2).

4. A point vector is created by assigning a point to the center of each pixel (Figure 4.24).

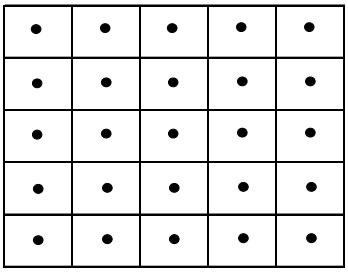

Figure 4.24: Point vector with centered points in each pixel.

5. The values obtained in step 3 for each map are entered in the database of the point vector. Thus, each point had 9 different attributes representing the logarithm of mean annual exceedance of each map (Figure 4.25).

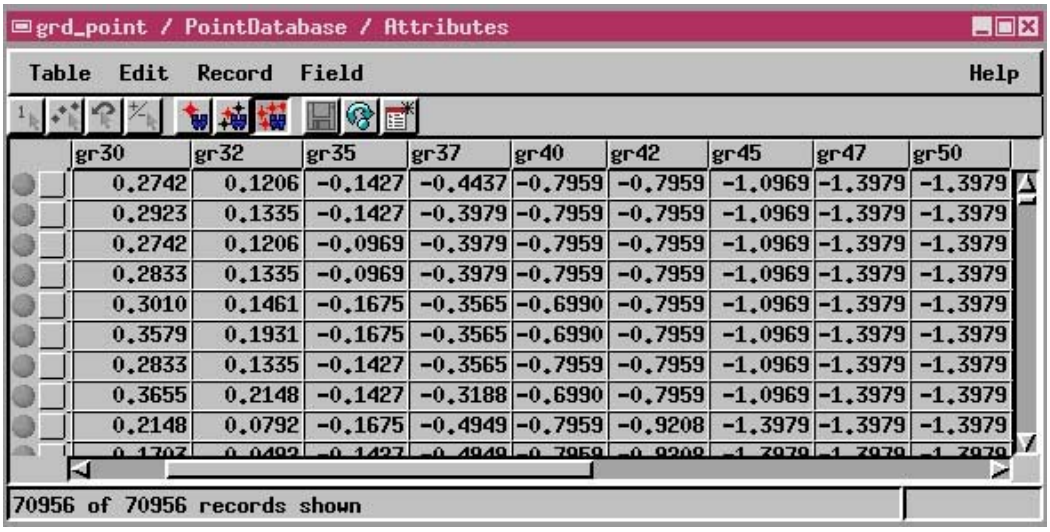

gr30	gr32	gr35	gr37	gr40	gr42	gr45	gr47	gr50
0.2742	0.1206	-0.1427	-0.4437	-0.7959	-0.7959	-1.0969	-1.3979	-1.3979
0.2923	0.1335	-0.1427	-0.3979	-0.7959	-0.7959	-1.0969	-1.3979	-1.3979
0.2742	0.1206	-0.0969	-0.3979	-0.7959	-0.7959	-1.0969	-1.3979	-1.3979
0.2833	0.1335	-0.0969	-0.3979	-0.7959	-0.7959	-1.0969	-1.3979	-1.3979
0.3010	0.1461	-0.1675	-0.3565	-0.6990	-0.7959	-1.0969	-1.3979	-1.3979
0.3579	0.1931	-0.1675	-0.3565	-0.6990	-0.7959	-1.0969	-1.3979	-1.3979
0.2833	0.1335	-0.1427	-0.3565	-0.7959	-0.7959	-1.0969	-1.3979	-1.3979
0.3655	0.2148	-0.1427	-0.3188	-0.6990	-0.7959	-1.0969	-1.3979	-1.3979
0.2148	0.0792	-0.1675	-0.4949	-0.7959	-0.9208	-1.3979	-1.3979	-1.3979

Figure 4.25: The snapshot of the point database with logarithm of mean annual exceedence values for different maps.

6. The point database is exported to MS Excel for convenience in further processes. The database is modified to obtain a meaningful regression line by excluding the “0” values and repeated values. Since “0” values, which were excluded from step 3, represent pixels having no, they have no meaning in terms of Gutenberg-Richter parameters. The repetitive values on the other hand are omitted because if a pixel belonging to identical row and column in all maps has same value in more than one map, then this value should belong to the map with the highest magnitude. Thus, the value of the map with the highest magnitude is kept while the other repetitive values are removed from the database (Table 4.3).

Table 4.3: An example of a row extracted from the point database. The shaded values are removed.

MAGNITUDE						
< = 3.0	< = 3.2	< = 3.5	< = 3.7	< = 4.0	< = 4.2	< = 4.5
-0,55280	-0,69900	-1,09690	-1,39790	-1,39790	-1,39790	0,00000

7. The “b” value is calculated for each row by using linear regression formula as stated below. The “b” value corresponds to the slope of the linear best line of the scatter plot of points within each row (Figure 4.26).

$$b = \frac{n\left(\sum xy\right) - \left(\sum x\right)\left(\sum y\right)}{n\left(\sum x^2\right) - \left(\sum x\right)^2} \tag{4.5}$$

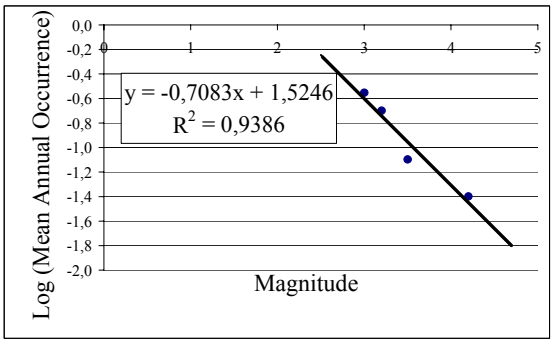

Figure 4.26: Plot of row in Figure 4.25.

8. The database with calculated “b” value is exported to TNTmips as point vector. The point vector is converted to raster using “b” values and in this way the “b” value map is obtained (Figure 4.27).

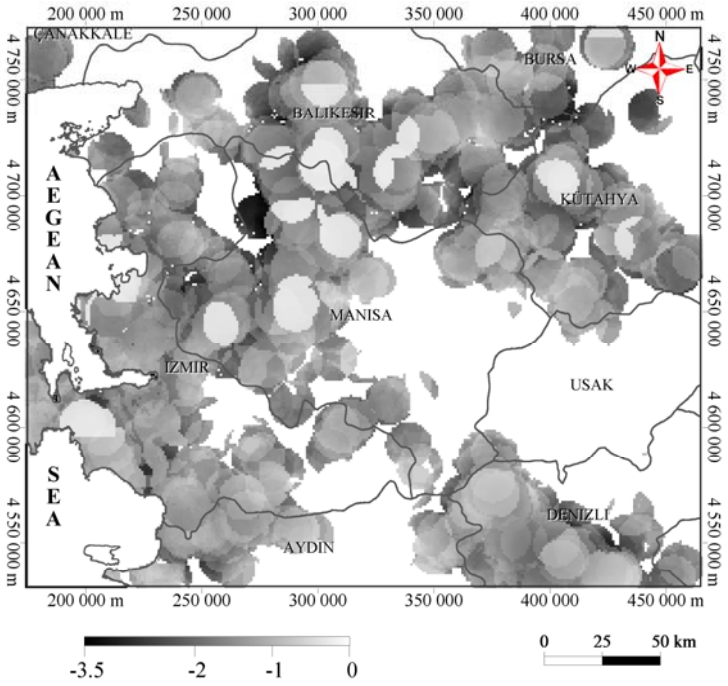

Figure 4.27: *b-value* map of the study area.

The procedure followed in constructructing the *b-value* map is shown schematically in Figure 4.28.

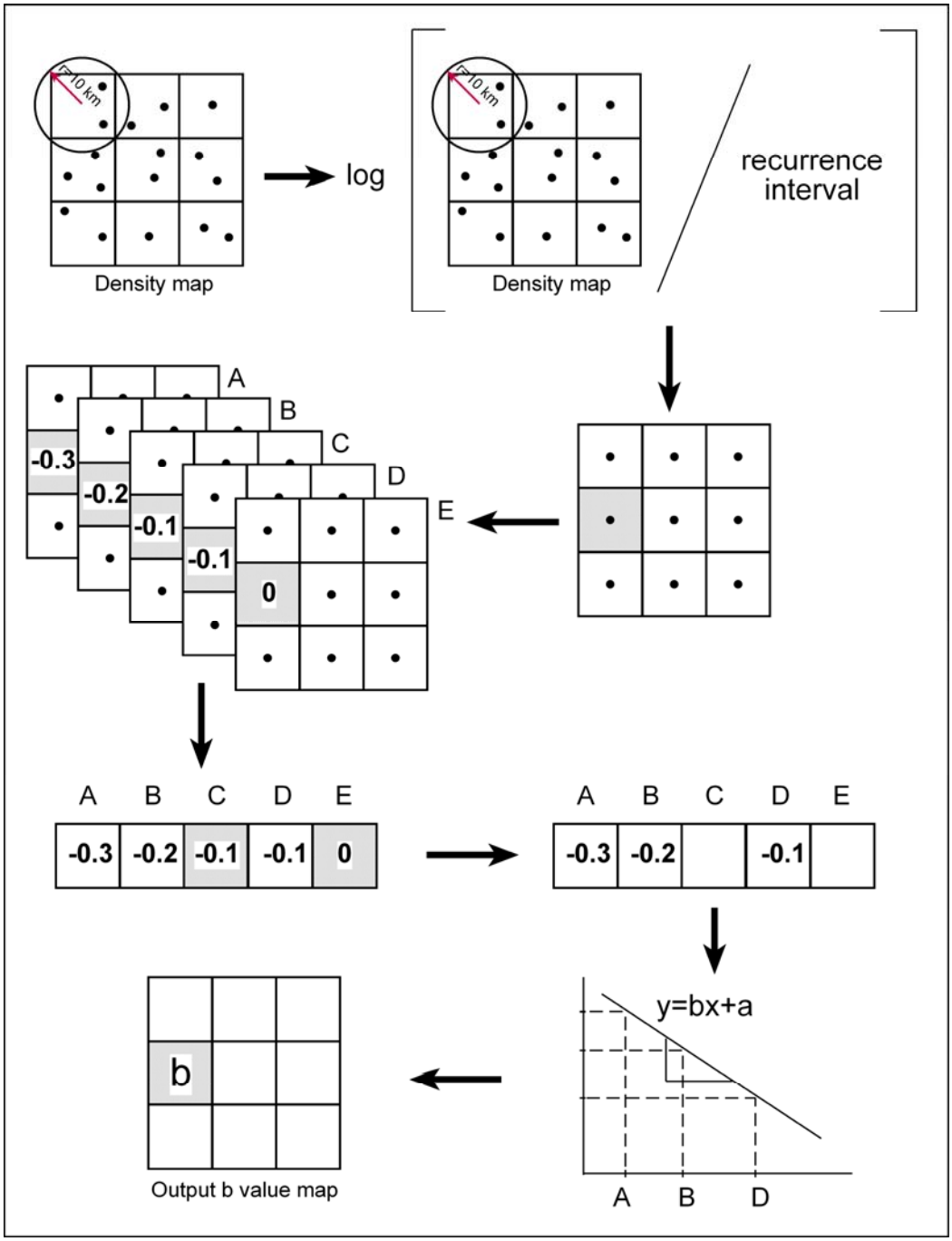

Figure 4.28: Schematic explanation for generation of b-value map.

Finally the map is overlaid by epicenter distribution map (Figure 4.29a) in order to observe the effect of magnitude and the *b-value*. As it is observed, high magnitudes corresponds to lower *b-values* when compared to low magnitudes. The same overlay operation is performed with geothermal occurrence points (Figure 4.29b) to investigate the relation of occurrences with the *b-value*.

As a final point, it is interpreted that nearly 75 % (58 out of 77) of the geothermal occurrences are related to seismic activity of low to medium magnitude earthquakes, while the rest 25 % (19 out of 77) occurrences seem not to be related to seismicity.

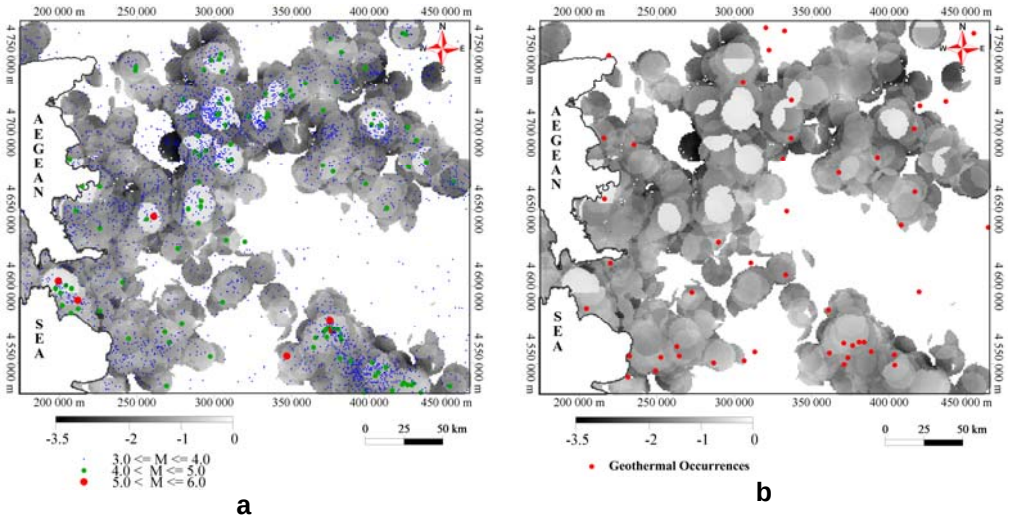

Figure 4.29: a) Overlay of b-value map with epicenter distribution map; **b)** Overlay of b-value map with distribution of geothermal occurrences map.

4.2.2 Distance to Lineament Map

Similar to earthquakes, the relation between lineaments and geothermal occurrences was investigated by means of clusters, and it was found out that there is a relation between the lineaments and the geothermal occurrences. However, the investigation of the cause of this relation is essential for the further analysis. As the faults, create a path to heated water beneath the surface then somewhat the occurrence of this water should be in some vicinity of the fault. To determine the amount of this vicinity, the lineament map which is in vector format is converted to distance raster. Each cell in the distance raster contains information on the orthogonal distance to the nearest line (Figure 4.30). According to the map nearly all of the geothermal occurrences are found out to be in the vicinity of less than 10 km.

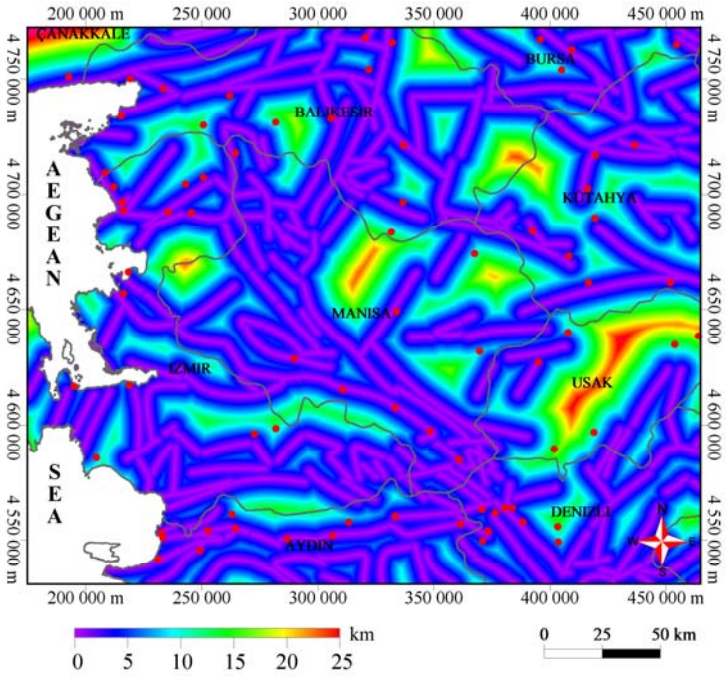

Figure 4.30: Distance to lineament map.

CHAPTER 5

ANALYSIS

Following the preliminary introduction about the relation between the geothermal occurrences and each raw data in chapter 4, the methods introduced in chapter 3 will be applied on the synthetic data. It should be noted that the aim of the methods is to predict the relative geothermal favorability within the study area.

The synthetic data layers are generally multiclass maps. However it was previously mentioned that both of the methods, Boolean logic model and WofE, are applied on binary maps. Thus, as a first step, the decision rules of binary classification are explained and then the multiclass maps are converted to binary maps. Then, the pairwise conditional independence of the maps is investigated. Afterwards, as a second step the binary maps are overlaid through two methods separately. The third step contains comparison of the output maps resulted from the Boolean Logic model and WofE method. Here, the methods are evaluated by means of their success of predicting the potential geothermal sites and it is also checked how well they coincide with each other. The last step, which is sensitivity analyses are carried out for the same methods but depending on different binarization techniques to ascertain the best binary classification procedure. Thus, in this step after the binary classification through different procedures is carried out, the previous three stages are repeated and accordingly output maps for both of the overlay methods is generated for each binary classification procedure. The scheme in Figure 5.1 summarizes the steps followed in this chapter.

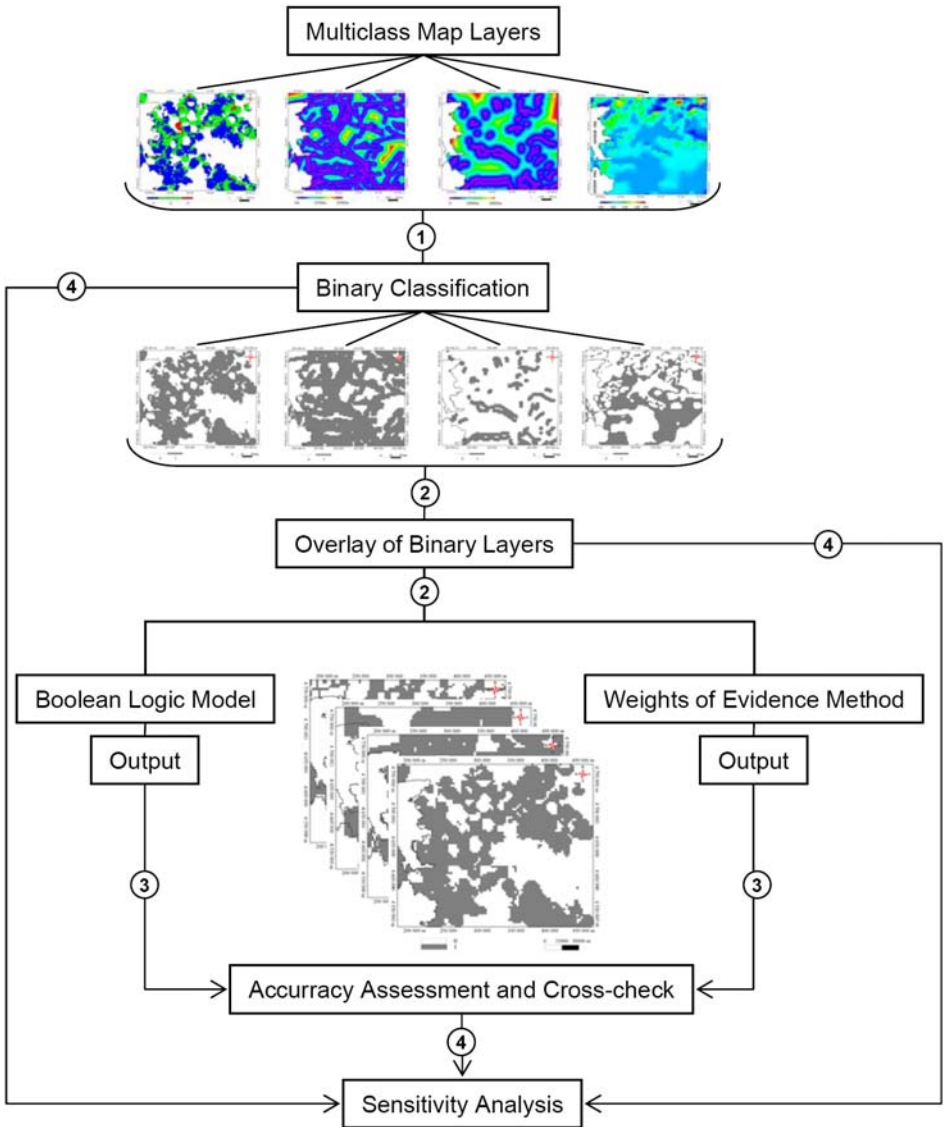

Figure 5.1: Scheme showing the steps in analysis.

5.1 Binary Classification of Evidential Themes

Binary classification process includes converting multiclass maps into two valued maps, where value of “1” indicates favorable and value of “0” indicate unfavorable areas for each map. In order to decide the threshold value of binary maps and maximizing the spatial association between the occurrences and evidential themes, the statistical relation of these maps and occurrences are investigated. The multiclass evidential themes and the geothermal occurrences on each theme are shown in Figure 5.2.

It can be visually interpreted that the geothermal occurrences lie in the vicinity of lineaments (Figure 5.2b) and estimated grabens (Figure 5.2c) before the statistical calculations are performed. For the “b” value map it can be said that the occurrences are related to “b” values between -1 and -2 (Figure 5.2a). However, no comment can be done by visual interpretation about spatial relation of occurrences with magnetic anomaly map, except an inference that the “geothermal” occur within negative magnetic anomaly, which covers rather wide range of the area (Figure 5.2d).

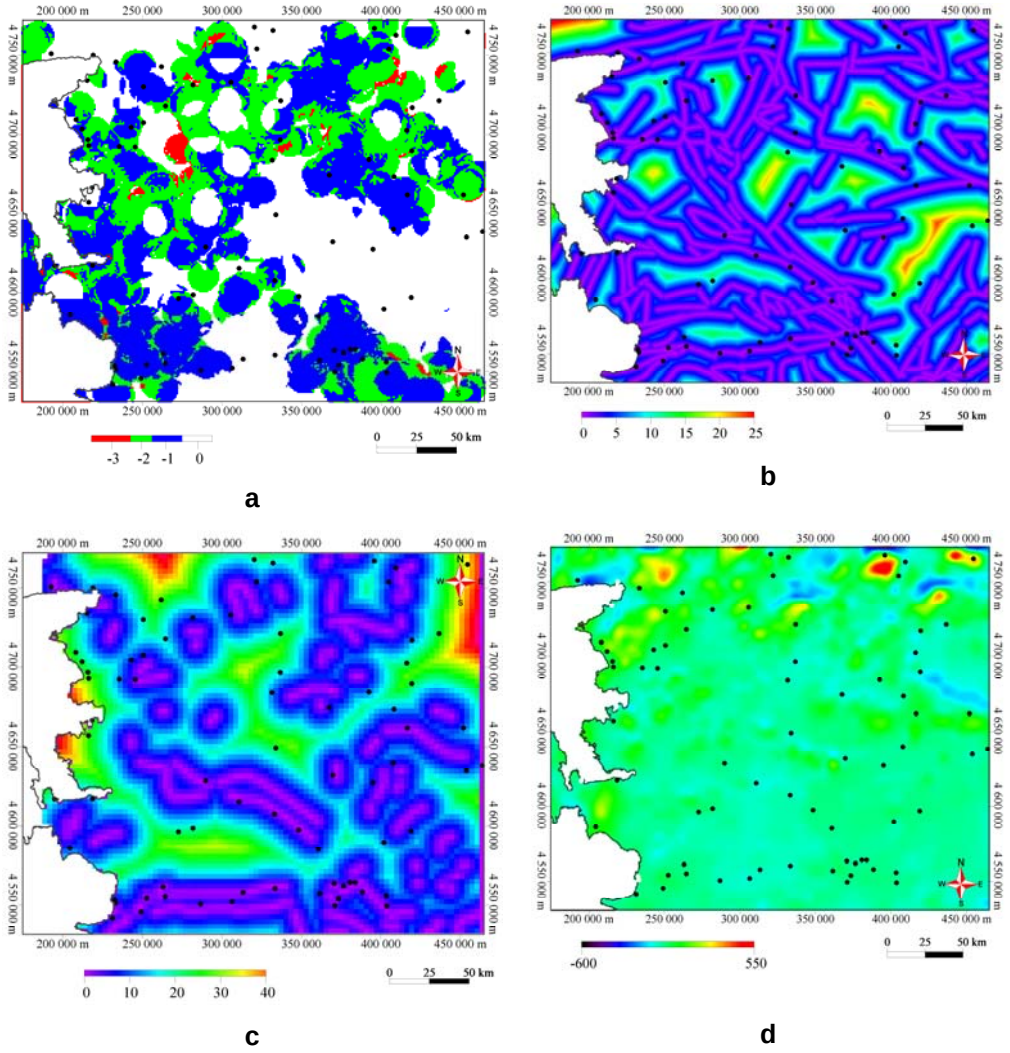

Figure 5.2: Multiclass evidential themes and geothermal occurrences; **a)** b-value map; **b)** Distance to lineament map; **c)** Distance to major grabens map; **d)** Magnetic anomaly map.

The basic problem in binary classification process is to decide about the cutoff value between 1 and 0. The class ranges falling in each of these two values should be decided so that minimum occurrences will be missed and the search area will be as narrow as possible. If the binary pattern is chosen to be too small then the data/case missing problem is quite possible to occur, while the second problem will arise when the binary pattern is too large, as every data/case will be included. Thus, it is vital to investigate statistically the values of evidential themes falling under the occurrences. In this way, if there is any, the preference values of geothermal occurrences for each predictor map will be figured out. In order to do this, the cell values falling under geothermal occurrence for each map is transferred to point database of geothermal occurrences (Figure 5.3).

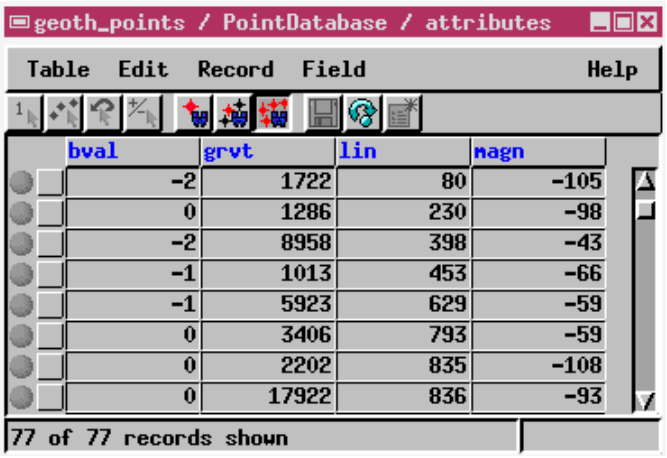

Figure 5.3: Point database of each evidential theme.

Using this database the descriptive statistics for each evidential theme is calculated and corresponding histograms with normal curves are produced (Table 5.1 and Figure 5.4). It is clear from the descriptive statistics that both gravity and lineament variables lay on a wide range. Their standard deviation is nearly close to their mean value. This is because both of the variables indicate distance to the closest feature. In other words, an occurrence may be present very close to either lineament or grabens, while the other may occur rather far from these features, which is the case. The minimum distances to grabens and lineaments are 210 m and 24 m, while the maximum distances are nearly 35 km and 15 km, respectively. Hence, there is a high deviation from the mean, which is supported with shallow wide normal curves on the histograms. The “b” value variable, on the other hand, includes only integers ranging from 0 to -3. Its mean do not deviate much as it can be also observed from its normal curve. The

magnetic anomaly variable has positive values as well as negative ones. However, it is clear from its histogram that the most values are negative and that is why its mean appear to be negative also. In addition, the deviation from the mean does not enter the positive range of this variable.

Table 5.1: Descriptive statistics of evidential theme values falling under each geothermal occurrence point.

	N	Range	Min.	Max.	Mean	Std. Dev.
"b" Value	77	3	-3	0	-,78	,772
Gravity	76	34653	210	34863	10561,5	8490,474
Lineament	76	15322	24	15346	3512,25	3324,481
Magnetic	76	438	-151	287	-61,30	62,748

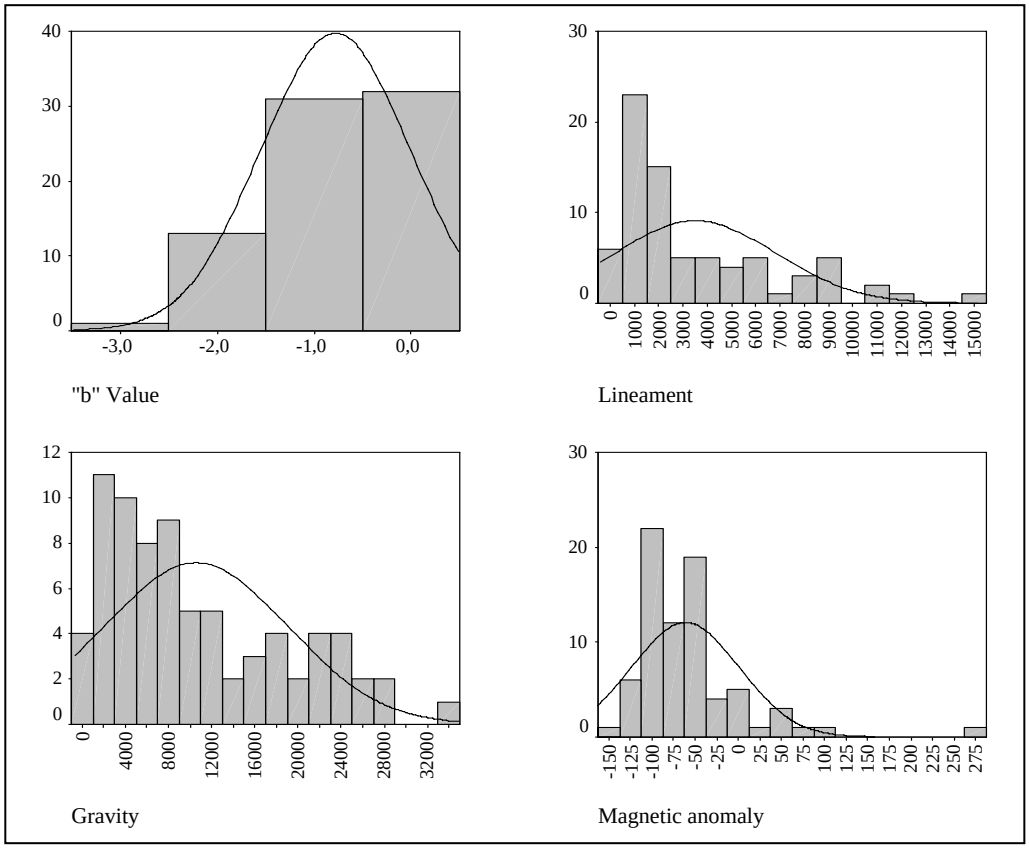

Figure 5.4: Histograms with normal curves belonging to each evidential theme.

Using the histograms and descriptive values it is decided to perform binary classification using the mean and the standard deviation values for each evidential theme. Thus, the range of “mean ± Standard deviation” is concluded to be represented by 1 and the rest by 0. In other words, the binary maps are obtained by assigning 1 to the areas falling in the range, while the rest of areas for each map are assigned the value of 0 (Figure 5.5).

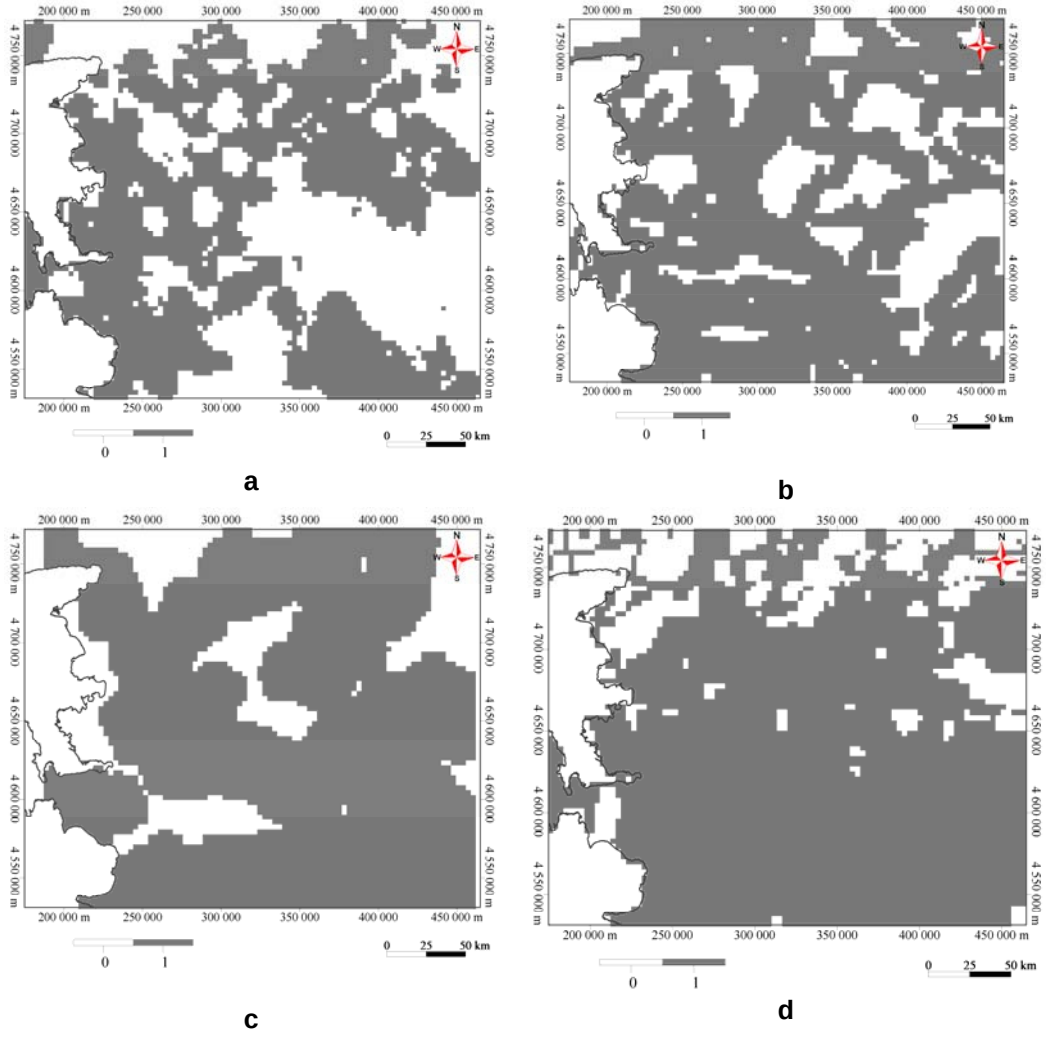

Figure 5.5: Binary pattern obtained by mean ± SD procedure; **a)** Binary map for “b” value evidential theme; **b)** Binary map for distance to lineament evidential theme; **c)** Binary map for distance to major grabens evidential theme; **d)** Binary map for magnetic anomaly evidential theme.

For the “b” value map, the mentioned range is roughly between -1.5 and 0 (-0.78 ± 0.772). However, “0” has no practical meaning for this evidential theme, as this value means that the recurrence of earthquakes having different magnitudes is same, which is

usually not possible. Thus, the range that will be represented by 1 in the binary map is chosen to be between -1 and -2. For the other three maps the range is chosen depending on deviation from the mean. The concluded ranges to be assigned as “1” for these maps are set up as following:

Distance to lineament: 0 – 7000 (3512.25 ± 3324.481)

Distance to major grabens: 0 – 20000 (10561.5 ± 8490.474)

Magnetic anomaly: 0 – (-120) ((-61.30) ± 62.748)

5.2 Conditional Independence

The conditional independence between each map pair should be checked in order to decide whether all of the maps are suitable for using in WofE analysis or not. If a pair is concluded to be dependent then one of the evidential themes within these pairs should be kept out of the analysis. To check the conditional independence, first observed and expected values are calculated according to equation 2.25 introduced in chapter 2 (Figure 5.6).

OBSERVED								
	B+	B-	G+	G-	L+	L-	M+	M-
B+			39	8	38	9	38	9
B-			23	8	22	9	23	8
G+					46	16	49	13
G-					14	2	12	4
L+							44	16
L-							17	1

EXPECTED								
	B+	B-	G+	G-	L+	L-	M+	M-
B+			31,0	8,0	30,0	9,0	30,5	8,5
B-			24,6	6,4	23,9	7,2	24,2	6,8
G+					47,7	14,3	48,5	13,5
G-					12,3	3,7	12,5	3,5
L+							46,9	13,1
L-							14,1	3,9

Figure 5.6: Observed and expected values for each map pair.

For each pair there are four possible conditions, where both are present or absent, or one of the pairs is absent. Here the presence of each map is indicated with (+) sign and absence with (-) sign. Each different letter stands for different binary evidential theme, that is “B” represent “b” value map, “G” represent distance to major graben map, “L” is used for distance to lineament map, and “M” for magnetic anomaly map.

After the pairwise calculation of observed and expected numbers of binary maps is performed, the X^2 test is applied using equation 2.26 where the null hypothesis assumes that map pairs are conditionally independent with significance level of 95% and 1 degree of freedom which is tabulated as 3.84 (Figure 5.7). As none of the

obtained X^2 values exceed the tabulated X^2 value, there is no reason to reject the null hypothesis of conditional independence.

X^2				
	B	**G**	**L**	**M**
B		2,6	2,8	2,2
G			1,3	0,1
L				3,6

Figure 5.7: X^2 values obtained for testing CI of map pairs with 95 % significance level and 1 degree of freedom, $X^2 = 3.84$.

5.3 Potential Areas According to Boolean Logic Model

The Boolean logic model constructed for determining relative favorability of geothermal occurrences includes the following constraints about the presence of the occurrences:

1. Be in certain distance to linear structures **OR**
2. Be in the vicinity of major grabens **OR**
3. Be in steep slope of “b” values indicating high recurrence for low magnitude earthquakes **OR**
4. Be in negative magnetic anomaly

Each layer is related with “OR” Boolean operation, because it is assumed that each of the evidential themes alone has equal influence on the geothermal occurrences. The “OR” operation is represented by the addition of the binary map layers rather than their union. In this way, the resulting map will have “0” value, where none of the layers are present, “1” where only one out of four layers is present, “2” where two of four, “3” where three of four and “4” where all layers are present (Figure 5.8).

The area of each cell in the resulting map is 10 km^2. Because it was previously assumed that wells and springs falling within 10 km^2 represent one geothermal occurrence, the value of each cell in the output map represent its favorability of containing a geothermal occurrence.

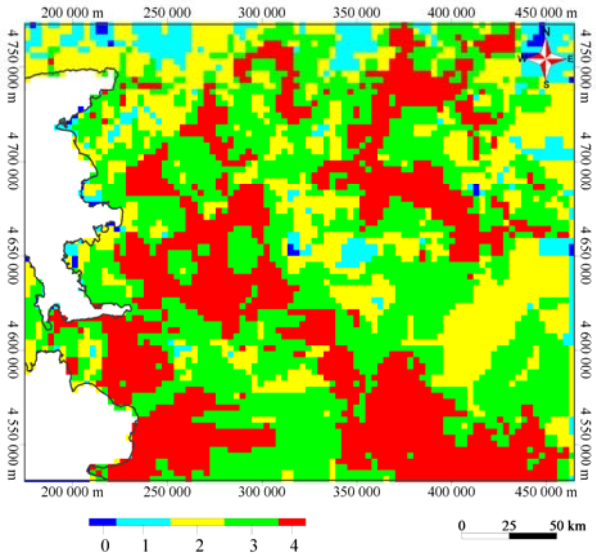

Figure 5.8: Result map of Boolean logic model.

As each layer is said to have equal influence, the areas where all of the layers are present can be accepted as very favorable, the areas where three of the layers exist as favorable, while the areas where two, one and none of the layers are present can be accepted as unfavorable. According to this assumption the resulting map is reclassified so that it ranges from 1 to 3, namely from unfavorable to very favorable, as shown in Table 5.2. After the reclassification the resulting map presented in Figure 5.9 is obtained.

Table 5.2: Real and reclassified cell values with their favorability condition.

Real cell value ranges	Reclassified cell value	Favorability
0-2	1	Unfavobale
3	2	Favorable
4	3	Very Favorable

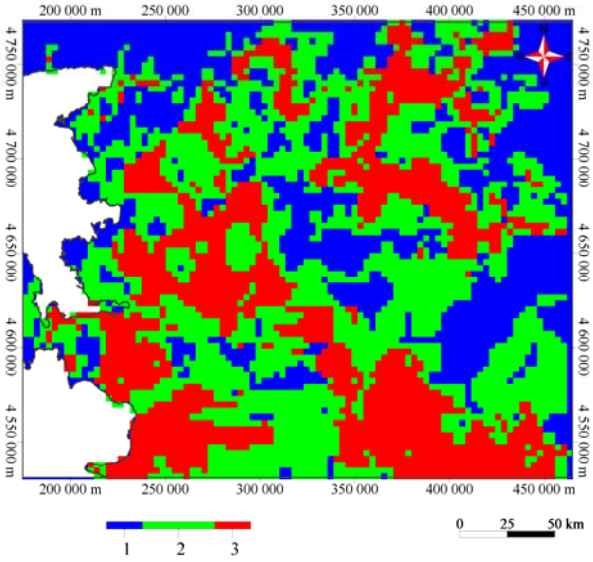

Figure 5.9: Reclassified Boolean output map.

5.4 Potential Areas According to WofE Method

Following the decision about the limits of binary maps and checking for the pairwise conditional independence, all layers are found out to be suitable for WofE analysis. The prior probability of geothermal occurrence within the whole area is found out to be 0.011. On the other hand, the positive and negative weights for each evidence layer, as well as their contrast and posterior probabilities are calculated using corresponding formulas introduced in chapter 2 (Table 5.3).

Table 5.3: Weights, contrast and posterior probabilities of evidence layers.

	W+	W-	Contrast	Posterior Probabiliy
"b" Value	0,2045	-0,2544	0,4589	0,0133
Distance to lineament	0,1303	-0,3585	0,4888	0,0124
Distance to grabens	0,0969	-0,3233	0,4202	0,0120
Magnetic anomaly	0,0386	-0,1256	0,1642	0,0115

In order to create the response map, namely the resulting map of probability of occurrences, each evidence layer is assigned its positive value where the pattern is

present and its negative value where the pattern is absent. Then all layers and the logit of prior probability are added and their exponential are taken to obtain posterior odds. Finally, the posterior probabilities of resulting map is obtained by dividing posterior odds by (1 + posterior odds). To clarify the idea, each step of the process is explained below (Modified from Bonham – Carter, 1996):

The prior logit of the prior probability of 0.0109:

Prilogit = Ln (0.011/(1 – 0.011))

For each cell calculate the probability by assigning W+ to cells where the pattern is present and W- where the pattern is absent:

B = If (bValue = = 1) Value = 0.2045

else Value = -0.2544

L = If (dist_linValue = = 1) Value = 0.1303

else Value = -0.3585

G = If (dist_grabenValue = = 1) Value = 0.0969

else Value = -0.3233

M = If (magnValue = = 1) Value = 0.0386

else Value = -0.1256

Posterior logit equals prior logit plus sum of weighted maps:

Pstlogit = Prilogit + B + L + G + M

Convert to posterior odds:

Pstodds = exp(pstlogit)

Convert to posterior probability:

Pstprob = pstodds / (1+pstodds)

The response theme is obtained:

OUT = pstprob

In this way the resulting map of posterior probabilities of geothermal occurrences are obtained (Figure 5.10).

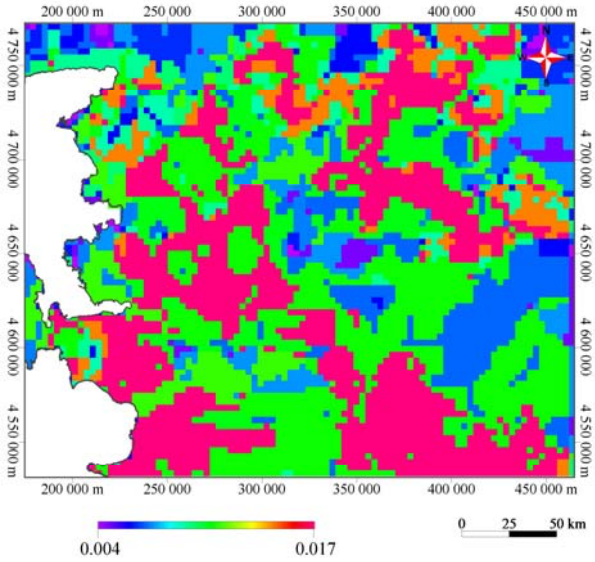

Figure 5.10: Resulting map of WofE method.

The response theme has several values ranging from 0.004 to 0.017. In this case, it should be decided about the threshold above which the occurrence will be accepted as favorable. Obviously, this threshold should be the value of prior probability. Because when there is no evidence layer, every cell within the map would be equally probable having the value of prior probability. However, decision about the threshold is not enough. The response theme should be reclassified so that it will have 3 classes ranging from unfavorable to very favorable. That is why the raster histogram of the response theme is investigated first (Figure 5.11). The mean value of raster cell is nearly equivalent to prior probability (0.011). Thus, the values lower than the mean are assigned as unfavorable. The favorable areas, on the other hand are decided to be those which are one standard deviation large from the mean (0.011 – 0.015). Finally, values greater than (mean + SD) are concluded to be very favorable (Figure 5.11). The exact ranges and assigned classes are tabulated in Table 5.4.

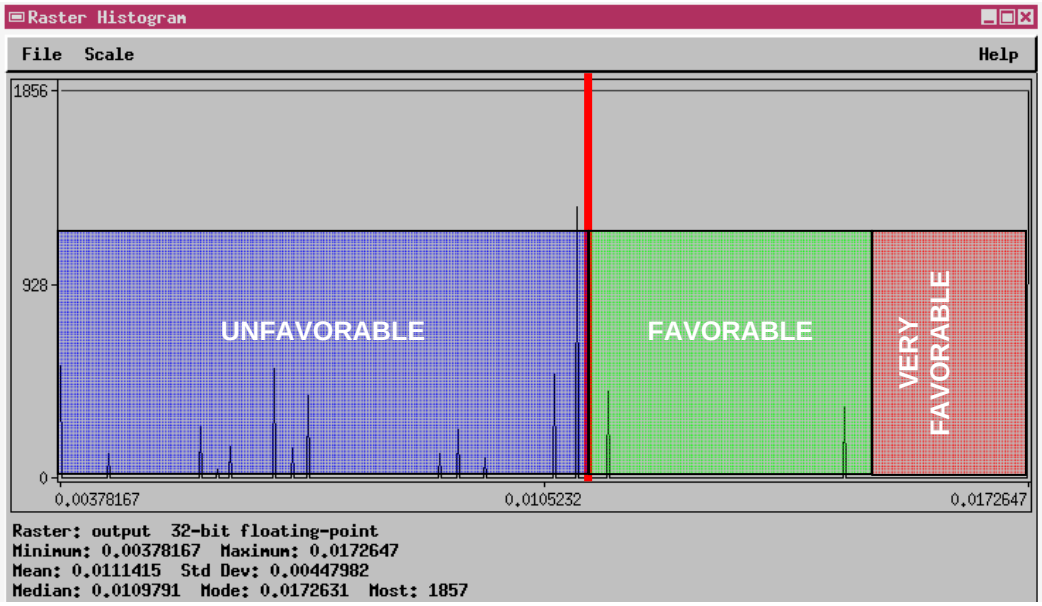

Figure 5.11: Raster histogram of response theme.

Table 5.4: Cell value ranges and reclassified cell values with their favorability condition.

Real cell value ranges	Reclassified cell value	Favorability
<0,011	1	Unfavobale
0,011-0,015	2	Favorable
>0,015	3	Very Favorable

According to this classification, the response theme is rearranged and the three classed result map shown in Figure 5.12 is obtained.

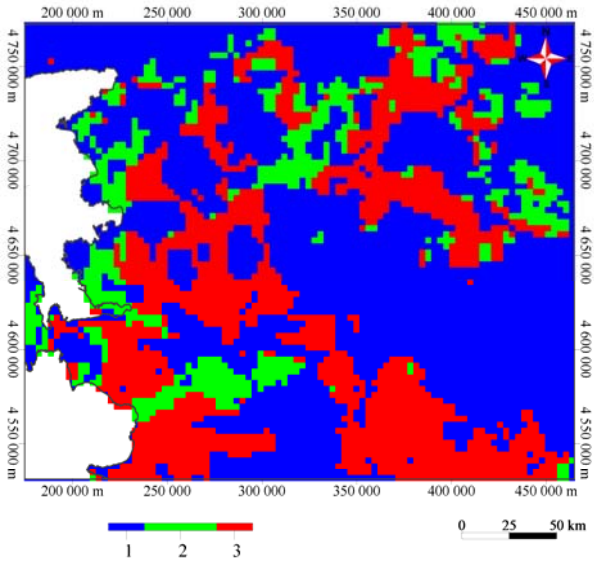

Figure 5.12: Reclassified map of the response theme.

5.5 Accuracy Assessment and cross-check of the Potential Areas

Comparison of two output maps obtained by Boolean logic model and WofE method is performed by checking the class values of both maps mutually (Figure 5.13a and b).

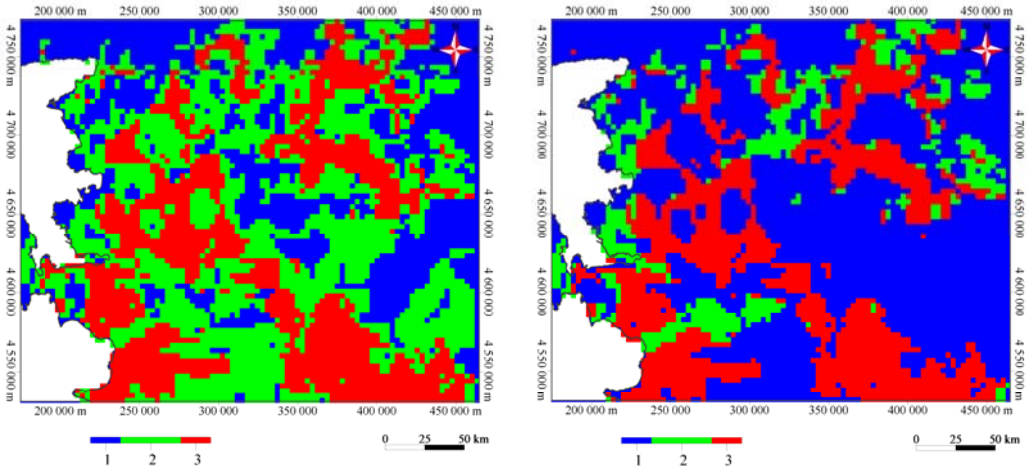

a **b**

Figure 5.13: a) The resultant map of Boolean logic model; **b)** The resultant map of WofE method.

The easy way of comparing two maps is to multiply one of the maps by 10 and adding the maps together. Thus, if the sum of a cell is 31 for example it means that for that cell the class value of the map multiplied by ten is 3, while this value is 1 for the other map. By using this method, two output favorability maps are compared and the matrix of the comparison as well as the bar diagram showing the percentages of the fit between cell values are shown in Figure 5.14a and b respectively.

Boolean \ WofE	1	2	3
1	1800	80	15
2	1688	582	253
3	222	72	1557

a

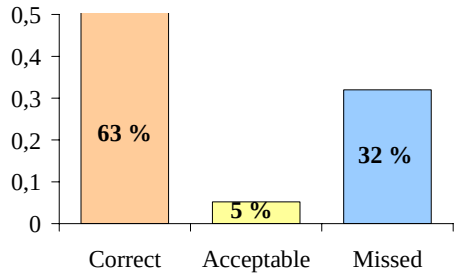

b

Figure 5.14: a) Matrix showing the comparison of two resultant map classes; **b)** The bar diagram showing correct, acceptable and missed classes after the comparison of two resultant maps.

As it is observed from the comparison matrix, the cell values of Boolean method usually goes beyond those of the WofE method. For example, most of the cells of Wofe which belong to class 1, that are unfavorable, appear to have value of class 2, which are favorable, for the Boolean method,. Similarly, the most of unfavorable areas in WofE turn to be favorable in Boolean model which can also be observed from the map in Figure 5.15. It is the classification map of correct, acceptable and missed classes obtained after the comparison of two resultant maps. In this map most of the blue areas, which represent missed classes, correspond to class 2 (favorable) in Boolean model (Figure 5.13a) and class 1 (unfavorable) in WofE (Figure 5.13b) model. Thus, it can be claimed that Boolean model overestimates the likelihood of favorability when compared to WofE method.

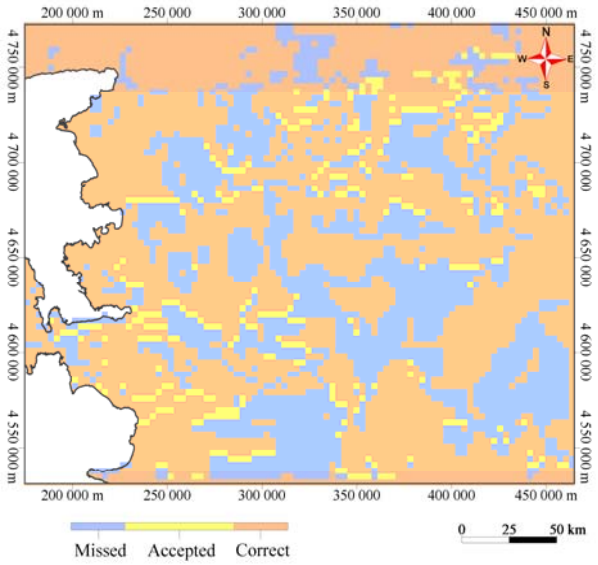

Figure 5.15: Classification map of correct, acceptable and missed classes.

In order to check how successful the Boolean output map is, the geothermal occurrence points falling in each class are counted and the resulting number is divided to the area of that class. In this way an index representing the success of the result map is obtained (Table 5.5).

Table 5.5: Point count in each resultant Boolean class and the success index.

Favorability	Reclassified cell value	Area	Point count	Index
Unfavobale	1	18950	23	0,00121
Favorable	2	25230	30	0,00119
Very Favorable	3	18510	24	0,0013

According to the table it is concluded that the Boolean logic method successfully predicts the areas where geothermal occurrences are present. At total it has predicted that 54 out of 77 occurrences lie on the favorable and very favorable areas.

Similar to the Boolean logic model, to check the success of the WofE output map from geothermal occurrence point of view the occurrences falling in each class are counted and the resulting number is divided to the area of that class to obtain the index of success (Table 5.6).

Table 5.6: Point count in each resultant WofE class and the success index.

Favorability	Reclassified cell value	Area	Point count	Index
Unfavobale	1	37100	41	0,00111
Favorable	2	7340	11	0,0015
Very Favorable	3	18250	25	0,00137

According to the calculated index it is concluded that the WofE method predicts some of the areas where geothermal occurrence is present. At total it has predicted that 36 out of 77 occurrences lie on the favorable and very favorable areas.

Although it seems that WofE method is worse predictor than the Boolean logic model due to the predicted number of occurrences, this is not the case. Due to the fact that this method restricts the area of favorability, it includes smaller amount of points in favorable areas. The Boolean method on the other hand, covers large areas of "favorable" regions because these areas are the intersection of any three maps out of four evidential layers. Thus, the prediction of favorability in Boolean method has rather high spatial range. That is why the success index depends on the number of points in each class divided by the area of that class. If the indices of both methods are taken into account it will be realized that the WofE method (0.00287) turns to be more successful than the Boolean logic model (0.00249).

5.6 Sensitivity Analysis

As previously mentioned the binary map classification constitutes the base of application of both methods. Therefore, the process needs to be applied with caution. In the preceding subchapter the binarization procedure was based on primary statistical characteristics of evidential themes. However, due to the nature of the maps the range which was considered as favorable and thus assigned value "1" for the binary maps appeared to be quite wide, leading to large binary pattern for some of the maps. Hence, here, with the purpose of optimizing the binary model two more binarization techniques will be introduced.

Besides the (mean ±SD) procedure, another approach can be used to decide about the binary pattern by evaluating weights, contrast and number of points present in each division of multiclass maps. In order to apply this procedure, first each map layer is assigned a class value which represents a particular range of the actual map value. Then, the positive and negative weights, the contrast and the number of points occurred in each division are calculated for every class. Afterwards, the class which maximizes, the positive weight, the contrast and the number points occurred, is decided to be in the

favorable category. Table 5.7 illustrates ranges of each map class, including their weights, contrasts, number of points existing within each class and the corresponding binary map value assigned for each map class.

Table 5.7: Weight contrast values and point numbers within each class of evidential themes.

	Map Value	Class	Number of Points	W^+	W^-	Contrast	Binary Map Value
b - value	0	0	25	-0,2475	0,1299	-0,3774	**0**
	-1	1	28	0,2507	-0,1008	0,3515	**1**
	-2	2	20	0,0690	-0,0190	0,0880	**0**
	-3	3	4	-0,9000	0,0619	-0,9618	
Distance to major grabens	< 5	1	26	0,5398	-0,1763	0,7162	**1**
	5-10	2	19	0,1475	-0,0439	0,1914	**0**
	10-15	3	10	-0,3491	0,0644	-0,4135	
	15-20	4	8	-0,2665	0,0360	-0,3025	
	20-25	5	7	0,0695	-0,0067	0,0762	
	> 25	6	7	-0,6848	0,1035	-0,7883	
Distance to lineament	< 2	1	34	0,5181	-0,2594	0,7775	**1**
	2-4	2	15	-0,1045	0,0270	-0,1316	**0**
	4-6	3	10	-0,0722	0,0112	-0,0835	
	6-8	4	5	-0,4116	0,0360	-0,4476	
	8-10	5	6	0,2277	-0,0171	0,2448	
	> 10	6	7	-0,8646	0,1478	-1,0123	
Magnetic anomaly	(-150)-(-100)	1	21	-0,0879	0,0351	-0,1230	**0**
	(-100)-(-50)	2	33	0,1635	-0,0863	0,2498	**1**
	(-50)-0	3	12	0,3438	-0,0523	0,3961	**0**
	0-50	4	5	0,4948	-0,0267	0,5216	
	50-100	5	2	0,1982	-0,0048	0,2029	
	100-150	6	1	0,1144	-0,0014	0,1158	

According to Table 5.7 the map value of b-map maximizing weights, contrast and number of points is “-1”, the distances to structural events are smaller than 5km for grabens and smaller than 2 km for lineaments, and the best class of magnetic anomaly map representing the occurrences of “geothermal” is set up between (-100) and (-50). All of these ranges are assigned 1 and the rest is given value of 0 and the maps are binarized (Figure 5.16).

Note that some of the positive weights are found to be negative. This is because on these classes the posterior probability for is smaller than the prior probability of the occurrence. That is to say, fewer points occur on this pattern than would occurr due to chance.

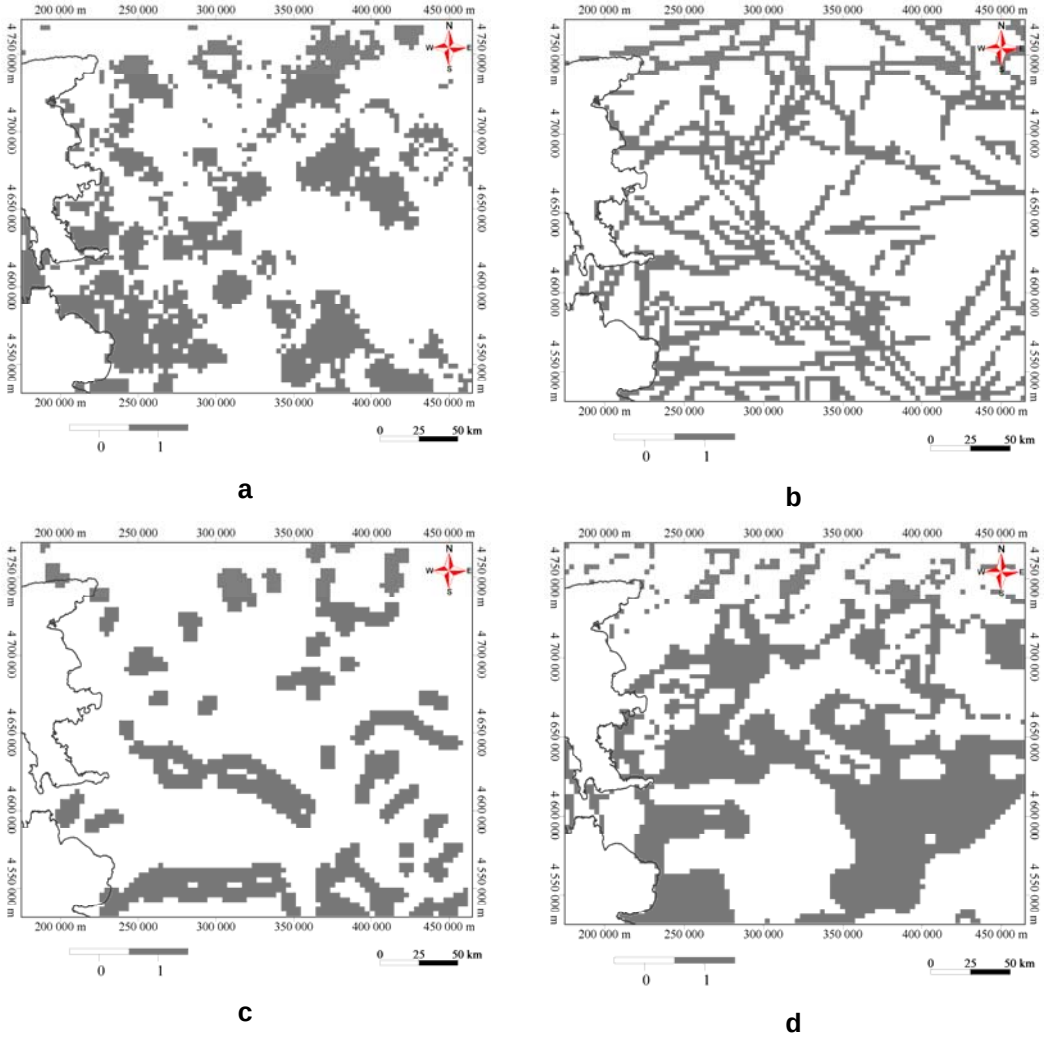

Figure 5.16: Binary patterns obtained by weight-contrast procedure; **a)** Binary map for "b" value evidential theme; **b)** Binary map for distance to lineament evidential theme; **c)** Binary map for distance to major grabens evidential theme; **d)** Binary map for magnetic anomaly evidential theme.

After the binarization the application of the methods is strightforward as defined previously. All of the maps are added to obtain Boolean output map (Figure 5.17a) and the weights tabulated in Table 5.8 are utilized for obtaining the response theme of WofE approach (Figure 5.17b).

Table 5.8: Weights assigned for absence and presence of each evidential theme for the weight-contrast procedure.

	W+	W-	Contrast	Posterior Probabiliy
"b" Value	0,2507	-0,1008	0,3515	0,0139
Distance to lineament	0,5181	-0,2594	0,7775	0,0181
Distance to grabens	0,5398	-0,1763	0,7162	0,0185
Magnetic anomaly	0,1635	-0,0863	0,2498	0,0128

After obtainig the output maps for each of the method they are reclassified so as to be compareble. The rearrangement procedure is performed in the same way as it was done earlier. The cell value ranges and the corresponding reclassified values are tabulated in Table 5.9.

Table 5.9: Cell value ranges for both methods and equivalent reclassified values (weight-contrast procedure).

Cell value ranges (Boolean)	Cell value ranges (WofE)	Reclassified cell value	Favorability
0-2	<0,011	1	Unfavobale
3	0,011-0,019	2	Favorable
4	>0.019	3	Very Favorable

The resultant reclassified maps are shown in Figure 5.17 c and d. It can be visually interpreted that the WofE method is affected too much from the high weight values of structural events, as the pattern have some linearity.

The output maps of Boolean logic model and WofE method are compared by means of their index values (Table 5.10 and Table 5.11). The Boolean model predicts 32 occurrences, while the WofE predicts 44 out of 77 in both favorable and very favorable aras. Due to the larger spatial distribution of favorable areas in WofE model it predicts much more points than the Boolean. However, the index number of these areas in WofE is also greater than that of Boolean indicating a reasonable prediction for WofE.

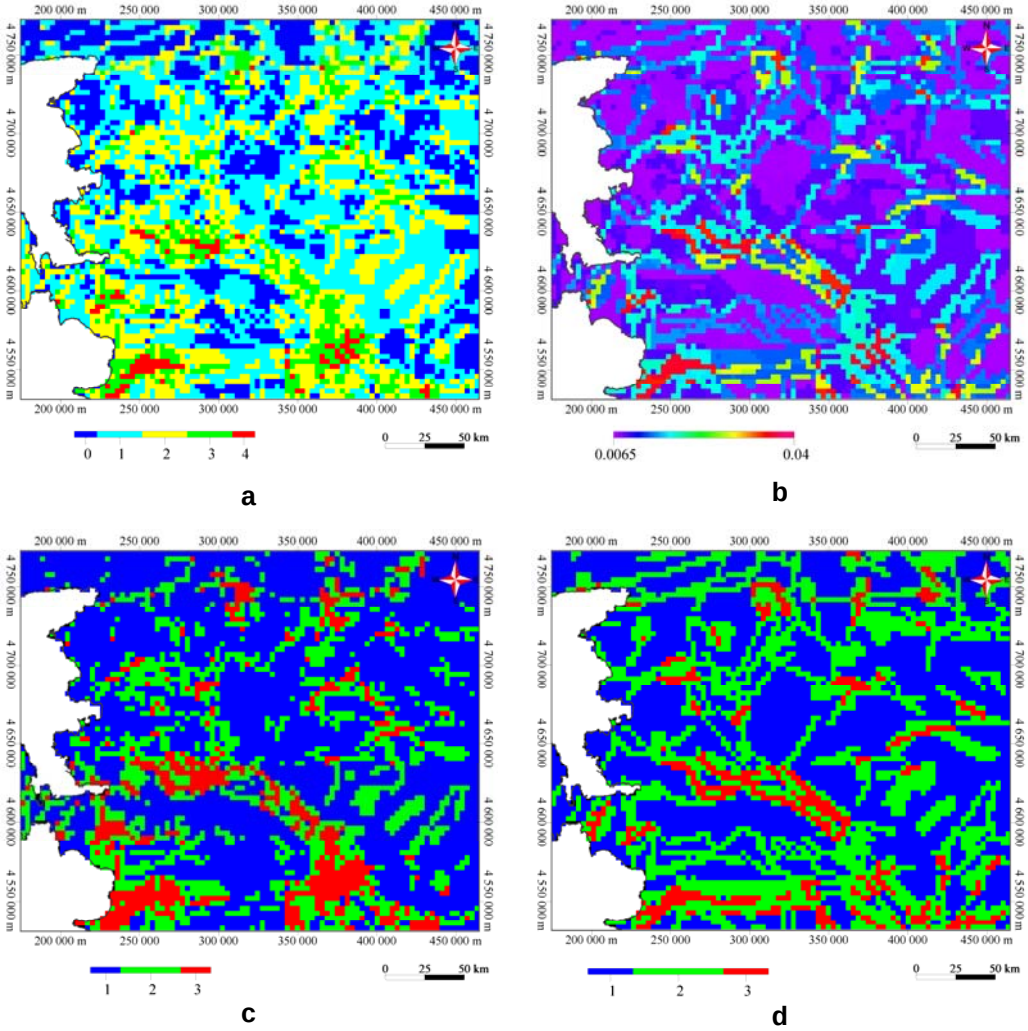

Figure 5.17: Output maps of two methods derived by weight-contrast procedure; **a)** Output map of Boolean model; **b)** Output map of WofE model; **c)** Reclassified map of Boolean model; **d)** Reclassified map of WofE model.

Table 5.10: Point count in each resultant Boolean class and the success index for weight-contrast procedure.

Favorability	Reclassified cell value	Area	Point count	Index
Unfavobale	1	39770	45	0,00113
Favorable	2	16200	16	0,00099
Very Favorable	3	6720	16	0,00238

Table 5.11: Point count in each resultant WofE class and the success index for weight-contrast procedure.

Favorability	Reclassified cell value	Area	Point count	Index
Unfavobale	1	35060	33	0,00094
Favorable	2	22440	29	0,00129
Very Favorable	3	5190	15	0,00289

Weight-contrast binarization procedure results in more successful output map for WofE method. However, some of the high weights of narrow binary patterns leads to the subjective output map for WofE. For this reason, new approach will be followed in binarization process by combining the previously introduced two procedures. In this approach the optimal binary pattern is selected for each map among the binary maps of both of the procedures. According to this, the binary patterns for b-value map and distance to lineament map are selected to be those derived from the mean±SD technique, because weight-contrast method narrowed these patterns so that the search area became too small. The binary maps for the rest of the layers, on the other hand, are chosen to be those found by weight-contrast method, due to the too large binary pattern obtained from the mean±SD approach (Figure 5.18).

Using these binary maps same way is followed to obtain and reclassify the output maps of both methods. Resultant maps are obtained through addition and weighting (Table 5.12) for Boolean and WofE model respectively (Figure 5.19 a and b). Then the reclassification (Figure 5.19 c and d) of the maps are performed using the ranges tabulated in Table 5.13. Finally, the reclassified maps are compared by the means of success indicies obtained for two of the methods (Table 5.14 and Table 5.15).

On the basis of the indices, it is concluded that this optimization method is the best among the three methods as calculated indices for both of the methods are greater than the indices presented in the previous methods. Another observation is that for all of the binarization procedures the resultant maps of WofE model appear to be more successful than the maps obtained for the Boolean model.

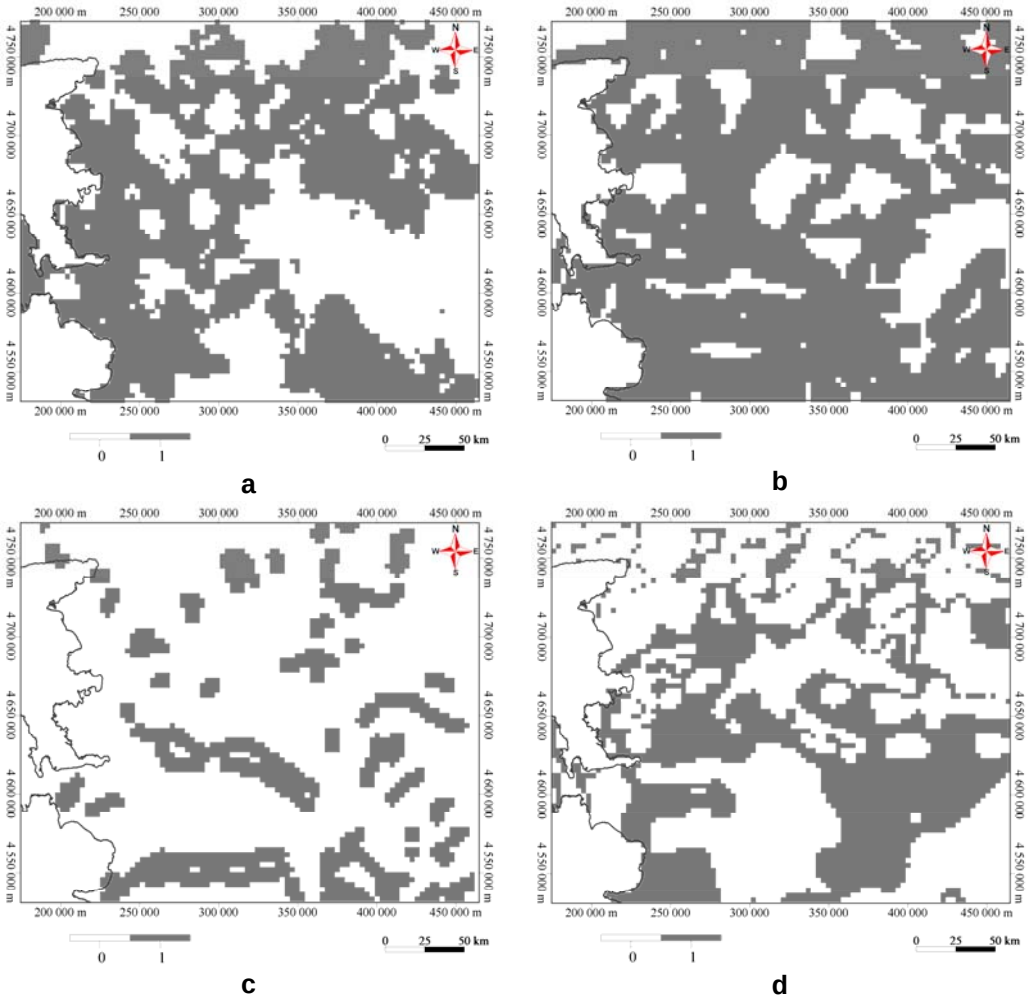

Figure 5.18: Binary patterns obtained by optimization procedure; **a)** Output map of Boolean model; **b)** Output map of WofE model; **c)** Reclassified map of Boolean model; **d)** Reclassified map of WofE model.

Table 5.12: Weights assigned for absence and presence of each evidential theme for the optimization procedure.

	W+	W-	Contrast	Posterior Probabiliy
"b" Value	0,2045	-0,2544	0,4589	0,0133
Distance to lineament	0,1303	-0,3585	0,4888	0,0124
Distance to grabens	0,5398	-0,1763	0,7162	0,0185
Magnetic anomaly	0,1635	-0,0863	0,2498	0,0128

Table 5.13: Cell value ranges for both methods and equivalent reclassified values (optimization procedure).

Cell value ranges (Boolean)	Cell value ranges (WofE)	Reclassified cell value	Favorability
0-2	<0,011	1	Unfavobale
3	0,011-0,025	2	Favorable
4	>0.025	3	Very Favorable

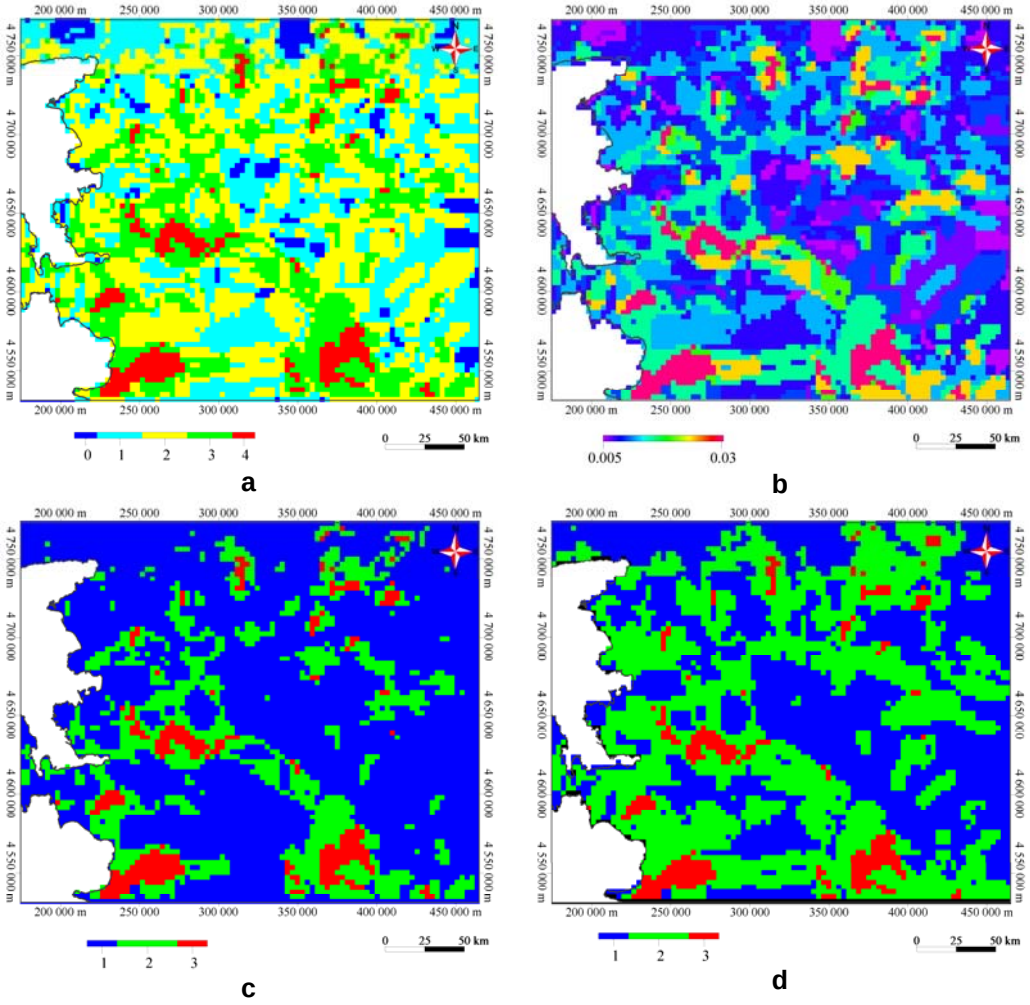

Figure 5.19: Output maps of two methods derived by optimization procedure; **a)** Output map of Boolean model; **b)** Output map of WofE model; **c)** Reclassified map of Boolean model; **d)** Reclassified map of WofE model.

Table 5.14: Point count in each resultant Boolean class and the success index for optimization procedure.

Favorability	Reclassified cell value	Area	Point count	Index
Unfavobale	1	45630	55	0,00121
Favorable	2	13740	11	0,0008
Very Favorable	3	3320	11	0,00331

Table 5.15: Point count in each resultant WofE class and the success index for optimization procedure.

Favorability	Reclassified cell value	Area	Point count	Index
Unfavobale	1	30060	32	0,00106
Favorable	2	29330	34	0,00116
Very Favorable	3	3300	12	0,00364

CHAPTER 6

DISCUSSION

This chapter discusses the accessibility and derivation methods of synthetic data used to examine the potential sites of geothermal occurrences. It also argues about the binarization techniques and compares two overlay methods, Boolean Logic Model and WofE Method, through their success of prediction. As a last point, by means of different binarization procedures the output maps of two methods are calculated and consequently result maps of each method and the reason of these results are evaluated and discussed (Figure 6.1).

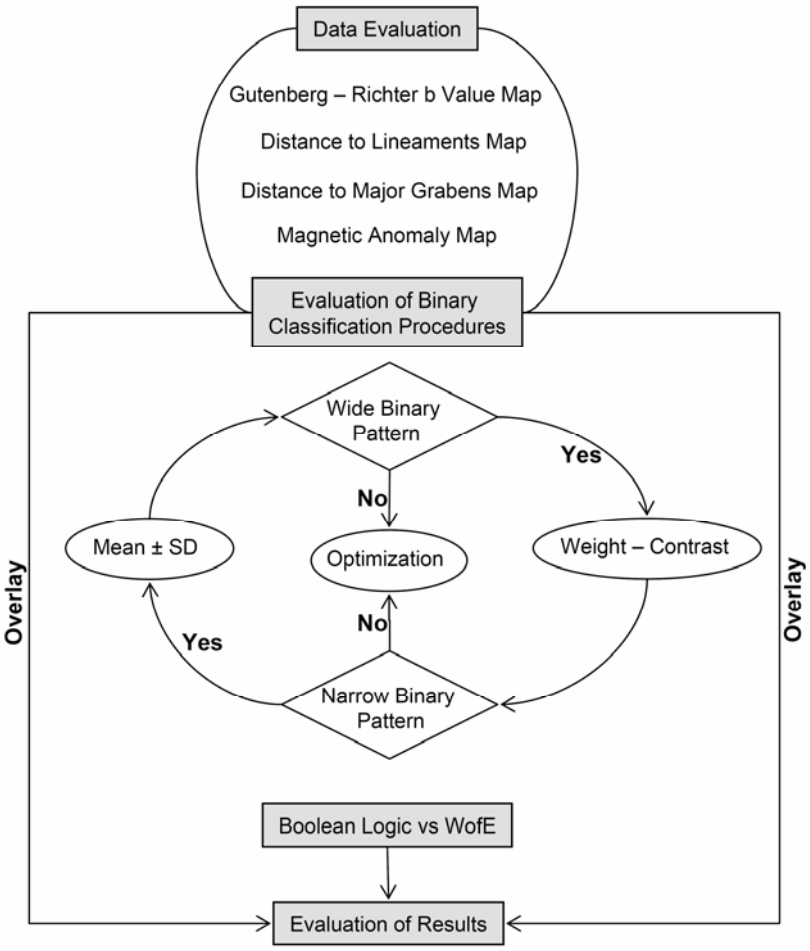

Figure 6.1: The scheme representing the discussed issues.

6.1 Evaluation of the Data

In this study spring and well clusters within 10 km^2 are assumed to belong to unique geothermal system and a point is assigned for each of these clusters. These points are used as training points in the further analysis. First, the distributions of all point and line data are investigated and the distribution of training points is found out to be nearly random. However, none of the geological occurrences are random. Their existence and formation depend on some other geological event. Thus, randomness of training points may be an indicator of arbitrary exploration.

Four synthetic maps which were produced from publicly available maps are used to create a statistical predictive model that will evaluate the undiscovered potential geothermal sites of greater part of Western Anatolia. These maps are Gutenberg-Richter *b-value* map, distance to lineaments map, distance to major grabens map and magnetic anomaly map. All of the data used in obtaining the evidence maps are gathered from the public sources and except the magnetic anomaly map, which is used directly in the analysis, the data is converted to synthetic data. The availability and function of each original (raw public data) and produced (synthetic data) layers are discussed individually.

Gutenberg-Richter *b-value* map: Before the conversion of the raw data into synthetic data the relation between the geothermal occurrences and earthquake related structures are explored. After finding some relation these data are converted to a far more meaningful version which is the synthetic data. Epicenter map is transferred to Gutenberg-Richeter *b-value* map to mirror the effect of magnitude and time of the earthquakes. This layer being produced from epicenter data enables to investigate the relation between the geothermal occurrences and the time and magnitude dependent seismic activity in a wide region. The production of this map includes equal sized multi source characterization which is generally unusual but effective when calculated for a broad area. Only *b value* of the Gutenberg – Richter relation is used because the aim is to emphasize the effect of earthquake magnitude related to time on geothermal occurrence.

Distance to lineaments: The lineament data is preferred to be used due to the availability of SRTM data. In fact, for the study area active fault map is also publicly available, however this would not be the case for every region in the world. The extraction of lineaments from SRTM data is an easy process for an expert structural geologist and it is usually consistent with the active fault data, where it will only lighten the morphological manifestations of faults. The lineament map is converted to distance to lineament map so that the selectivity of geothermal occurrences, if there is any, in terms of distance to lineament is worked out. The distance is calculated for both side of

a line. However, the geothermal occurrence should be expected on hanging wall block as the hot water would find a path along the slope direction of the fault. Though, the dip directions of the slopes is usually not known for the area, thus the distance from the both sides of a line is calculated. Actually, assuming that the geothermal occurrence will show the dip direction, it becomes a useful tool for interpreting the slope direction of a fault where it is unknown.

Distance to major grabens: The geophysical data, which is in continuous form, is evaluated through their pixel values and shape of the contours. In this context, a map representing the slopes of gravity contours is generated. The apparent output demonstrated the boundary of major horst- graben systems within the area. These areas are then represented by a line vector showing the faults and then a map presenting distance to these faults is prepared. Therefore, similar to the lineaments, distance to major grabens map was produced from the gravity anomaly map. Generally in horst-graben systems it is found out that geothermal occurrences are presented either within graben or along the faults comprising the boundary between horsts and grabens.

Magnetic anomaly: For the magnetic anomaly, however, neither exploration of pixel values nor the contour patterns gave distinct evidences and thus this map is decided to be used in its original form.

Finally, all maps are resampled in order to have same pixel size, which is 10km^2. Because each spring and well cluster within 10 km^2 area was previously assumed to belong to distinctive geothermal system, the area of each pixel is decided to be 10 km^2. Thus, each pixel will have some potential of containing an occurrence. In addition, if the pixel area is selected to be wider the decision rules would have a wide range, while if it is chosen to be narrower, then it would be too much case dependent.

6.2 Evaluation of Map Binarization

Binary map classification includes application of logical values. Each location of occurrence is tested to determine whether it belongs to the set of locations. In the language of sets, set membership is expressed only with binary 1(true) or 0 (false) with no possibility of “maybe” (Bonham-Carter, 1996). Each of the binary maps is assumed to be a requirement for occurrence of particular evidence. Thus, each binary map layer is an evidential theme for training points of occurrences. These layers are combined with Boolean operators and WofE method separately to support a specific hypothesis. Hence, the driven hypothesis in this study is “this area is favorable for geothermal occurrences”.

Conversion of multiclass maps to binary map pattern should be performed so that the spatial association between the binary pattern and the training points is optimal.

Two methods are applied in this study for the binarization process. The first is simple statistical application which gives importance to mean and standard deviation values of maps where training point is present (Figure 6.2a and d). The second method depends on the contrast value and number of training points present in each class of the maps (Figure 6.2b and c). Both methods have some positive and negative points. The first one for example chooses very large area for magnetic anomaly map and thus reduces the effectiveness of this pattern for narrowing the search area (Figure 6.2a). The second method, on the other hand, prefers very small area for distance to lineament map due to the high contrast of selected class (Figure 6.2c). Thus, this layer when put in WofE analysis underestimates the weights of the other layers and acts as if it is the only effective evidence for geothermal occurrence.

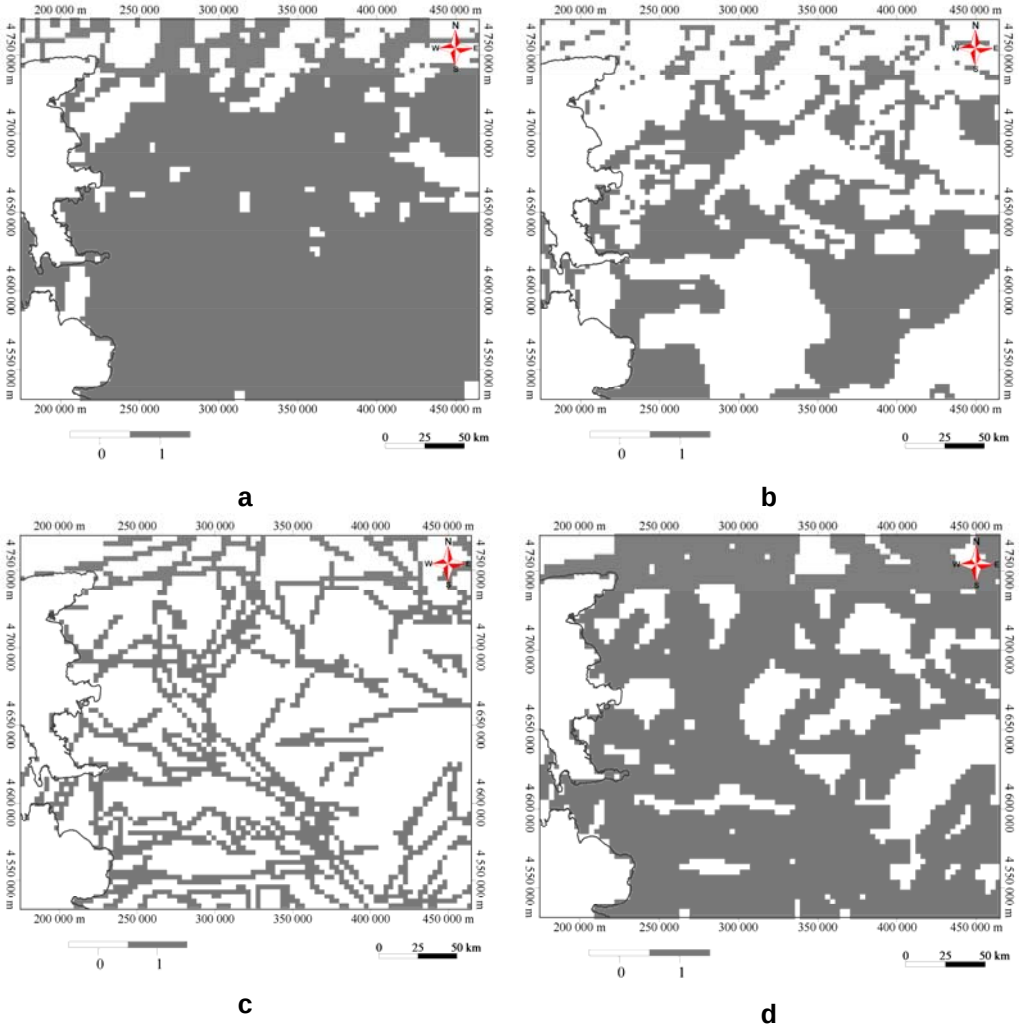

Figure 6.2: Binary patterns obtained by weight-contrast and mean ± SD procedure **a)** Binary pattern of magnetic anomaly performed by mean±SD method; **b)** Binary pattern of magnetic anomaly performed by contrast-occurrence method; **c)** Binary pattern of distance to lineament performed by contrast-occurrence method; **d)** Binary pattern of distance to lineament performed by mean±SD method.

Consequently, to achieve these problems both of the methods have to be evaluated with caution and the most appropriate binary pattern which will neither make the search area too small nor too large should be chosen.

6.3 Comparison of Methods

The assumptions made about a hypothesis regarding any geological occurrence depend on some knowledge which is based on the opinion of an exploration geologist. Thus the geologist using his/her experience and knowledge constructs a set of rules for any occurrence so that the factors important for finding it are introduced. If the evidences are related to each other with a set of rules, the resulting network is sometimes called decision tree. Decision trees are one of the tools which denote knowledge in an expert system. They are used in many fields, like in the construction of keys for the optical identification of minerals, or for the identification of biological taxa from morphological and other characteristics (Bonham-Carter, 1996).

Both methods applied for investigating the potential geothermal sites can be employed using the expert's opinion and assessment. However, if the study area is large, it is nearly impossible to expect from the expert to have a detailed knowledge about every single locality in the area. In this case, it is more appropriate to use the data-driven methods.

The advantage of the Boolean approach is its simplicity. In cases where a set of rules for an occurrence are set up by law or code, Boolean combinations are practical and easily-applied method. However, application of this approach is only dependent on rules expressing the inter-relation among the evidence layers. In other words, it gives equal importance to each criteria being combined. Though, evidence layers needs to be weighted so that their relative importance for occurrences is reflected to the analysis. For example, being close to a lineament is a far more important indicator than the magnetic anomaly but in the Boolean logic approach both kinds of evidence are treated equally.

The advantage of WofE method is that it eliminates the weight problem in the Boolean model. The method is unbiased and avoids the particular choice of weighting factors. The extraction of weighting factors and combination of multiple map patterns are straightforward to program with a modeling language. The combination of input maps assumes that the maps are conditionally independent and providing the conditional independence among the map layers is the hardest part of the method. Hence, if possible, the layers having probability of being dependent need to be binarized in such a way that the dependence disappears.

The application of WofE method requires well known occurrences. In the exploration regions where only a few occurrences are known, the calculated weights will be in error and they will have large variances. For that reason the WofE model is not always applicable in poorly explored regions. However, in partly explored regions, where sufficient number of occurrences is known the calculated weights will not greatly alter.

6.4 Evaluation of the Results

Analysis part of the study was performed through three different binarization techniques. The first depend on mean and the standard deviation of the map values, the second depend on contrast, weight and existing points of each class, while the third one is the combination of first two. Three of the methods support the idea that WofE method is better estimator than the Boolean model by means of calculated indices.

When three output maps obtained for each method through different binarization techniques are investigated within themselves it is observed that the third technique which is the optimization procedure gives the most successful outputs (Figure 6.3 and 6.4).

After the evaluation of output maps for each binarization procedure two more maps, one for Boolean model and the other for WofE method, are generated. These maps were produced using the intersection of very favorable and favorable areas of the maps obtained from the three procedures. Thus, Figure 6.5 is the representation of Boolean output obtained from intersection of the maps in Figure 6.3. Similarly, Figure 6.6 demonstrates the output of WofE model derived from intersections of the maps in Figure 6.4.

Both resultant maps agree in potential sites, which are Aydın, Denizli and Manisa, with different sizes. Boolean method has wide range while the WofE keep the size of potential areas narrow.

Having a potential in Denizli and Aydın areas is not surprising. These areas have been explored well since now and thus, this resulted in many training points present in these areas. Including much more training points in a particular area when compared to others, results in larger weights for a particular property of evidence layers lying in these locations. Hence the areas, with similar properties give similar results in terms of favorability. Therefore, it can be claimed that the favorable area in Manisa have alike properties to those present in Aydın and Denizli.

MEAN±SD

Favorability	Point count	Index
Unfavobale	23	0,00121
Favorable	30	0,00119
Very Favorable	24	0,0013

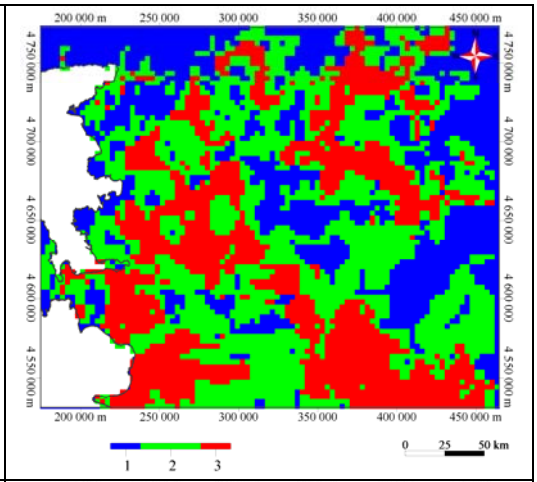

WEIGHT-CONTRAST

Favorability	Point count	Index
Unfavobale	45	0,00113
Favorable	16	0,00099
Very Favorable	16	0,00238

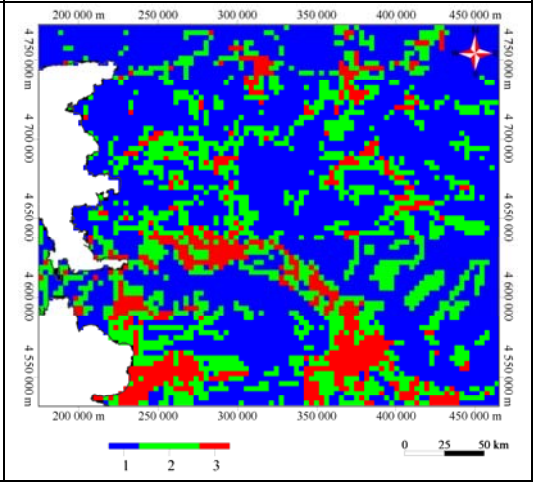

OPTIMIZED

Favorability	Point count	Index
Unfavobale	55	0,00121
Favorable	11	0,0008
Very Favorable	11	0,00331

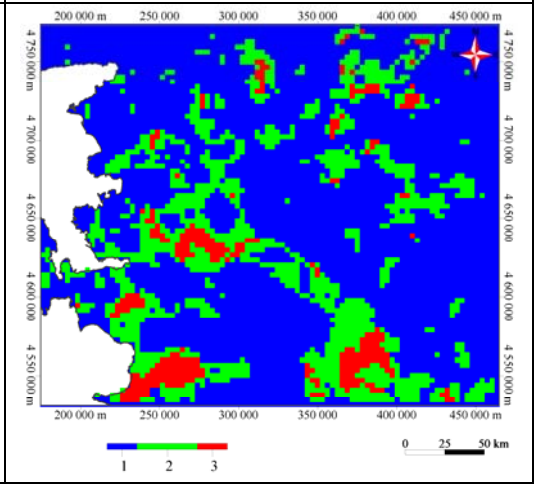

Figure 6.3: Output maps of Boolean model obtained from three different binarization techniques with their corresponding indices.

	Favorability	Point count	Index
MEAN±SD	Unfavobale	41	0,00111
	Favorable	11	0,0015
	Very Favorable	25	0,00137

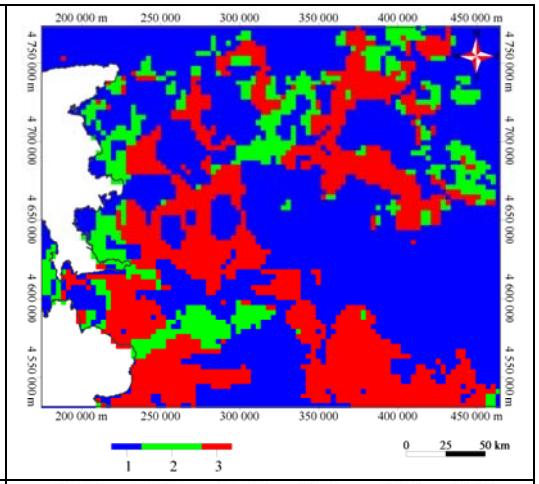

	Favorability	Point count	Index
WEIGHT-CONTRAST	Unfavobale	33	0,00094
	Favorable	29	0,00129
	Very Favorable	15	0,00289

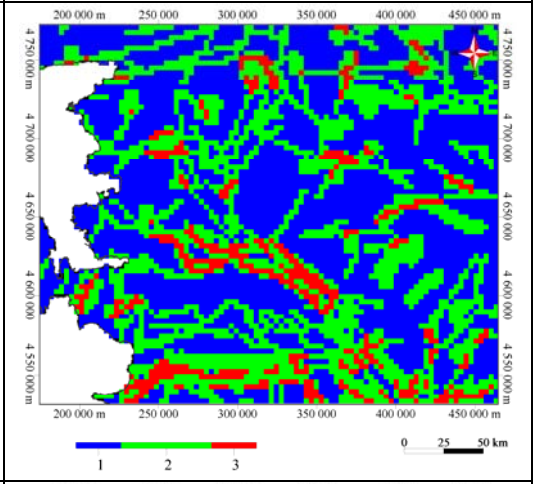

	Favorability	Point count	Index
OPTIMIZED	Unfavobale	32	0,00106
	Favorable	34	0,00116
	Very Favorable	12	0,00364

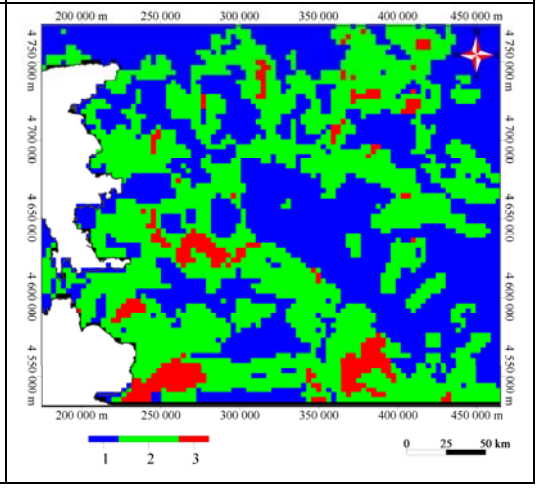

Figure 6.4: Output maps of WofE model obtained from three different binarization techniques with their corresponding indices.

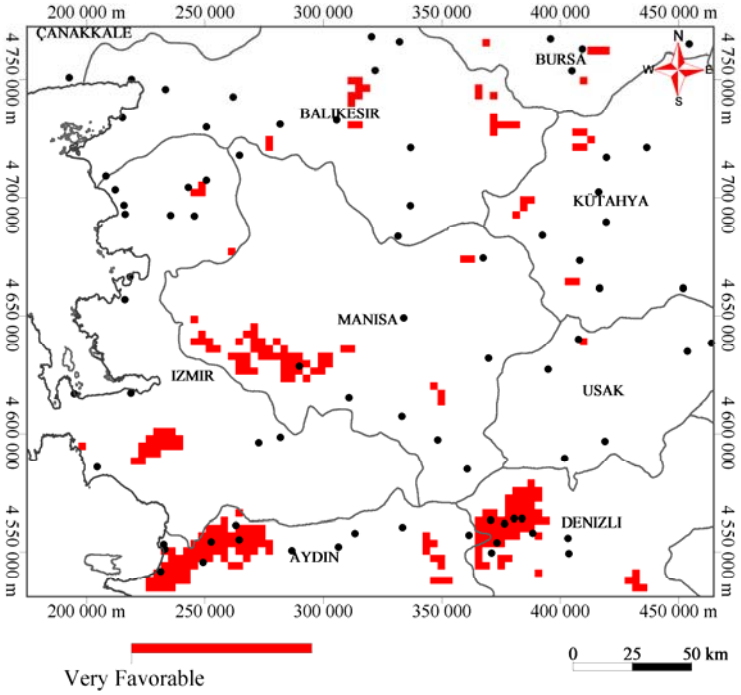

Figure 6.5: Output map of Boolean method obtained from intersection of resulting maps derived by means of three different binarization procedures.

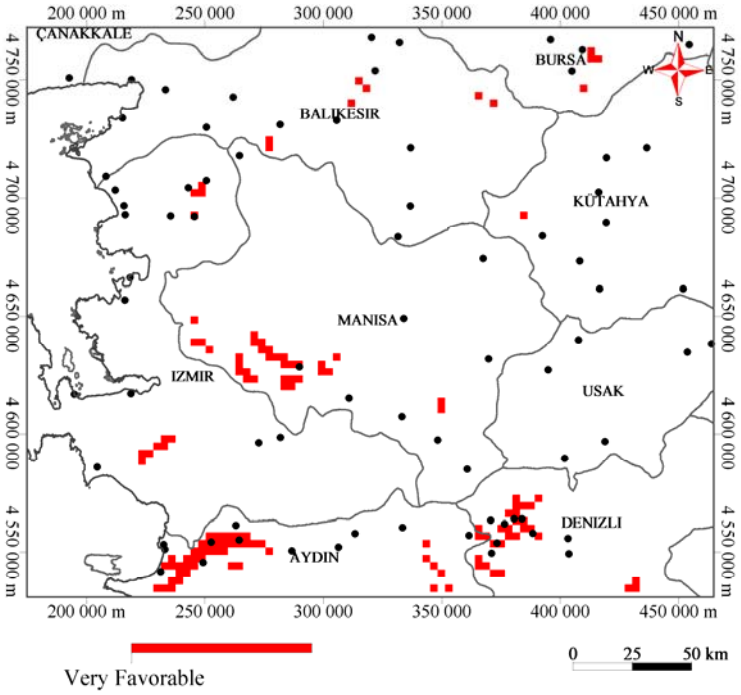

Figure 6.6: Output map of WofE method obtained from intersection of resulting maps derived by means of three different binarization procedures.

CHAPTER 7

CONCLUSION

Potential of geothermal occurrence of western Anatolia is promising due to its appropriate geological condition. A high fractured system in the area constitutes a suitable medium for geothermal waters to percolate and to rise to the surface.

Due to the importance of the geologic structures in the area; the relationship between geothermal occurrences and the two main geologic issues which make the area exceptional in terms of the “geothermal” is investigated. One of them includes the basic reason of extensional regime, namely earthquakes, and the consequences of these earthquakes, that is faults which are interpreted from lineaments in this study. The other concept involves the rock units presented beneath the surface of the study area, which are basically predicted by means of geophysics.

Four maps namely evidential themes, are used to examine the spatial relation of the “geothermal” and its surroundings. One of the maps is Gutenberg-Richter *b-value* map, which is an indicator of seismicity of the area depending on earthquake magnitude and time. The other two maps are distances to lineaments and grabens. The last map used is magnetic anomaly map of the area.

The maps are combined through two different methods, Boolean logic model and Weights of Evidence (WofE) Method. Boolean method depends on logical numbers of 1 and 0 and combination of these are performed with the Boolean operators (AND, OR, XOR, NOT). WofE method on the other hand assigns weights to each evidential theme by using the logic of Bayesian probability. Both methods require binary map classification of the evidential themes, which is the hardest process of the analysis.

Three different techniques are performed for the decision of binary map classification. The first depends on the means and standard deviations of the map values, while the second method is weight dependent. The disadvantage of the first method is that it reveals large binary pattern for some of the map layers. The inconvenience of the second approach, on the other hand, is that it concludes in too narrow binary patterns for some of the maps, and that the output map generated from these narrow patterned binary maps is much more influenced by the layers having a significant weight. Thus, a third method which is combination of these two is applied. In these method the binary maps having too narrow search area due to the weighting method, are eliminated and for these the ones obtained from the first method are put in

the analysis. Similarly, if the map obtained from the first method had too large binary pattern it is replaced with its binary pattern obtained from the second method.

Hence, for each combination method three output maps are obtained and compared. According to this comparison it is concluded that WofE method is much more advanced predictor than the Boolean logic model, because its estimation of geothermal occurrences depending on the area of favorability is better. However, when a quick prediction for an area is essential the Boolean logic model can be used to get an idea about the region, and after if a detailed exploration is expected the WofE method can be utilized. As a final point, the binarization techniques are evaluated according to their success. It is found out that the second method is a better estimator than the first one while the best one is discovered to be the third method which is mixture of the first two.

The resultant favorability maps for both of the methods are obtained by intersecting the very favorable areas predicted through different binarization procedures. As a result, it is found out that the most promising areas are Denizli, Aydın and Manisa. However, Denizli and Aydın areas are already explored and the potential here is evident. Though, this is not the case for Manisa, thus it is concluded that this region is worth to be explored in geothermal potential point of view. Nevertheless, it is important to note that the resultant maps are obtained from data layers calculated for a wide region and the precision of the results are in 10 km^2 area. Thus, Manisa, found to be a promising region, should be further investigated locally with much more data layers including evidential themes having higher resolution.

REFERENCES

Adelfio, S. A., Nolan, C. F., 1964, Principles and applications of Boolean Algebra, Hayden Book Company, Inc., New York, 319 pages.

Agterberg, F., P., Cheng, Q., 2002, Conditional independence test for weight of evidence modeling, Natural Resources Research, Vol.11, No.4, pp.249-255.

Akkuş, İ., Aydoğdu, Ö., Akıllı, H., Gökmenoğlu, O., Sarp, S., 2005, Geothermal Energy and Its Economic Dimension in Turkey, World Geothermal Congress 2005, Antalya, Turkey.

Aldanmaz, E., Pearce, J.A., Thirlwall, M.F., Mitchell, J.G., 2000, Petrogenetic evolution of late Cenozoic, post-collision volcanism in Western Anatolia, Turkey. J. Volcanol. Geotherm. Res., Vol. 102 (1–2), pp. 67– 95.

Altherr, R., Keuzer, H., Wendt, I., Lenz, H., Wagner, G.A., Keller, J., Harre, W., Hohndorf, A., 1982, A Late Oligocene/Early Miocene high temperature belt in the Attic-Cycladic crystalline complex (SE Pelagonian, Greece), Geol. Jahrb., Vol. 23, pp. 97–164.

Altunel E., 1999, Geological and geomorhological observations in relation to the 20 September 1899 Menderes earthquake, Western Turkey, J. Geol. Soc., London, Vol. 156, pp. 241–246.

Altunel E., 1998, Evidence for damaging historical earthquakes at Priene, Western Turkey, Turkish J Earth Sci., Vol. 7, pp. 25–35.

Ambraseys N.N., Jackson J.A., 1998, Faulting associated with historical and recent earthquakes in the Eastern Mediterranean region, Geophys. J. Inter. Vol. 133, pp. 390–406.

Ambraseys N.N., 1988, Engineering seismology, Earthq. Engineer. Struct. Dynam., Vol. 17, pp. 1–105.

Arpat, E., Şaroğlu, F., 1975, Türkiye'deki bazı önemli genç tektonik olaylar, Türkiye Jeoloji Kurumu Bülteni, in Turkish, Vol. 18, pp. 91–101.

Arpat, E., Şaroğlu, F., 1972, The East Anatolian fault system: thoughts on its development. Bull. Min. Res. Expl. Inst. Turkey, Vol. 78, pp. 33–39.

Barka, A.A., 1992, The North Anatolian Fault zone, Annales Tecton., Vol. 6, pp. 164–195.

Başarır, E., 1970, The petrology and geology of the eastern flank of the Menderes Massif on the east of Lake Bafa: Scientific Report of the Faculty of Science, Ege University, No: 102.

Blumental, M., 1951, Batı Toroslarda Alanya Ard Ülkesinde Jeolojik Araştırmalar, M.T.A. Enst. Yayını, Seri D, No. 5, 134 sayfa.

Bonham-Carter, G.F., 1996, Geographic Information Systems for Geoscientists: Modelling with GIS, Pergamon, 398 pages.

Bonham-Carter, G.F., Agterberg, F.P., Wright, D.F., 1988, Integration of geological datasets for gold exploration in Nova Scotia: Photogrammetric Engineering and Remote Sensing, Vol. 54(11), pp. 1585-1592.

Bowen, R., 1989, Geothermal Resources, 2nd Edition: Elsevier Science Inc., New York, NY, 485 p.

Bozkurt, E., 2001, Neotectonics of Turkey – a synthesis, Geodinamica Acta, Vol. 14, pp. 3-30.

Bozkuş, C., 1996, Kavacık (Dursunbey-Balıkesir) Neojen grabeninin stratigrafisi ve tektoniği, Turkish J. Earth Sci., Vol. 5, pp. 161–170 (in Turkish with English abstract).

Canıtez, N., Üçer, S.B., 1967, Computer determinations of the fault plane solutions in and near Anatolia, Tectonophysics, Vol. 4, pp. 235–244.

Condie, K.C., 1976, Plate Tectonics and Crustal Evolution, Pergamon Press Inc., New York.

Darracott, B.W., Fairhead, D., Girdler, W., 1972, Gravity and Magnetic surveys in northern Tanzania and southern Kenya, Tectonophysics, Vol. 15, pp. 131–141.

Davis, J. C., 2002, Statistics and Data Analysis in Geology, John Wiley & Sons, Inc., USA, 637 pp.

Delaloye, M., Bingöl, E., 2000, Granitoids from Western and Northwestern Anatolia: geochemistry and modelling of geodynamic evolution, Int. Geol. Rev., Vol. 42, pp. 241–268.

Demirbaş, A., 2002, Turkey's Geothermal Energy Potential, Energy Sources, Vol. 24, pp. 1107-1115.

Dewey J.F., Helman M.L., Turco E., Hutton D.H.W., Knott S.D., 1989, Kinematics of the western Mediterranean, in: Coward M.P., Dietrich D., Park R.G. (Eds.), Alpine Tectonics, Geological Society Special Publication no. 45, Geological Society, London, pp. 265–283.

Dewey J.F., Hempton M.R., Kidd W.S.F., Şaroğlu F., Şengör A.M.C., Shortening of continental lithosphere: the neotectonics of eastern Anatolia – a young collision zone, in: Coward M.O., Ries A.C. (Eds.), 1986, Collisional Tectonics, Geological Society Special Publication no. 19, Geological Society, London, pp. 3–36.

Dewey, J.F., Şengör, A.M.C., 1979, Aegean and surrounding regions: complex multiplate and continuum tectonics in a convergent zone, Geol. Soc. Am. Bull., Part I, Vol. 90, pp. 84–92.

Dora O., Candan, O., Dürr, S., Oberhanslı, R., 1997, New evidence on the geotectonic evolution of the Menderes Massif. In: Pişkin O, Ergün M, Savaşcın Y., Tarcan, G., (eds) Proc International Earth Sciences Colloquium on the Aegean Region, İzmir-Güllük, Turkey, pp 53–72

Dumont, J.F., Uysal, Ş., Şimşek, Ş., 1979, Karamanderesi, I.H., Letouzcy, F., Güneybatı Anadolu'daki grabenlerin oluşumu, Min. Res. Expl. Inst. Turkey Bull., Vol. 92, pp. 7–17.

Dürr, S., Atherr, R., Keller, J., Okkursch, M., Seidel, E., 1978, The Median Aegean crystalline Belt. Stratigraphy, structure, metamorphism, magmatism: Alps, Apennins, Hellenids: Inter-Union Commission on Geodynamics, Scientific Report, No. 38, pp. 454–477.

Duvarcı, E., 2001, Geolectric structure of inland area of the Gökova rift, southwest Anatolia and its tectonic implications, J. Geodyn., Vol. 31, pp. 33–48.

Erdoğan, B., Güngor, T., 1992, Menderes Masifinin Kuzey Kanadının Stratigrafisi ve Tektonik Evrimi, Turk. Assoc. Petrol. Geol. Bull., Vol. 4, pp. 9 – 34.

Eyidoğan H., 1988, Rates of crustal deformation in western Turkey as deduced from major earthquakes, Tectonophysics, Vol. 148, pp. 83–92.

Eyidoğan, H., Jackson, J.A., 1985, A seismological study of normal faulting in the Demirci, Alaşehir and Gediz earthquake of 1970 in western Turkey: implications for the nature and geometry of deformation in the continental crust, Geophys. J. Royal Astronom. Soc., Vol. 81, pp. 569–607.

Flóvenz, Ó. G., Björnsson, G., Sæmundsson, K., 2001, Pressure signals in geothermal systems in S-Iceland caused by two large earthquakes in June 2000, Iga News, no. 43, Orkustofnun, Reykjavik.

Fridleiffsson, I., B., 2001, Geothermal Energy for the Benefit of the People, Renewable and Sustainable Energy Reviews, Vol. 5, pp. 299-312.

Fytikas M., Innocenti F., Manetti P., Mazzuoli R., Peccerillo A., Villari L., 1984, Tertiary to Quaternary evolution of the volcanism in the Aegean region, in: Dixon J.E., Robertson A.H.F. (Eds.), The Geological Evolution of the Eastern Mediterranean, Geological Society Special Publication, Vol. 17, Geological Society, London, pp. 687–700.

Gemici, Ü., Tarcan, G., 2002, Hydrogeochemistry of the Simav geothermal field, western Anatolia, Turkey, Journal of volcanology and geothermal research, Vol. 116, pp. 215-233.

Görür, N., Şengör, A.M.C., Sakınç, M., Tüysüz, O., Akkök, R., Yiğitbaş, E., Oktay, F.Y., Barka, A.A., Sarıca, N., Ecevitoğlu B., Demirbağ, E., Ersoy, Ş., Algan, O., Güneysu, C., Akyol, A., 1995, Rift formation in the Gökova region, southwest Anatolia: implications for the opening of the Aegean Sea, Geol. Mag., Vol. 132, pp. 637–650.

Griffiths, D.H., 1965, Applied Geophysics for Engineers and Geologists, Pergamon Press, Oxford, London, 215 p.

Gutenberg, B., Richter, C.F., 1944, Frequency of Earthquakes in California, Bulletin of the Seismological Society of America, Vol. 34, No. 4, pp. 1985-1988

Hempton M.R., 1987,Constraints on Arabian plate motion and extensional history of the Red Sea, Tectonics, Vol. 6, pp. 687–705.

Hepbaşlı, A., Özgener, L., 2004, Development of geothermal energy utilization in Turkey: a review, Renewable and Sustainable Energy Reviews, Vol. 8, pp. 433-460.

Hoernes, G. E., Heilweil, M. F., 1964, Introduction to Boolean Algebra and Logic Design, McGraw-Hill Book Company, 306 pages.

Innocenti, F., Agostini, S., Di Vincenzo, G., Doglionic, C., Manetti, P., Savaşçin, M. Y., Tonarini, S., 2005, Neogene and Quaternary volcanism in Western Anatolia: Magma sources and geodynamic evolution, Marine Geology, Vol. 221, pp. 397-421.

Innocenti, F., Kolios, N., Manetti, P., Rita, F., Villari, L., 1982, Acid and basic late Neogene volcanism in central Aegean Sea: its nature and geotectonic significance. Bull. Volcanol., Vol. 45, pp. 87– 97.

İzdar, E., 1971. Introduction to geology and metamorphism of the Menderes Massif of Western Turkey. Geology and history of Turkey, Petroleum Explor. Soc. of Libya, Tripoli, pp. 495–500.

Jackson J.A., King G., Vita-Finzi C., 1992, The neotectonics of the Aegean: an alternative view, Earth Planet. Sci. Lett., Vol. 61, pp. 303–318.

Jackson J.A., McKenzie D.P., 1988, Rates of active deformation in the Aegean Sea and surrounding regions, Basin Res., Vol. 1, pp. 121–128.

Kaygusuz, K., Kaygusuz, A., 2004, Geothermal energy in Turkey: the sustainable Future, Renewable and Sustainable Energy Reviews, Vol. 8, pp. 545-563.

Ketin, I., 1983. Türkiye Jeolojisine Giriş, Istanbul Teknik Üniversitesi Yayını, No. 32.

Koçyiğit, A., Yusufoğlu, H., Bozkurt, E., 1999, Evidence from the Gediz graben for episodic two-stage extension in western Turkey, J. Geol. Soc., London, Vol. 156, pp. 605–616.

Kramer, S.L., 1996, Geotechnical Earthquake Engineering, Prentice Hall, Upper Saddle River, New Jersey, 653 pp.

Le Pichon, X., Angelier J., 1981, The Aegean Sea, Philop. Trans. R. Soc. London Ser. A., Vol. 300, pp. 357–372.

Le Pichon X., Angelier J., 1979, The Aegean arc and trench system: a key to the neotectonic evolution of the eastern Mediterranean area, Tectonophysics, Vol. 60, pp. 1–42.

Lund, J., W., Feeston, D., H., 2001, World-wide direct uses of geothermal energy 2000, Geothermics, Vol. 30, pp. 29-68.

Lytel, A., 1963, ABC's of Boolean Algebra, W. Foulsham & Co. Ltd., 112 pages.

Mart, Y., Woodside, J., 1994, Preface: Tectonics of the Eastern Mediterranean, Tectonophysics, Vol. 234, pp. 1–3.

Mc Kenzie D.P., 1978, Active tectonics of the Alpine–Himalayan belt: the Aegean Sea and surrounding regions, Geophys. J. Royal Astron. Soc., Vol. 55, pp. 217–254.

Mc Kenzie, D.P., 1972, Active tectonics of the Mediterranean region, Geophys. J. R. Astron. Soc., Vol. 30, pp. 109–185.

Mc Kenzie D.P., 1969, Speculations on the consequence and causes of plate motions, Geophys. J. Royal Astron. Soc.,Vol. 18, pp. 1–32.

Mertoğlu, O., 2005, Geothermal Applications in Turkey", World Geothermal Congress 2005.

Mertoğlu, O., Bakır, N., Kaya, T., 2003, Geothermal applications in Turkey, Geothermics, Vol. 32, pp. 419-428.

Meulenkamp J.E., Wortel W.J.R., Van Wamel W.A., Spakman W., Hoogerduyn Strating E., 1988, On the Hellenic subduction zone and geodynamic evolution of Crete in the late middle Miocene, Tectonophysics, Vol. 146, pp. 203–215.

Ministry of Energy and Natural Resources (MENR). Energy report of Turkey. Ankara, Turkey, 2002, Available from http://www.m enr.gov.tr.

Möller, P., Dulskia, P., Savascin, Y., Conrad, M., 2004, Rare earth elements, yttrium and Pb isotope ratios in thermal spring and well waters of West Anatolia, Turkey: a hydrochemical study of their origin, Chemical Geology, Vol. 206, pp. 97-118.

MTA, General Directorate of Mineral Research and Exploration, Turkey, 1996, Geothermal Inventory.

Mutlu, H., Güleç, N., 1998, Hydrogeochemical outline of thermal waters and geothermometry applications in Anatolia (Turkey), Journal of volcanology and geothermal research, Vol. 85, pp. 495-515

Nebert, K., 1960, Tavşanlı'nın batı ve kuzeyindeki linyit ihtiva eden Neojen sahasının mukayeseli stratigrafisi ve tektoniği, Min. Res. Expl. Inst. Turkey Bull., Vol. 54, pp. 7–35 (in Turkish with English abstract).

O'Leary, D.W., Friedman, J.D., Pohn, H.A., 1976, Lineament, linear, lineation: Some proposed new standards for old terms, *Geological Society of America Bulletin,* vol.87, pp. 1463- 1469.

Özelçi, F., 1973,Gravity anomalies of the Eastern Mediterranean. M.T.A. Enstitüsü Dergisi 1973; Vol. 80.

Öztürk, A., Koçyiğit, A., 1983, A structural approach to the basement covers relationship of Menderes group rocks, (Selimiye-Mugla), Bull. Geol. Soc. Turkey, Vol. 2, pp. 99–106.

Papazachos B.C., Comninakis P.E., 1971, Geophysical and tectonic features of the Aegean arc, J. Geophys. Res., Vol. 76, pp. 8517–8533.

Parasnis, D.S., 1972, Principles of Applied Geophysics, Chapman and Hall Ltd, London, 203 p.

Pe-Piper, G., Piper, D.J.W., Kotopouli, C.N., Panagos, A.G., 1995, Neogene volcanoes of Chios, Greece: the relative importance of subduction and back-arc extension. In: Smellie, J.L. (Ed.), Volcanism Associated with Extension at Consuming Plate Margins. Geol. Soc. Spec. Publ. London, pp. 213–231.

Rabinowitz, P.D., Ryan, W.B.F., 1970, Gravity anomalies and crustal shortening in the Eastern Mediterranean, Tectonophysics, Vol. 10, pp. 285–608.

Raines, G., L., Bonham–Carter, G., F., Kemp, L., 2000, Predictive Probabilistic Modeling Using ArcView GIS, ArcUser, pp. 45-48

Reilinger, R.E., McClusky, S.C., Oral, M.B., King W., Toksöz M.N., 1997, Global Positioning, System measurements of present-day crustal movements in the Arabian–Africa-Eurasia plate collision zone, J. Geophy. Res., Vol. 102, pp. 9983–9999.

Reiter, L., 1990, Earthquake Hazard Analysis: Issues and Insights, Columbia University Press, New York, 254 pp.

Ring, U., Gessner, K., Güngfr, T., Passchier, C.W., 1999, The Menderes Massif of western Turkey and the Cycladic Massif in the Aegean—do they really correlate?, J. Geol. Soc. (Lond.), Vol. 156, pp. 3–6.

Robert, U., Foden, J., Varne, R., 1992, The Dodecanese Province, SE Aegean: a model for tectonic control on potassic magmatism, Lithos, Vol. 28, pp. 241– 260.

Robertson A.H.F., Grasso M., 1995, Overview of the late Triassic-Recent tectonic and palaeo-environmental development of the Mediterranean region, Terra Nova, Vol. 7, 114–127.

Sarı, C., Şalk, M., 2005, Sediment thicknesses of the Western Anatolia graben structures determined by 2D and 3D analysis using gravity data, Journal of Asian Earth Sciences, In Press

Savasçın, Y., Güleç, N., 1990, Relationship between magmatic and tectonic activities in western Turkey, International Earth Sciences Congress on Aegean Regions, Proceedings, Vol. II, İzmir.

Şengör A.M.C., 1987, Cross-faults and differential stretching of hanging walls in regions of low-angle normal faulting: examples from western Turkey, in: Coward M.P., Dewey J.F., Hancock P.L. (Eds.), Continental Extensional Tectonics, Geological Society Special Publication no., Vol. 28, Geological Society, London, pp. 575–589.

Şengör, A.M.C., Görür, N., Şaroğlu, F., 1985, Strike-slip faulting and related basin formation in zones of tectonic escape: Turkey as a case study, in: Biddle K.T., Christie-Blick N. (Eds.), Strike-slip Faulting and Basin Formation, Soc. Econ. Paleontol. Mineral. Sp. Pub., Vol. 37, pp. 227–264.

Şengör A.M.C., Yılmaz Y., 1981, Tethyan evolution of Turkey: a plate tectonic approach, Tectonophysics, Vol. 75, pp. 181–241.

Şengör, A.M.C., 1979, The North Anatolian Transform Fault: its age, offset and tectonic significance, J. Geol. Soc., London, Vol. 136, pp. 269–282.

Seyitoğlu G., Scott B., 1992, The age of the Büyük Menderes Graben (western Turkey) and its tectonic implications, Geol. Mag., Vol. 129, pp. 239–242.

Seyitoğlu G., Scott B., Late C., 1991, Cenozoic crustal extension and basin formation in west Turkey, Geol. Mag., Vol. 128, pp. 155–166.

Spakman W.A.V., Wortel M.J.R., Vlaar N.J., 1988, The Aegean subduction zone: a tomographic image and its geodynamic implications, Geophys. Res. Lett., Vol. 15, pp. 60–63.

Tarcan, G., Gemici, Ü., Aksoy, N., 2005, Hydrogeological and geochemical assessments of the Gediz Graben geothermal areas, western Anatolia, Turkey, Environmental Geology, Vol. 47, pp. 523-534.

Tarcan, G., 2004, Mineral saturation and scaling tendencies of waters discharged from wells (>150 °C) in geothermal areas of Turkey, Journal of Volcanology and geothermal research, in press

Taymaz T., 1993, The source parameters of the Çubukdağ (W. Turkey) earthquake of October 11, Geophys. J. Inter., Vol. 113, pp. 260–267.

Taymaz T., Jackson J., McKenzie D.P., 1991, Active tectonics of the North and Central Aegean Sea, Geophy. J. Inter., Vol. 106, pp. 433–490.

Vengosh, A., Helvacı, C., Karamanderesi, İ. H., 2002, Geochemical constraints for the origin of thermal waters from western Turkey , Applied Geochemistry, Vol. 17, pp.163-183.

Whitesitt, J. E., 1962, Boolean Algebra and its Applications, Addison-Wesley Publishing Company, Inc., USA, 177 pages.

Yilmaz, Y., Genç, S.C., Karacık, Z., Altunkaynak, S., 2001, Two contrasting magmatic associations of NW Anatolia and their tectonic significance, J. Geodyn., Vol. 31, pp. 243– 271.

Yılmaz, Y., Genç, S.C., Gürer, O.F., Bozcu, M., Yılmaz, K., Karacık, Z., Altunkaynak, Ş., Elmas, A., 2000, When did the western Anatolian grabens begin to develop in: Bozkurt E., Winchester J.A., Piper J.D.A. (Eds.), Tectonics and magmatism in Turkey and the surrounding area, Geological Society Special Publication, Vol. 173, Geological Society, London, pp. 353–384.